1-1-2014

Interference Modeling And Control In Wireless Networks

Xin Che
Wayne State University,

INTERFERENCE MODELING AND CONTROL IN WIRELESS NETWORKS

by

XIN CHE

DISSERTATION

Submitted to the Graduate School

of Wayne State University,

Detroit, Michigan

in partial fulfillment of the requirements

for the degree of

DOCTOR OF PHILOSOPHY

2014

MAJOR: COMPUTER SCIENCE

Approved by:

_____

Advisor Date

_____

_____

_____

DEDICATION

To my wife, Xue Zhang, and my parents, Shu-Pin Che and Jin-Lian Guo

ACKNOWLEDGEMENTS

First, I would like to thank my advisor, Dr. Hongwei Zhang, for his continuous and enormous support in the past 7 years. He has invest so many hours discussing research, answering my questions and giving me advice. Without his commitment, this dissertation would not have been possible without him. I would also like to thank my committee members, Dr. Monica Brockmyer, Dr. Feng Lin, Dr. Wei-Song Shi and Dr. Le-Yi Wang, for their valuable time reading my thesis and giving me feedback.

Second, I would thank all my colleagues at Dependable Networking and Computing research group at Wayne State University, Dr. Qiao Xiang, Xiaohui Liu, Chuan Li and Yu Chen, for the great discussions and wonderful time we had.

Last but not least, I sincerely acknowledge the love from my family, especially from my wife, Xue Zhang. Their unconditional love carries me through the difficulties that would otherwise crush me so many times. Thanks to Rev. David Chang, Clifton Tally, Gary Chen, Zhaoming Zhu, Zhi-Gang Tie, Dr. Li-jun Wang, Dr. Yan-hua Zhang, Dr. Wei Song, Emily Zhang, Dr. Chang Liu, Dr. Su-hui Wang, Dr. Ning Wen, Dr. Bo Zhao, Dong-Shu Liu, Dr. Shaobai Kan, Dr. Yi Wang, Dr. Xiaodong Liu, Xin Wang, Ji Yan, Dr. Jun Wang. The life-sharing and pray with you all transform my life and build my character. You have lift my life to a new horizontal.

TABLE OF CONTENTS

LIST OF TABLES

LIST OF FIGURES

CHAPTER 1

INTRODUCTION

1.1 Inteference: a key challenge of wireless networks

With a succesful commercialization of IEEE802.11 standard, wireless networks have become a tight-knit of our daily life. Besides Wireless Local Area Network(LANs), different types of wireless networks have been designed and deployed. For example, there are Wireless Sensor Networks [5], Wireless Mesh Networks [6], Wireless Multimedia Networks [4]. Recently, the development of networked embeded sensing and control expands the application territories of wireless networks into the field of mission-critical applications such as industrial monitoring and control [18]. This is evidenced by the recent industry standards such as WirelessHART [70] and ISA SP100.11a [63] which target wireless networked sensing and instrumentation. In supporting real-time, mission-critical tasks, these wireless networks are required to ensure real-time, reliable data delivery. Nonetheless, wireless communication is subject to various dynamics and uncertainties. Due to the broadcast nature of wireless communication, in particular, concurrent transmissions may interfere with one another and introduce co-channel interference. Co-channel interference not only reduces the reliability and throughput of wireless networks, it also increases the variability and uncertainty in data communication [64, 80, 77].

Therefore, effectively scheduling concurrent transmissions to control co-channel interference has become critical for enabling reliable, predictable wireless communication. A basis of interference control is the interference model which *predicts* whether a set of concurrent transmissions may interfere with one another. Two commonly used models are the physical interference model and the protocol interference model [25]. In the physical model, a set of concurrent transmissions are regarded as not interfering with one another if the resulting signal-

to-interference-plus-noise-ratio (SINR) at every receiver is no less than a threshold value γ_0; in the protocol model, a transmission is regarded as not being interfered by an interferer if the interferer is at least K times the transmitter-receiver distance away from the receiver[1]. For simplicity, we also call the physical model the *SINR model* and the protocol model the *ratio-K model* in this paper, and we regard scheduling based on the SINR model and the ratio-K model SINR-based scheduling and ratio-K-based scheduling respectively. The SINR model is a high fidelity model in general, but the interference relations defined by it are non-local and combinatorial. This is because whether one transmission interferes with another is modeled as *explicitly* depending on all the other transmissions in the network. Accordingly, SINR-based scheduling usually requires network-wide coordination. Since the coordination delay slows down protocol convergence [11, 73] and increases uncertainty [74], it is difficult to use the SINR model in *distributed* protocol design. This is especially the case when network traffic pattern and environmental conditions are dynamic and potentially unpredictable.

Unlike the SINR model, the ratio-K model defines local, pair-wise/non-combinatorial interference relations where interference is regarded as existent only between nodes in a local neighborhood. Accordingly, the ratio-K model is suitable for distributed protocol design since ratio-K-based scheduling only requires coordination among nodes in their local neighborhood. The locality of ratio-K-based scheduling can also enable agile protocol adaptation for addressing the challenges of unpredictable traffic pattern and environmental dynamics. Nonetheless, the ratio-K model is an approximate model in nature, and it does not ensure reliable data delivery in general. For instance, the RTS-CTS-based channel access control can only enable a data delivery ratio of $\sim$50% in our field wireless sensor networks [7, 76]; via testbed-based measurement study of event-detection sensor networks, Choi et al. have also shown that CSMA- and RTS-CTS-based channel access control mechanisms may only enable a data delivery ratio of 16.9% and 36.8% respectively [19]. To enable the design of distributed MAC protocols for

[1]We replace the original notation of $(1 + \Delta)$ [25] with K for simplicity. Also note that the commonly used K-hop model [54] is a special case of the protocol model in geometric graphs.

agile, predictable interference control, an *open question* is whether it is possible to develop an interference model that has both the locality of the ratio-K model and the high fidelity of the SINR model.

1.2 Contribution of this dissertation

To answer that question, we propose the *physical-ratio-K (PRK) interference model* as a reliability-oriented instantiation of the ratio-K model, where the link-specific choice of K adapts to network and environmental conditions as well as application QoS requirements to ensure certain minimum reliability of every link. Given that the ratio-K model is local and can enable agile, distributed protocols, we explore the possibility of extending the ratio-K model to preserve its locality while addressing the low performance issue of ratio-K-based scheduling. To this end, we first study the behavior of ratio-K-based scheduling, and a summary of our findings are as follows:

- We analyze, for both grid and random networks, how network traffic load, link length, node distribution density, and wireless signal attenuation affect the effective instantiation of the ratio-K model. We find that, as traffic load increases and wireless signal attenuation decreases, the optimal K for maximizing network throughput and the minimum K for satisfying certain link reliability tends to increase. As link length increases, the minimum K for satisfying certain link reliability also tends to increase, but the optimal K for maximizing network throughput can both increase and decrease. We also find that fixing K to a constant number, as in most existing studies [14, 40, 44], can lead to significant performance loss when network and environmental settings change. For instance, deviation from the optimal K by up to 1 can cause up to 68% throughput loss, and fixing K to 2 may lead to a link reliability less than 80%. These findings suggest that it is important to choose the right K when studying ratio-K-based scheduling, otherwise the performance evaluation will be biased.

- We also find that there is inherent tradeoff between reliability and throughput when instantiating the ratio-K model. Maximum network throughput is usually achieved not at the minimum K for ensuring certain link reliability, but at a smaller K. For instance, $\sqrt{2}$ is the optimal K for maximizing throughput in many scenarios, but, with non-negligible probability, $\sqrt{2}$ is unable to guarantee an 80% link reliability. Moreover, as K increases from the minimum one required for satisfying certain link reliability, network throughput tends to decrease, especially when link reliability requirement is high.

The above analytical results give us insight into the behavior of ratio-K-based scheduling in uniform grid and random networks with a wide range of system configurations (on factors such as traffic load, link length, and wireless signal attenuation). We have verified these insight through simulation as well as measurement study in both the NetEye and the MoteLab wireless sensor network testbeds which reflect real-world properties such as non-uniform network settings.

On the other hand, the interference among the transmissions, when scheduling them for a same time slot, limits the number of concurrent transmissions in the slot. Optimal interference-oriented scheduling in wireless networks has been shown to be NP-complete in general [23, 54], and the research community has proposed different polynomial-time approximation algorithms accordingly. Most approximation algorithms are greedy in nature, and two representatives are Longest-Queue-First (LQF) [35, 30, 9] and GreedyPhysical [10, 66]. When scheduling concurrent transmissions for a time slot, LQF greedily adds to the slot non-interfering links in a decreasing order of their senders' queue lengths; GreedyPhysical selects non-interfering links for the slot in a decreasing order of their interference numbers, where the interference number of a link ℓ is defined as the number of other links that do not share any end-node with ℓ but can be interfered by ℓ. Different from the greedy algorithms, Goussevskaia et al. proposed the algorithm LengthDiversity [23]. In LengthDiversity, the links of a network are grouped into different classes based on their lengths. Links in different classes are scheduled independent

of one another, and links in the same class are scheduled using virtual-grid-based coloring.

In approximation algorithms where links are added to a time slot in a sequential manner until reaching the interference limit,[2] the order in which links are added determines the accumulation of interference at the receivers and thus affects the number of concurrent links schedulable in the slot (see Section 3.3 for an example). Nonetheless, existing scheduling algorithms either do not take this ordering effect into account (e.g., in LQF) or do not explicitly optimize for the ordering effect (e.g., in GreedyPhysical and LengthDiversity). Thus the *open questions* are: 1) how to explicitly optimize the ordering of link addition in wireless scheduling? and 2) how does link ordering affect the throughput and delay of data delivery?

To address these open questions for insight into wireless scheduling, we formulate the concept of *interference budget* that, given a set of scheduled transmissions in a time slot, characterizes the additional interference power that can be tolerated by all the receivers without violating the application requirement on link reliability. Then, by modeling the scheduling problem as a knapsack problem, we propose the scheduling algorithm *iOrder* that optimizes link ordering by considering both interference budget and queue length in scheduling. When constructing the schedule for a time slot, iOrder first picks a link with the maximum number of queued packets; then iOrder adds links to the slot one at a time in a way that maximizes the interference budget at each step; this process repeats until no additional link can be added to the slot without violating the application requirement on link reliability. To understand the impact of link ordering on scheduling, we first analytically prove the approximation ratio of iOrder in Poisson random networks, then we comparatively study the performance of iOrder and existing algorithms via simulation and testbed-based measurement. We observe that optimizing link ordering can improve the performance of existing algorithms by a significant.

[2]For example, the SINR at some receiver falls below a minimum threshold.

1.3 Organization of this dissertation

The rest of this paper is organized as follows. We first analysis the performance of the *Ratio-K* model and compare its peformance of different instantiation with the *SINR model* in Chapter 2. Based on the analytical result, we propose our model, the PRK model. With the insight of controlling interference *locally* from the *PRK model*, we explore a similar method to handle the interference *globally* in the network link scheduling problem. The effort of this study leads to the result of *iOrder* and we will discuss it in detail in Chapter 3. In Chapter 4, we will explore the potential of using PRK model in milt-channel scheduling. In the end, we will conclude our work and the future work in Chapter 5.

CHAPTER 2

PRK INTERFERENCE MODEL

2.1 Preliminaries

Here we present the wireless channel and radio model used in the analytical part of the work.

Channel model When a wireless signal propagates, it is subject to the impact of diffraction, reflection, and scattering. These effects affect the power of the signal in two different ways: first, the signal power decays exponentially with respect to distance traveled; second, for a given distance *d*, the signal strength is random and log-normally distributed around the mean distance-dependent value [58].

To characterize signal attenuation in wireless networks, we use the log-normal path loss model [50] which is widely adopted in protocol design and analysis. This model could be used for large and small coverage systems [52]. Moreover, empirical studies have shown that the log-normal model provides more accurate multipath channel models than the well-known Nakagami and Rayleigh models for indoor environment [48].

By this model, the power P_r (in dBm) of the received signal at a node distance d away from the transmitter is computed as follows:

$$P_r = P_t - PL(d_0) - 10\alpha log_{10}\frac{d}{d_0} + N(0, \sigma^2) \tag{2.1}$$

where P_t is the transmission power, $PL(d_0)$ is the power decay at the reference distance d_0, α is the path loss exponent, $N(0, \sigma)$ is a Gaussian random variable with mean 0 and variance σ. In our study, we use different instantiations of α and σ to represent different wireless

environments.

Radio model. The reception capability of a radio can be characterized by the bit error rate (BER) and the packet delivery rate (PDR) in decoding signals with specific signal-to-interference-plus-noise-ratios (SINR). Focusing on wireless sensing and control networks, we base our study mainly on the commonly-used, IEEE 802.15.4-compatible CC2420 radios; For CC1000 radios, Zuniga $et\ al.$ have derived the formula for computing the expected PDR for a given distribution of SINR values at a receiver [75]. Since CC2420 radios are compatible with the IEEE 802.15.4 standard and tend to be more popular than CC1000 today, the analysis of this paper is based on the CC2420 radio. For CC2420 radio, the BER for a SINR of γ is computed as follows [2]:

$$\text{BER}(\gamma) = \frac{8}{15} \times \frac{1}{16} \times \sum_{k=2}^{16} (-1)^k \binom{k}{16} e^{(20 \times \gamma \times (\frac{1}{k} - 1))} \tag{2.2}$$

Accordingly, the PDR for a SINR of γ is computed as follows:

$$\text{PDR}(\gamma, f) = (1 - \text{BER}(\gamma))^{8f} \tag{2.3}$$

where f is the packet length (in units of bytes) including overhead such as packet header.

Remark. For analytical tractability, the aforementioned models do not capture all the real-world phenomena such as the irregularity in wireless communication [79]. But the analysis based on these models gives us insight into the behaviors of wireless interference models, and the analytical results have also been verified through testbed-based measurement which captures complex real-world phenomena as we discuss in Section 2.7.

To compute the expected PDR for a CC2420 receiver at a specific location, we first derive the PDR-SINR relation for CC2420 radios, then we compute the expected PDR based on the distribution of SINR values at the receiver using the method of [81].

Interference model. We consider the ratio-K and SINR interference models. In the ratio-K

model, a concurrent transmitter n_i does not interfere with the transmission from n_s to n_r if and only if the following holds:

$$d(n_i, n_r) \geq K \times d(n_s, n_r) \tag{2.4}$$

where $d(n_i, n_r)$ is the distance between n_i and n_r, and $d(n_s, n_r)$ is the distance between n_s and n_r. In the SINR model, a set of concurrent transmitters S_i does not interfere with the transmission from n_s to n_r if and only if the following holds:

$$\frac{P(n_s, n_r)}{N_0 + \sum_{n_i \in S_i} P(n_i, n_r)} \geq \gamma_0 \tag{2.5}$$

where N_0 is the background noise power, $P(n_s, n_r)$ is the strength of signals reaching n_r from n_s, $P(n_i, n_r)$ is the strength of signals reaching n_r from n_i, and γ_0 is a SINR threshold chosen to satisfy certain requirement on PDR.

Network and environment model. For mathematical tractability in our study, we only focus on grid networks and Poisson random networks (where nodes are distributed in a Poisson manner spatially), and we assume that signal attenuation follows the geometric rule as shown in Equation 3.1. As we will show in Section 2.2, however, the insight gained from our study also shed light on system analysis and protocol design in non-uniform networks where node distribution and signal attenuation may not be uniform. Thus, we expect that the observations of this paper be of generic interest to different wireless networks even though we focus on uniform networks for in this paper.

2.2 Instantiation of the ratio-K model

To explore effective methods of instantiating the ratio-K model, we first analyze the performance of ratio-K-based scheduling, then we numerically study how system properties and design objectives affect the effective instantiation of the ratio-K model.

Performance of ratio-K-based scheduling

Here we analyze network throughput and link reliability in ratio-K-based scheduling when the ratio-K model is instantiated with different Ks. Focusing on link-layer behavior, we consider the optimization objective of maximizing channel spatial reuse (i.e., maximizing the number of concurrent transmissions) in ratio-K-based scheduling. In Sections 2.2 and 2.4 accordingly, by network throughput, we mean network spatial throughput as defined by Formula (2.6); in our measurement study in Section 2.7, we consider end-to-end throughput which directly reflects network-wide behavior.

Towards characterizing the computational complexity of ratio-K-based scheduling in general, we first prove that the ratio-K-based scheduling is NP-hard as follows:[1]

Proposition 1. *The problem of maximizing the number of interference-free concurrent transmissions is NP-hard when the interference model is the ratio-K model.* □

Proof. We consider the case when $K > 1$, as is usually the case in practice. Then, the NP-hardness of ratio-K-based scheduling with maximum spatial reuse can be proved through a polynomial time reduction from the 3-CNF-SAT problem to ratio-K-based scheduling. The proof is the same as the proof for Theorem 2 of [55] (which shows the NP-hardness of the Maximum Weighted K-Valid Matching problems) except for the following changes to the reduction:

- Instead of an abstract graph, the graph G is embedded onto a 2D plane where each node has a fixed location in the plane.

- For the subgraph corresponding to the s-th ($s = 1..m$) clause of the 3-CNF boolean formula, locate the nodes such that the links $(v^s_{i,f}, v^s_{i,b})(i = 1..3)$ are orthogonal to the links $(v^s_{i,f}, v^s_{i+1,f})(i = 1, 2)$ and that links $(v^s_{1,f}, v^s_{2,f})$ and $(v^s_{2,f}, v^s_{3,f})$ are along the same line. In addition, make the lengths of the links $(v^s_{i,f}, v^s_{i,b})(i = 1..3)$ and $(v^s_{i,f}, v^s_{i+1,f})(i = 1, 2)$ to be of one unit.

[1] Even though the NP-hardness of K-hop-interference-model-based scheduling has been proved [54], the NP-hardness of ratio-K-based scheduling has not been analyzed yet.

- Place all the subgraphs on the plane (e.g., in a big circle) such that every link connecting two subgraphs is at least $K (K > 1)$ units long.

Based on this new reduction method for constructing the graph G, the rest of the proof for Theorem 2 of [55] is applicable to our proof here without any change.

□

We consider both grid and Poisson random networks in our analysis, but, given the NP-hardness of general ratio-K-based scheduling, we only consider the following special cases of the problem for computational tractability and for deriving closed-form formula for scheduling performance:

- To avoid the complication introduced by boundary effects in small, finite networks, we only consider infinite sized networks. (Note that infinite sized networks also approximate large networks such as those envisioned for industrial control in large oil fields.)

- For grid networks, we only consider cases where the data transmission links are of equal length ℓ and ℓ is a multiple of grid hop length. We also assume a uniform traffic pattern where all the transmissions follow the same direction along the grid-line, which enables the maximum degree of spatial reuse in grid networks (see Appendix II for the proof).

- For 2D Poisson random networks, we assume that nodes are distributed with an average density of λ nodes per unit area. The traffic pattern is such that the average link length is ℓ; each transmitter T sends packets to a receiver R such that the distance between T and R is the closest to ℓ, and if multiple such receivers exist, T randomly picks one as its receiver.

- For both grid and random networks, we assume that each transmitter has data packets buffered for transmission with probability β at any moment in time.

The analytical results derived based on the above assumptions give us insight into the behavior

of ratio-K-based scheduling in uniform grid and random networks with a wide range of system configurations (on factors such as traffic load, link length, and wireless signal attenuation); the analytical insight has been verified through testbed-based measurement and simulation where finite networks and non-uniform traffic patterns are considered without the above assumptions. We will present the measurement results in Section 2.7, and, the detail simulation results in Section 2.3

In data transmission scheduling, we consider both reliable reception of data at receivers and reliable reception of link-layer acknowledgments at transmitters. Let the length of a link L be ℓ, and T and R be the transmitter and receiver of L respectively. Then ratio-K-based scheduling defines two circular exclusion regions centered at T and R respectively, each with a radius $K\ell$, such that no other node in the exclusion regions can transmit concurrently with T. We regard the union of the transmitter- and receiver-side exclusion regions as the exclusion region of link L, and we denote it by $\mathbb{ER}(L, K)$. For instance, Figure 2.1 shows the exclusion

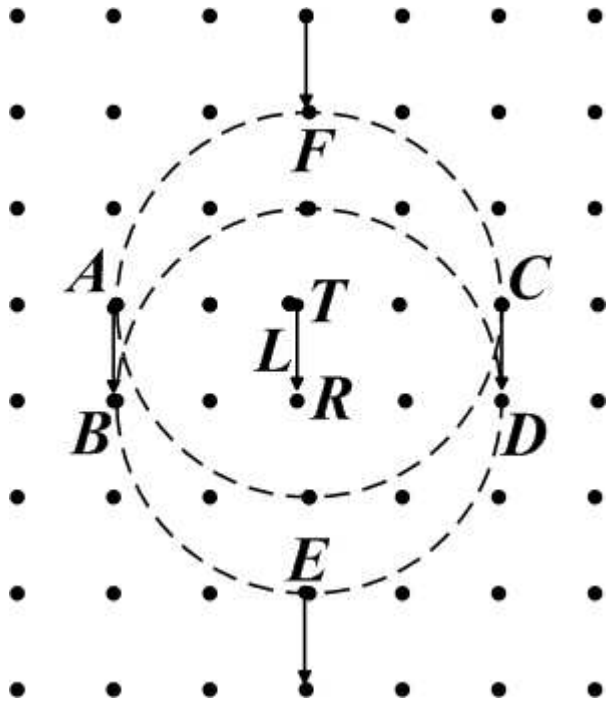

Figure 2.1: Example: scheduling based on the ratio-2 model in grid networks

region of link L in a grid network when K = 2. For convenience, we also use $\mathbb{ER}(L, K)$ to denote the set of nodes within the exclusion region, not including those on the boundary.

Given the uniform network and traffic conditions we consider and based on the concept of *spatial throughput* [60], we define as follows the throughput T_{net} of an infinite network:[2]

$$T_{net} = E_L[\frac{T_L}{|\mathbb{ER}(L, K)|}] \tag{2.6}$$

where L is an arbitrary link in the network, T_L is the throughput along link L, and $|\mathbb{ER}(L, K)|$ is the number of nodes in L's exclusion region.[3] Denoting the length of L as ℓ, T_L is such that its time average can be computed as

$$E_t[T_L] = (BW \times \beta \times \text{PDR}) \times \ell \tag{2.7}$$

where BW is the radio transmission rate in terms of number of packets per unit time, β is the probability that a node has data packets buffered for transmission at any moment in time, and PDR is the packet delivery reliability over L. Note that, by the above definitions, the unit for T_L is "packet-distance-product per unit time", and the unit for T_{net} is "packet-distance-product per unit time per node". T_{net} characterizes the average throughput from every node to its one-hop neighbors in the network; even though T_{net} only indirectly reflects the achievable multi-hop throughput, our testbed-based measurement study in Section 2.7 will show that the insight gained in the analysis applies to the case of multi-hop convergecast. Also note that T_{net} is of direct interest to the applications of inter-vehicle sensing and control, where one typical traffic pattern is single-hop communication between neighboring vehicles.

Grid networks. The interference incurred at a receiver depends on the spatial distribution

[2]Focusing on link-layer behavior, Sections 2.2 and 2.4 adopt this notion of network throughput; in our measurement study in Section 2.7, we consider end-to-end throughput which directly reflects network-wide behavior.

[3]We consider the expected value of $\frac{T_L}{|\mathbb{ER}(L,K)|}$ to account for non-deterministic factors such as probabilistic packet transmissions and probabilistic node distribution in random networks.

of concurrent transmitters, which depends on the specific K used in ratio-K-based scheduling. For clarity of presentation, we only present the case of $K = 2$ as shown in Figure 2.1, and we relegate the discussion of other Ks to Section 2.3

In what follows, we prove the fact, that

Proposition 2. *the uniform traffic pattern where all the transmissions follow the same direction along the grid-line enables the maximum degree of spatial reuse in grid networks*

Proof. For convenience, we call *same-direction schedules* the schedules generated for the traffic pattern where all the transmissions follow the same direction along the grid-line, and we call *different-direction schedules* the schedules generated for the traffic pattern where transmissions follow different directions and different grid-lines. To achieve the maximal spatial reuse, we must minimize the average area shared by a link. Given a ratio-K model, we find the minimum area-per-link in optimal same-direction schedules and different-direction schedules, and we denote them by $A_{min}(k)$ and $A'_{min}(k)$ respectively. We will prove that $A_{min}(k) > A'_{min}(k)$ for all the cases we study.

Given an infinite grid network, we pick one node as the origin to set up the coordinate system. So the coordinate of any node in grid networks, say (x, y), is such that $x, y \in \mathbb{Z}$. As discussed in Section 2.2, here we only consider cases where link length ℓ is a multiple of grid hop length. For simplicity of presentation in the following discussion, we also set the unit of variables as multiples of ℓ.

Suppose that the coordinates of a end-node of a link and one of its closest interferers are (x, y), (x', y') respectively. In grid networks, the following holds:

$$\begin{cases} |x - x'| = a \\ |y - y'| = b \\ \sqrt{a^2 + b^2} = k \end{cases}$$

where $a, b \in \mathbb{Z}^+$ and K is the parameter of the ratio-K model. The values of a and b in different ratio-K models are shown in Table 2.1.

Table 2.1: a and b in ratio-K model

K	(a, b)	K	(a, b)
$\sqrt{2}$	(1, 1)	2	(0, 2)
$\sqrt{5}$	(1, 2)	$\sqrt{8}$	(2, 2)
3	(0, 3)	$\sqrt{10}$	(1, 3)
$\sqrt{13}$	(2, 3)	4	(0, 4)
$\sqrt{18}$	(3, 3)	$\sqrt{20}$	(2, 4)
5	(0, 5)/(3,4)	$\sqrt{26}$	(1, 5)
$\sqrt{29}$	(2, 5)	$\sqrt{32}$	(4, 4)
$\sqrt{34}$	(3, 5)	$\sqrt{6}$	(0, 6)

For same-direction transmissions, there are four possible patterns of tightest spatial reuse, as shown in Figures 2.2, 2.3, 2.4, 2.5. Denote these patterns of patter I, II, III, and IV respectively. The average area-per-link for each spatial reuse pattern is shown in Equations 2.8, 2.9, 2.10, and 2.11 below:

$$A_I(a,b) = (a+1)(a+b) + b(b-a), \text{if } a > 0, \tag{2.8}$$

$$A_{II}(a,b) = 2b \times (a+1), \text{if } 2b > \sqrt{a^2+b^2}, 2a+1 > \sqrt{a^2+b^2} \tag{2.9}$$

$$A_{III}(a,b) = 2a \times (b+1), \text{if } 2a > \sqrt{a^2+b^2}, 2b+1 > \sqrt{a^2+b^2} \tag{2.10}$$

$$A_{IV}(a,b) = b \times (b+1), \text{if } a = 0 \tag{2.11}$$

To achieve the highest spatial reuse for same-direction transmissions, we define a set of candidate schedule types $Sch_{a,b} = \{i | (a,b)$ satisfies the requirement of schedule pattern $i, i \in I, II, III, IV\}$. So the average area-per-link is $A_{min} = \min\{A_i, i \in Sch_{a,b}\}$.

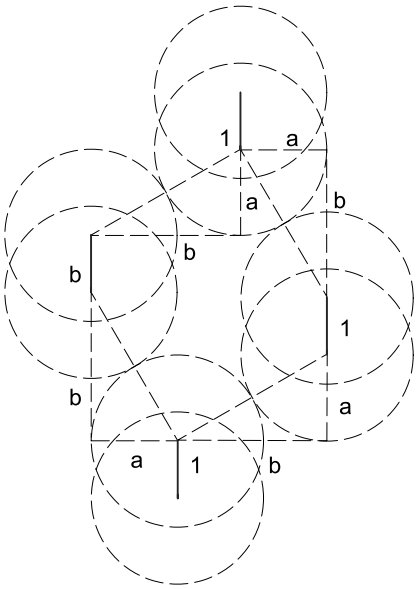

Figure 2.2: Type I schedule

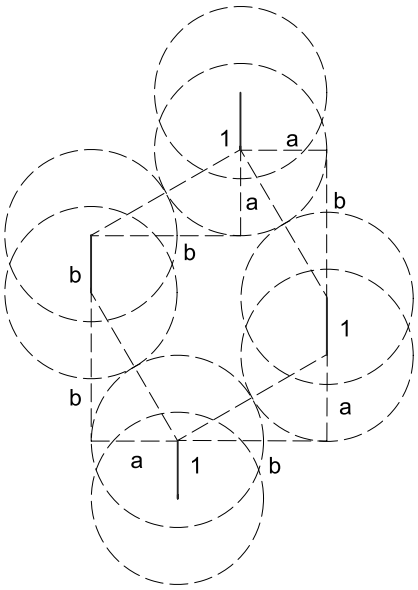

Figure 2.3: Type II schedule

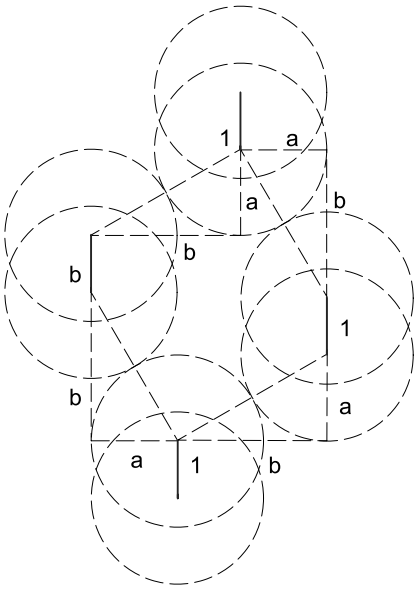

Figure 2.4: Type III schedule

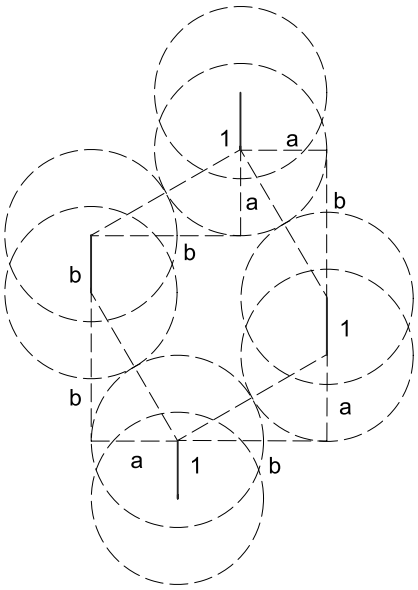

Figure 2.5: Type IV schedule

For different-direction transmissions, there are also find four types of tightest schedules, namely as $V, VI, VII, VIII$ as shown in Figures 2.6, 2.7, 2.8, and 2.9. The average area-per-link for each spatial reuse pattern is shown in Equations 2.12, 2.13, 2.14, 2.15.

Similar to the case of same-direction transmissions, we define $Sch'_{a,b} = \{i|(a,b)$ satisfies the requirement of schedule pattern $i, i \in V, VI, VII, VIII\}$. So the average area-per-link is $A'_{min} = \min\{A_j, j \in Sch'_{a,b}\}$.

$$A_V(a,b) = \frac{(a+b+1)^2 + (b-a)^2}{2}, \text{if } a > 0, \tag{2.12}$$

$$A_{VI}(a,b) = \frac{(2a+1)(2b+1)}{2}, \text{if } 2a \geq \sqrt{a^2+b^2}, 2b \geq \sqrt{a^2+b^2} \tag{2.13}$$

$$A_{VII}(a,b) = \frac{b(3b+a+2)}{2}, \text{if } a > 0, b = a+1 \tag{2.14}$$

$$A_{VIII}(a,b) = (2b+1)(b+1), \text{if } a = 0 \tag{2.15}$$

We compute A_{min} and A'_{min} for different ratio-K instantiations, and Table 2.2 shows the results. We see that same-direction schedules always has smaller area-per-link than the corresponding different-direction schedules do. This implies that same-direction traffic pattern enables the maximum degree of spatial reuse.

Done. □

For the transmission along an arbitrary link L as shown in Figure 2.1, six nodes (i.e., A - F) on the boundary of the exclusion region of L can be involved, either as a transmitter or a receiver, in concurrent transmissions to generate the tightest tessellation of concurrent transmissions and to enable maximum spatial reuse. In a tightest tessellation of concurrent transmissions in ratio-2-based scheduling, this pattern of 4 concurrent transmissions/receptions

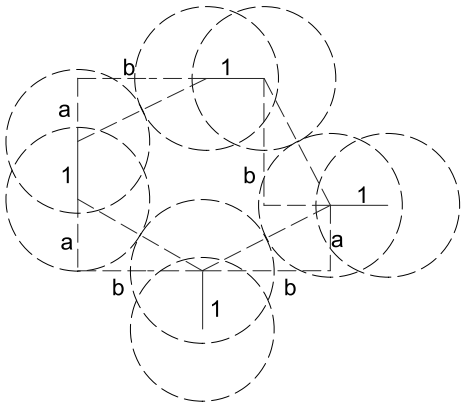

Figure 2.6: Type V schedule

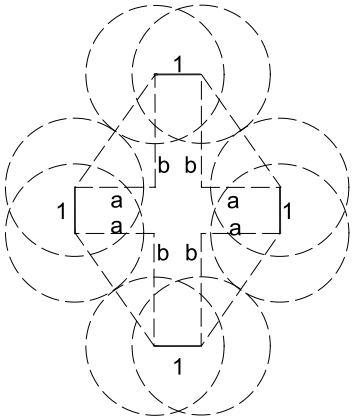

Figure 2.7: Type VI schedule

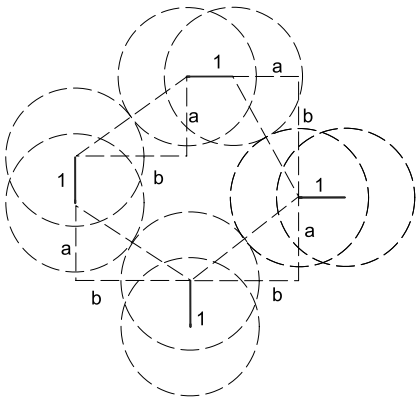

Figure 2.8: Type VII schedule

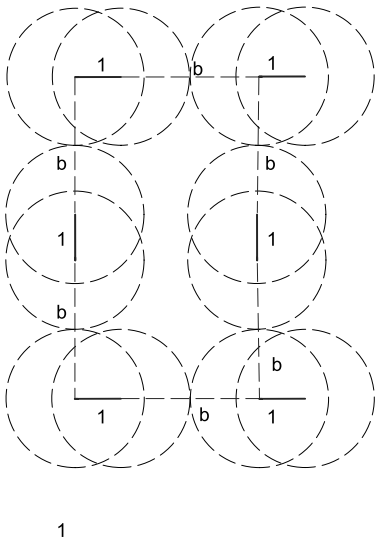

Figure 2.9: Type $VIII$ schedule

Table 2.2: A_{min} and A'_{min} in ratio-K based scheduling

K	$A_{min}(k)$	$A'_{min}(k)$
$\sqrt{2}$	4	4.5
2	6	7.5
$\sqrt{5}$	8	8.5
$\sqrt{8}$	12	12.5
3	12	14
$\sqrt{10}$	12	14.5
$\sqrt{13}$	16	17.5
4	20	22.5
$\sqrt{18}$	24	24.5
$\sqrt{20}$	24	26.5
5	30	33
$\sqrt{26}$	32	32.5
$\sqrt{29}$	36	36.5
$\sqrt{32}$	40	40.5
$\sqrt{34}$	36	38.5
6	42	45.5

around L applies to every other transmission in the network, thus we can derive the set $\mathcal{S}_i$ of concurrent transmitters that serve as interferers to the transmission along L. If we define a coordinate system where the coordinates of R and T are $(0, 0)$ and $(0, \ell)$ respectively, then

$$\mathcal{S}_i = \{(2m\ell, (3n+1)\ell) : m \in \mathbb{Z}, n \in \mathbb{Z}, m^2 + n^2 \neq 0\} \tag{2.16}$$

where $\mathcal{S}_i$ is identified by the locations of the nodes in it, and $\mathbb{Z}$ is the set of all integers. In Figure 2.1, for instance, transmitter C's location is (2ℓ, ℓ) and the corresponding m and n are 1 and 0 respectively. Then,

Proposition 3. *When $K = 2$, the expected total interference I at a receiver R in an infinite*

grid network is as follows:

$$
\begin{aligned}
&I = \textstyle\sum_{n_i \in \mathcal{S}_i} I_i = P_t \times \beta \times \sum_{n_i \in S_i} d(n_i, R)^{-\alpha} = P_t \times \beta \times \\
&\ell^{-\alpha} \times \Bigg(\textstyle\sum_{m=1}^{\infty} \big(\frac{2}{((2m)^2+1)^{\alpha/2}} + \frac{1}{(3m+1)^{\alpha/2}} + \frac{1}{(3m-1)^{\alpha/2}} \big) + \\
&2 \times \textstyle\sum_{m=1}^{\infty} \sum_{n=1}^{\infty} \Big(\frac{1}{[(2m)^2+(3n+1)^2]^{\alpha/2}} + \frac{1}{[(2m)^2+(3n-1)^2]^{\alpha/2}} \Big) \Bigg)
\end{aligned}
\tag{2.17}
$$

where I_i is the interference introduced by concurrent transmitter n_i, P_t is the transmission power, $d(n_i, R)$ is the distance from n_i to R, β is the node transmission probability, and α is the wireless path loss exponent. I is finite as long as $\alpha > 2$. □

Proof. When $K = 2$,

$$\mathcal{S}_i = \{(2m\ell, (3n+1)\ell) : m \in \mathbb{Z}, n \in \mathbb{Z}, m^2 + n^2 \neq 0\}$$

Thus I is the sum of the expected interference introduced by each concurrent transmitter n_i in $\mathcal{S}_i$. Based on the link model discussed in Section 3.2, we have

$$
\begin{aligned}
&I = \textstyle\sum_{n_i \in S_i} I_i \\
&= P_t \times \beta \times \textstyle\sum_{n_i \in S_i} d(n_i, R)^{-\alpha} \\
&= P_t \times \beta \times \ell^{-\alpha} \times \\
&\Bigg(\textstyle\sum_m \sum_n \big(\frac{1}{[(2m)^2+(3n+1)^2]} \big)^{\alpha/2} \Bigg)
\end{aligned}
\tag{2.18}
$$

After some simple derivations, Equation 2.18 becomes equal to Equation 2.17.

When $\alpha > 2$, the following holds:

$$\sum_{m=1}^{\infty} \frac{1}{((2m)^2+1)^{\alpha/2}} < \sum_{m=1}^{\infty} \frac{1}{m^{\alpha/2}}$$

The right hand side of the above inequality is a type of p-series where $p = \frac{\alpha}{2}$, and it converges when $p > 1$. Accordingly, $\sum_{m=1}^{\infty} \frac{1}{((2m)^2+1)^{\alpha/2}}$ converges when $\alpha > 2$. Using similar approach,

we can prove that the other items of Equation 2.17 converges if $\alpha > 2$. Therefore, I converges and is finite as long as $\alpha > 2$. □

Note that, in grid networks, the total interference I is a function of link length ℓ but not the node distribution density (e.g., as characterized by the grid-hop length $\frac{\ell}{n}$ for some positive integer n).

Using Equation 2.17, we can compute the interference and thus the SINR at R, based on which we can compute link reliability and network throughput for the case of $K = 2$. Similar approaches can be used to derive I for other Ks; interested readers can find the details in Appendix-I.

Random networks. In ratio-K-based scheduling for maximizing spatial reuse in Poisson random networks, the spatial distribution of concurrent transmitters can be modeled as a variant of the Matern hard-core process [59]. More specifically, it can be specified by a dependent thinning process as follows. Let's denote the stationary Poisson process corresponding to the random network as Φ. We mark each node X of Φ with a random number $m(X)$ uniformly distributed over $(0, 1)$; a link L with transmitter T and receiver R is marked with a number $m(L) = \frac{m(T)+m(R)}{2}$. We define the links incident to a node X as the set of links whose transmitter or receiver is X, and we denote it by $\mathbb{L}(X)$; we also denote the link whose transmitter is X by $L(X)$. Then, the dependent thinning process retains a transmitter $X \in \Phi$ if the mark of $L(X)$ is the smallest among those of all the links incident to some node within the exclusion region $\mathbb{ER}(L(X), K)$ of link $L(X)$. That is, the thinned process of concurrent transmitters is defined as follows:

$$\begin{aligned} \Phi_t = \{X \in \Phi : \quad & m(L(X)) < m(L), \\ & \forall L \in \cup_{Y \in \mathbb{ER}(L(X),K)} \mathbb{L}(Y)\} \end{aligned} \tag{2.19}$$

Then, the thinned process Φ_t can be approximated by a spatial Poisson process [59], and we derive its density λ_t as follows:

Proposition 4. *The density of the thinned process Φ_t of concurrent transmitters computes as follows:*

$$\lambda_t = \frac{1 - exp(-\lambda c)}{c} \tag{2.20}$$

where $c = C(\ell, K) + (C(\ell, K+1) - C(\ell, K)) \int_0^\ell \frac{2arccos(\frac{\ell^2 + \ell'^2 + 2K\ell\ell'}{2\ell(k\ell+\ell')})}{360\ell} d\ell'$, $C(\ell, K)$ *and* $C(\ell, K+1)$ *is the area of the exclusion region* $\mathbb{ER}(L, K)$ *and* $\mathbb{ER}(L, K+1)$ *of a* ℓ*-long link* L *respectively.*

Proof. From the results in Section 5.4 of [59], the intensity λ_t of Φ_t is given by

$$\lambda_t = p_t \lambda$$

where p_t is the *Palm retaining probability* of a 'typical point' of Φ. p_t is given by

$$p_t = \int_0^1 r(t)dt = \frac{1 - exp(\lambda c)}{\lambda c} \tag{2.21}$$

where $r(t) = exp(-\lambda c t)$, with $c = C(\ell, K) + (C(\ell, K+1) - C(\ell, K)) \int_0^\ell \frac{2arccos(\frac{\ell^2 + \ell'^2 + 2K\ell\ell'}{2\ell(k\ell+\ell')})}{360\ell} \mathrm{d}\ell'$, is the retaining probability of a node T whose associated link $L(T)$ has a mark t (i.e., $m(L(T)) = t$).

The equation for $r(t)$ follows from the observation that the point process

$$\{X \in \Phi : m(X) < t\}$$

is simply a t-thinning of the Poisson process Φ, hence itself is a Poisson process of intensity λt. Therefore, $r(t)$ is the probability that an exclusion region $\mathbb{ER}(L, K+1)$ of a ℓ-long link contains no node who has an associated link with mark less than t, that is, containing no nodes of the t-thinned process.

In computing $r(t)$, the reason why c equals $C(\ell, K) + (C(\ell, K+1) - C(\ell, K)) \int_0^\ell \frac{2arccos(\frac{\ell^2 + \ell'^2 + 2K\ell\ell'}{2\ell(k\ell+\ell')})}{360\ell} \mathrm{d}\ell'$

instead of $C(\ell, K)$ is because $\cup_{Y \in \mathbb{ER}(L(X),K)} \mathbb{L}(Y)$ may well contain links whose transmitter is in $\mathbb{ER}(L, K+1)$ but not in $\mathbb{ER}(L, K)$.

For a transmitter $T' \in \mathbb{ER}(L, K+1) \setminus \mathbb{ER}(L, K)$ that is $K\ell + \ell'$ $(0 < \ell' \leq \ell)$ from the transmitter T of link L as shown in Figure 2.10, the probability that T' transmits to a

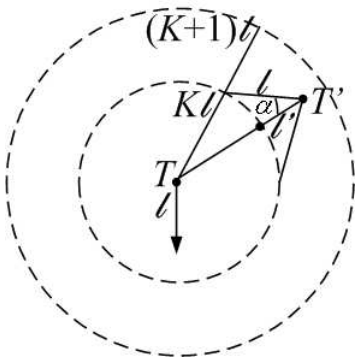

Figure 2.10: Probability that a transmitter $T' \in \mathbb{ER}(L, K+1) \setminus \mathbb{ER}(L, K)$

node in $\mathbb{ER}(L, K)$ is $\frac{2\alpha}{360}$ since the receiver of T' is at any direction around T' with equal probability. Since $(K\ell)^2 = \ell^2 + (K\ell + \ell')^2 - 2\ell(K\ell + \ell')cos\alpha$, $\alpha = arccos(\frac{\ell^2 + \ell'^2 + 2K\ell\ell'}{2\ell(K\ell + \ell')})$. Therefore, the probability that an arbitrary transmitter in $\mathbb{ER}(L, K+1) \setminus \mathbb{ER}(L, K)$ has its receiver in $\mathbb{ER}(L, K)$ is $\int_0^\ell \frac{2\alpha}{360} \frac{1}{\ell} \mathrm{d}\ell' \int_0^\ell \frac{2arccos(\frac{\ell^2 + \ell'^2 + 2K\ell\ell'}{2\ell(k\ell + \ell')})}{360\ell} \mathrm{d}\ell'$, and the expected number of nodes in $\mathbb{ER}(L, K+1) \setminus \mathbb{ER}(L, K)$ whose receivers are in $\mathbb{ER}(L, K)$ is $\lambda(C(\ell, K+1) - C(\ell, K)) \int_0^\ell \frac{2arccos(\frac{\ell^2 + \ell'^2 + 2K\ell\ell'}{2\ell(k\ell + \ell')})}{360\ell} \mathrm{d}\ell'$. Thus we have the formula for c. □

Then we can compute the total interference I at an arbitrary receiver R as follows:

Proposition 5. *With ratio-K-based scheduling, the expected total interference I at a receiver R in an infinite Poisson random network is as follows:*

$$I = \frac{2\pi\lambda_t P_t \beta}{(\alpha - 2)} (K\ell)^{2-\alpha} \tag{2.22}$$

where λ_t is given by Equation 2.20, P_t is the transmission power, β is the node transmission probability, α is the wireless path loss exponent, and ℓ is the link length. □

Proof. In [68], the authors derived as follows, for an arbitrary receiver, the total interference from nodes more than r distance away from the receiver when $\beta = 1$ and interferers are Poisson distributed with density λ:

$$m(\lambda) = \frac{2\pi\lambda P_t}{(\alpha - 2)} r^{2-\alpha} \tag{2.23}$$

Accordingly, for an arbitrary transmission probability β, the total interference is

$$m(\lambda, \beta) = \frac{2\pi\lambda P_t \beta}{(\alpha - 2)} r^{2-\alpha} \tag{2.24}$$

Based on the analysis earlier in this section, the set of concurrent transmitters in the tightest ratio-K-based scheduling are Poisson distributed with density λ_t as shown in Equation 2.20. The concurrent transmitters are also more than $K\ell$ distance away from the receiver. Therefore, we can see from Equation 2.24 that I can be computed as follows:

$$I = m(\lambda_t, \beta) = \frac{2\pi\lambda_t P_t \beta}{(\alpha - 2)} (K\ell)^{2-\alpha} \tag{2.25}$$

Q.E.D. □

2.3 Analysis of the interference in grid networks

we analyze, for the tightest tessellation of concurrent transmissions in grid networks, the receiver-side interference when different ratio-K models are used. The key to this analysis is to identify the spatial distribution of concurrent transmitters (i.e., interferers), based on which the interference introduced by each interferer can be derived from the distance between the interferer and the receiver. Accordingly, we use a coordinate system where the receiver R is located at the origin and its transmitter is located at location (0,1) (i.e., we treat the link length l from R to its transmitter as the unit of distance). So the distance between R and an interferer n_i at location (x, y) is $\sqrt{x^2 + y^2}$. Then, our main task is to identify the coordinates of all the interferers when different ratio-K models are used for the scheduling in grid networks. In

what follows, we analyze the coordinates of interferers in scheduling based on different ratio-K models.

When $K = \sqrt{2}$, Figure 2.11 shows the spatial distribution of concurrent transmissions. Given a link L, we can find four nodes, say A, B, C and D, on the boundary of the exclusion region of link L such that each is involved in a concurrent transmission (either as a sender or as a receiver).

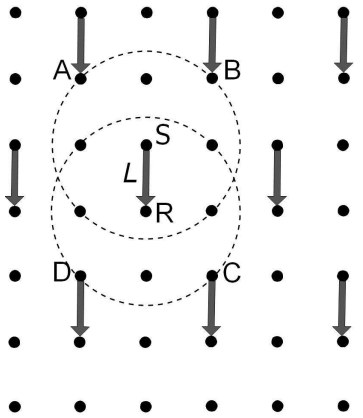

Figure 2.11: Concurrent transmissions when $K = \sqrt{2}$

By symmetry, we can expand this spatial distribution of concurrent transmissions to the rest of the network, and thus the coordinates of interferers are

$$\begin{cases} x = 2n + Q \\ y = 4m + 1 + 2Q \end{cases}$$

where $m, n \in \mathbb{Z}$, $Q \in \{0, 1\}$ and $m^2 + n^2 + Q \neq 0$. So the receiver-side interference when $K = \sqrt{2}$ is as follows:

$$I = P_t \times \beta \times \ell^{-\alpha} \times \left(\sum_{\substack{m=-\infty \\ m^2+n^2 \neq 0}}^{\infty} \sum_{n=-\infty}^{\infty} \frac{1}{[(2n)^2+(4m+1)^2]^{\alpha/2}} + \sum_{m=-\infty}^{\infty} \sum_{n=-\infty}^{\infty} \frac{1}{[(2n+1)^2+(4m+3)^2]^{\alpha/2}} \right)$$

For other Ks, we can derive interferers' coordinates in a similar fashion. For conciseness, we ignore the detailed derivation here and only give the results as follows.

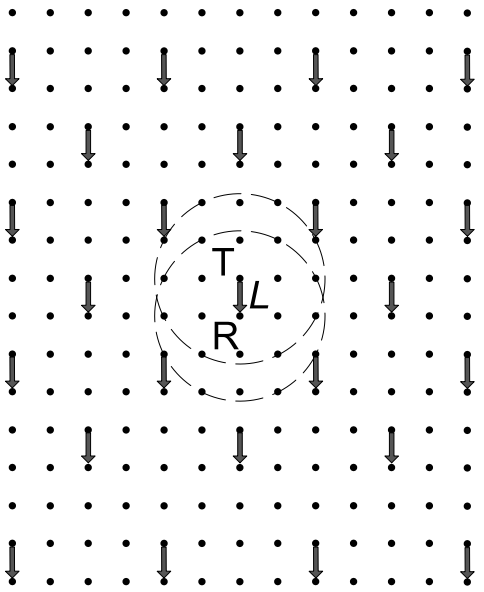

Figure 2.12: Concurrent transmissions when $K = \sqrt{5}$

When $K = \sqrt{5}$, the spatial distribution of concurrent transmission are shown in Figure 2.12 and the coordinates of interferers are

$$\begin{cases} x = 4n + 2Q \\ y = 4m + 1 + 2Q \end{cases}$$

where $m, n \in \mathbb{Z}$, $Q \in \{0, 1\}$ and $m^2 + n^2 + Q \neq 0$. So the receiver-side interference is

$$I = P_t \times \beta \times \ell^{-\alpha} \times \left(\sum_{\substack{m=-\infty \\ m^2+n^2 \neq 0}}^{\infty} \sum_{n=-\infty}^{\infty} \frac{1}{[(4n)^2+(4m+1)^2]^{\alpha/2}} + \sum_{m=-\infty}^{\infty} \sum_{n=-\infty}^{\infty} \frac{1}{[(4n+2)^2+(4m+3)^2]^{\alpha/2}} \right)$$

When $K = \sqrt{8}$, the spatial distribution of concurrent transmission are shown in Figure 2.13 and the coordinates of interferers are

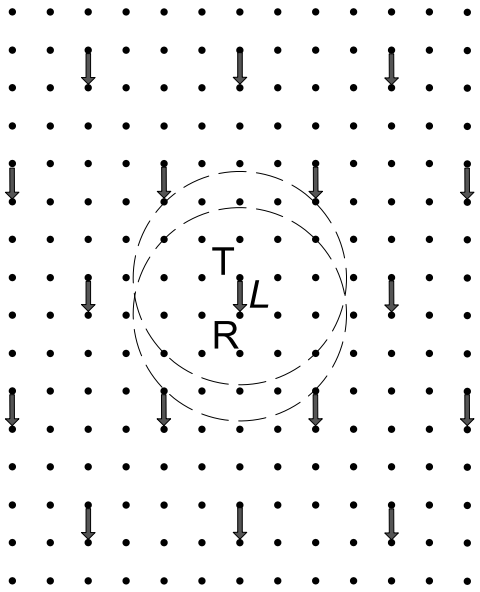

Figure 2.13: Concurrent transmissions when $K = \sqrt{8}$

$$\begin{cases} x = 4n + 2Q \\ y = 6m + 1 + 3Q \end{cases}$$

where $m, n \in \mathbb{Z}$, $Q \in \{0, 1\}$ and $m^2 + n^2 + Q \neq 0$. So the receiver-side interference is

$$I = P_t \times \beta \times \ell^{-\alpha} \times \left(\sum_{\substack{m=-\infty \\ m^2+n^2 \neq 0}}^{\infty} \sum_{n=-\infty}^{\infty} \frac{1}{[(4n)^2+(6m+1)^2]^{\alpha/2}} + \sum_{m=-\infty}^{\infty} \sum_{n=-\infty}^{\infty} \frac{1}{[(4n+2)^2+(6m+4)^2]^{\alpha/2}} \right)$$

When $K = 3$, the spatial distribution of concurrent transmission are shown in Figure 2.14 and the coordinates of interferers are

$$\begin{cases} x = 3n \\ y = 4m + 1 \end{cases}$$

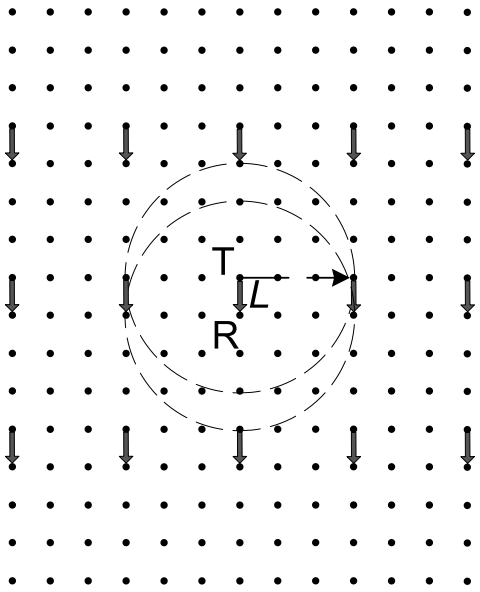

Figure 2.14: Concurrent transmissions when $K = 3$

where $m, n \in \mathbb{Z}$ and $m^2 + n^2 \neq 0$. So the receiver-side interference is

$$I = P_t \times \beta \times \ell^{-\alpha} \times \left(\sum_{\substack{m=-\infty \\ m^2+n^2 \neq 0}}^{\infty} \sum_{n=-\infty}^{\infty} \frac{1}{[(3n)^2+(4m+1)^2]^{\alpha/2}} \right)$$

When $K = \sqrt{10}$, the spatial distribution of concurrent transmission are shown in Figure 2.15 and interferers are divided into 7 groups, denoted as $G_1, G_2, \ldots, G_7$, and we let $I = \sum_{i=1}^{7} I_i$, where I_i is the interference from nodes of group G_i. The coordinates of nodes in G_1 are

$$\begin{cases} x = 7n \\ y = 14m + 1 \end{cases}$$

where $m, n \in \mathbb{Z}$ and $m^2 + n^2 \neq 0$. And I_1 is given by

$$I_1 = P_t \times \beta \times \ell^{-\alpha} \times \sum_{\substack{m=-\infty \\ m^2+n^2 \neq 0}}^{\infty} \sum_{n=-\infty}^{\infty} \frac{1}{[(7n)^2+(14m+1)^2]^{\alpha/2}}$$

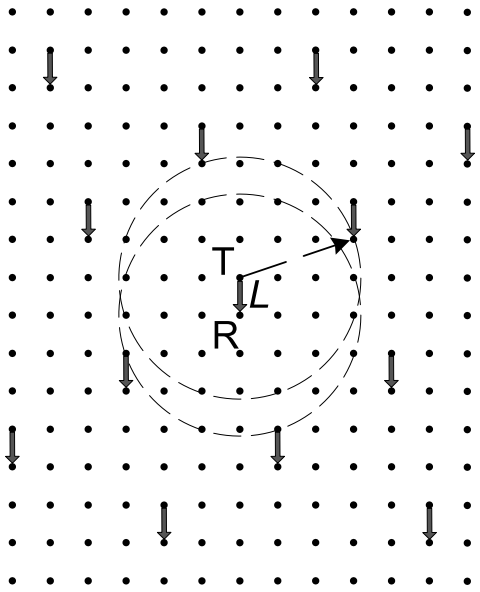

Figure 2.15: Concurrent transmissions when $K = \sqrt{10}$

The coordinates of nodes in G_2

$$\begin{cases} x = 7n + 4 \\ y = 14m - 1 \end{cases}$$

where $m, n \in \mathbb{Z}$ and $m^2 + n^2 \neq 0$. And I_2 is given by

$$I_2 = P_t \times \beta \times \ell^{-\alpha} \times \sum_{m=-\infty}^{\infty} \sum_{n=-\infty}^{\infty} \frac{1}{[(7n+4)^2+(14m-1)^2]^{\alpha/2}}$$

The coordinates of nodes in G_3

$$\begin{cases} x = 7n + 1 \\ y = 14m - 3 \end{cases}$$

where $m, n \in \mathbb{Z}$ and $m^2 + n^2 \neq 0$. And I_3 is given by

$$I_3 = P_t \times \beta \times \ell^{-\alpha} \times \sum_{m=-\infty}^{\infty} \sum_{n=-\infty}^{\infty} \frac{1}{[(7n+1)^2+(14m-3)^2]^{\alpha/2}}$$

The coordinates of nodes in G_4

$$\begin{cases} x = 7n + 5 \\ y = 14m - 5 \end{cases}$$

where $m, n \in \mathbb{Z}$ and $m^2 + n^2 \neq 0$. And I_4 is given by

$$I_4 = P_t \times \beta \times \ell^{-\alpha} \times \sum_{m=-\infty}^{\infty} \sum_{n=-\infty}^{\infty} \frac{1}{[(7n+5)^2+(14m-5)^2]^{\alpha/2}}$$

The coordinates of nodes in G_5

$$\begin{cases} x = 7n + 2 \\ y = 14m - 7 \end{cases}$$

where $m, n \in \mathbb{Z}$ and $m^2 + n^2 \neq 0$. And I_5 is given by

$$I_5 = P_t \times \beta \times \ell^{-\alpha} \times \sum_{m=-\infty}^{\infty} \sum_{n=-\infty}^{\infty} \frac{1}{[(7n+2)^2+(14m-7)^2]^{\alpha/2}}$$

The coordinates of nodes in G_6

$$\begin{cases} x = 7n + 6 \\ y = 14m - 9 \end{cases}$$

where $m, n \in \mathbb{Z}$ and $m^2 + n^2 \neq 0$. And I_6 is given by

$$I_6 = P_t \times \beta \times \ell^{-\alpha} \times \sum_{m=-\infty}^{\infty} \sum_{n=-\infty}^{\infty} \frac{1}{[(7n+6)^2+(14m-9)^2]^{\alpha/2}}$$

The coordinates of nodes in G_7

$$\begin{cases} x = 7n + 3 \\ y = 14m - 11 \end{cases}$$

where $m, n \in \mathbb{Z}$ and $m^2 + n^2 \neq 0$. And I_7 is given by

$$I_7 = P_t \times \beta \times \ell^{-\alpha} \times \sum_{m=-\infty}^{\infty} \sum_{n=-\infty}^{\infty} \frac{1}{[(7n+3)^2+(14m-11)^2]^{\alpha/2}}$$

When $K = \sqrt{13}$, the spatial distribution of concurrent transmission are shown in Figure 2.16 and the coordinates of interferers are

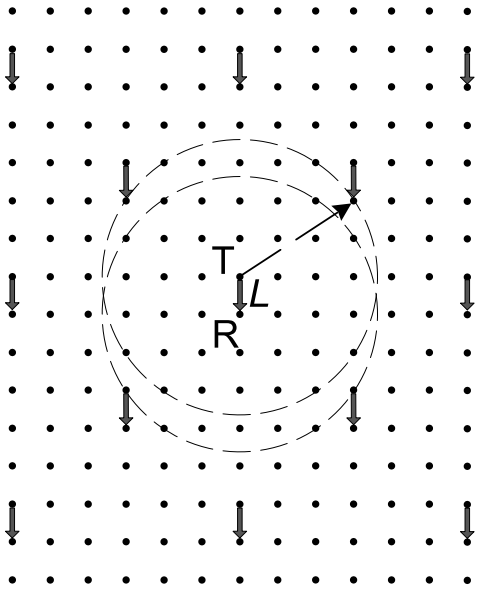

Figure 2.16: Concurrent transmissions when $K = \sqrt{13}$

$$\begin{cases} x = 4n + 2Q \\ y = 8m + 4Q + 1 \end{cases}$$

where $m, n \in \mathbb{Z}$, $Q \in \{0, 1\}$ and $m^2 + n^2 + Q \neq 0$. So the receiver-side interference is

$$I = P_t \times \beta \times \ell^{-\alpha} \times \left(\sum_{\substack{m=-\infty \\ m^2+n^2 \neq 0}}^{\infty} \sum_{n=\infty}^{\infty} \frac{1}{[(4n)^2+(8m+1)^2]^{\alpha/2}} + \sum_{m=-\infty}^{\infty} \sum_{n=-\infty}^{\infty} \frac{1}{[(4n+2)^2+(8m+5)^2]^{\alpha/2}} \right)$$

When $K = 4$, the spatial distribution of concurrent transmission are shown in Figure 2.17 and the coordinates of interferers are

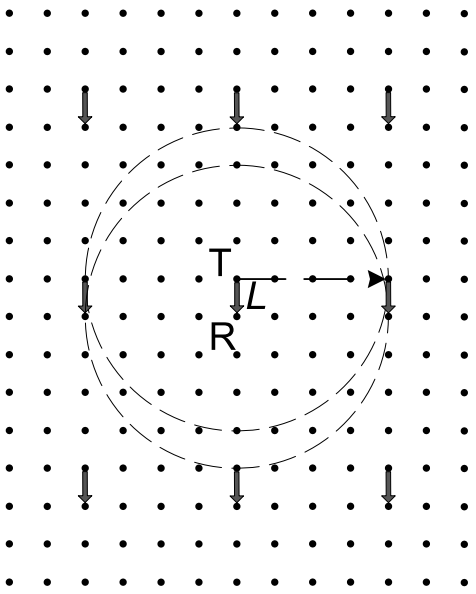

Figure 2.17: Concurrent transmissions when $K = 4$

$$\begin{cases} x = 6n \\ y = 5m + 1 \end{cases}$$

where $m, n \in \mathbb{Z}$ and $m^2 + n^2 \neq 0$. So the receiver-side interference is

$$I = P_t \times \beta \times \ell^{-\alpha} \times \left(\sum_{\substack{m=-\infty \\ m^2+n^2 \neq 0}}^{\infty} \sum_{n=-\infty}^{\infty} \frac{1}{[(6n)^2+(7m+1)^2]^{\alpha/2}} \right)$$

When $K = \sqrt{18}$, the spatial distribution of concurrent transmission are shown in Fig-

ure 2.18 and the coordinates of interferers are

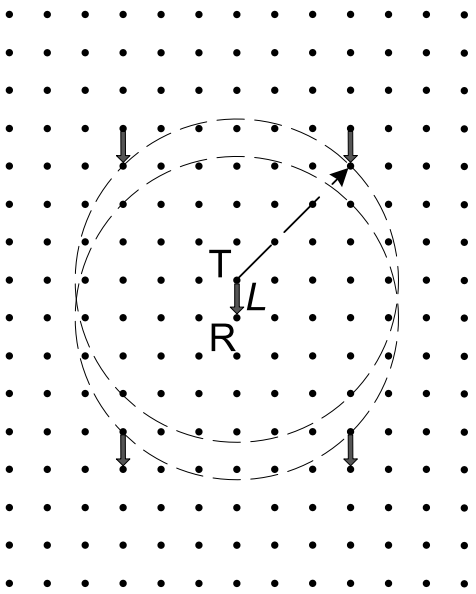

Figure 2.18: Concurrent transmissions when $K = \sqrt{18}$

$$\begin{cases} x = 6n + 3Q \\ y = 7m + 3Q + 1 \end{cases}$$

where $m, n \in \mathbb{Z}$, $Q \in \{0, 1\}$ and $m^2 + n^2 + Q \neq 0$. So the receiver-side interference is

$$I = P_t \times \beta \times \ell^{-\alpha} \times \left(\sum_{\substack{m=-\infty \\ m^2+n^2 \neq 0}}^{\infty} \sum_{n=-\infty}^{\infty} \frac{1}{[(6n)^2+(7m+1)^2]^{\alpha/2}} + \sum_{m=-\infty}^{\infty} \sum_{n=-\infty}^{\infty} \frac{1}{[(6n+3)^2+(7m+4)^2]^{\alpha/2}} \right)$$

When $K = \sqrt{20}$, the spatial distribution of concurrent transmission are shown in Figure 2.19 and the coordinates of interferers are

$$\begin{cases} x = 8n + 4Q \\ y = 6m + 3Q + 1 \end{cases}$$

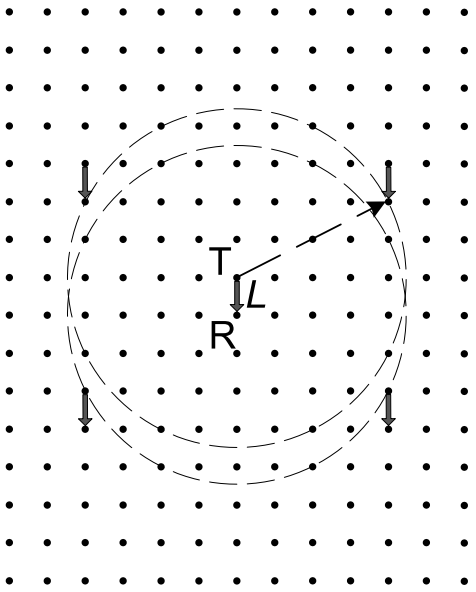

Figure 2.19: Concurrent transmissions when $K = \sqrt{20}$

where $m, n \in \mathbb{Z}$, $Q \in \{0, 1\}$ and $m^2 + n^2 + Q \neq 0$. So the receiver-side interference is

$$I = P_t \times \beta \times \ell^{-\alpha} \times \left(\sum_{\substack{m=-\infty \\ m^2+n^2 \neq 0}}^{\infty} \sum_{n=-\infty}^{\infty} \frac{1}{[(8n)^2+(6m+1)^2]^{\alpha/2}} + \sum_{m=-\infty}^{\infty} \sum_{n=-\infty}^{\infty} \frac{1}{[(8n+4)^2+(6m+4)^2]^{\alpha/2}} \right)$$

When $K = 5$, the spatial distribution of concurrent transmission are shown in Figure 2.20 and the coordinates of interferers are

$$\begin{cases} x = 5n \\ y = 6m + 1 \end{cases}$$

where $m, n \in \mathbb{Z}$ and $m^2 + n^2 \neq 0$. So the receiver-side interference is

$$I = P_t \times \beta \times \ell^{-\alpha} \times \left(\sum_{\substack{m=-\infty \\ m^2+n^2 \neq 0}}^{\infty} \sum_{n=-\infty}^{\infty} \frac{1}{[(5n)^2+(6m+1)^2]^{\alpha/2}} \right)$$

When $K = \sqrt{26}$, the spatial distribution of concurrent transmission are shown in Fig-

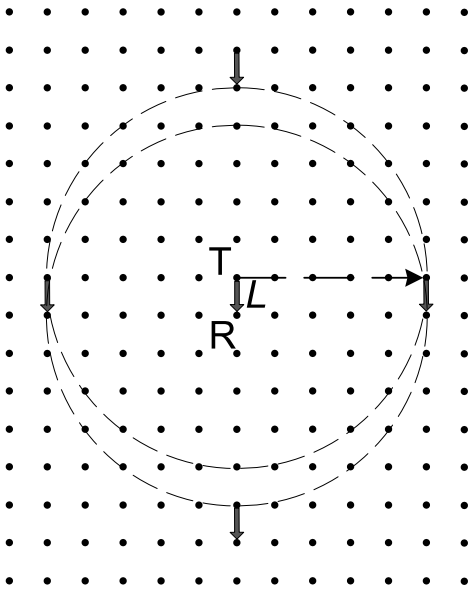

Figure 2.20: Concurrent transmissions when $K = 5$

ure 2.21 and the coordinates of interferers are

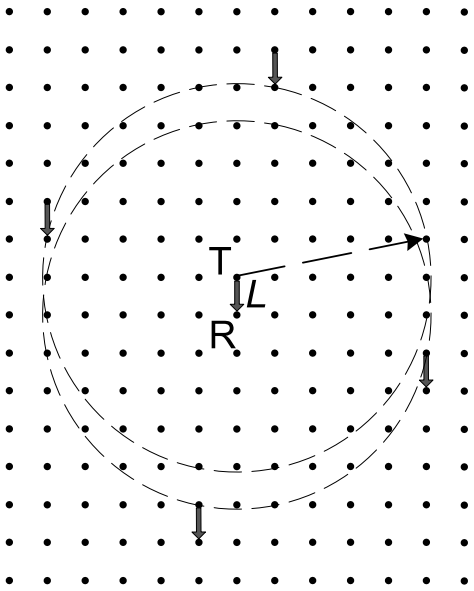

Figure 2.21: Concurrent transmissions when $K = \sqrt{26}$

$$\begin{cases} x = 5n + m \\ y = -2n + 6m + 1 \end{cases}$$

where $m, n \in \mathbb{Z}$ and $m^2 + n^2 \neq 0$. So the receiver-side interference is

$$I = P_t \times \beta \times \ell^{-\alpha} \times \left(\sum_{\substack{m=-\infty \\ m^2+n^2 \neq 0}}^{\infty} \sum_{n=-\infty}^{\infty} \frac{1}{[(5n+m)^2 + (-2n+6m+1)^2]^{\alpha/2}} \right)$$

When $K = \sqrt{29}$, the spatial distribution of concurrent transmission are shown in Figure 2.22 and the coordinates of interferers are

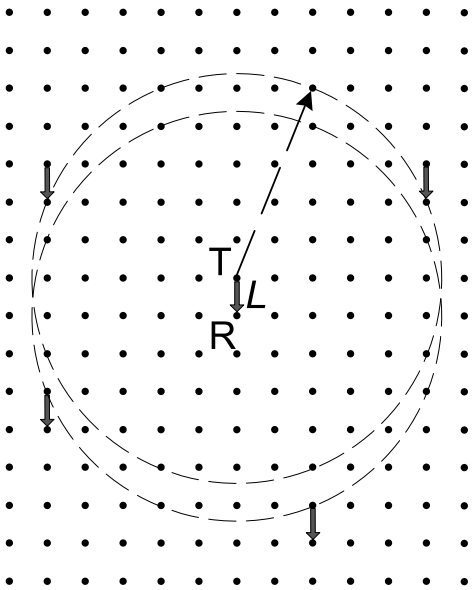

Figure 2.22: Concurrent transmissions when $K = \sqrt{29}$

$$\begin{cases} x = 5n + 2m \\ y = 3n - 6m + 1 \end{cases}$$

where $m, n \in \mathbb{Z}$ and $m^2 + n^2 \neq 0$. So the receiver-side interference is

$$I = P_t \times \beta \times \ell^{-\alpha} \times \left(\sum_{\substack{m=-\infty \\ m^2+n^2 \neq 0}}^{\infty} \sum_{n=-\infty}^{\infty} \frac{1}{[(5n+2m)^2 + (3n-6m+1)^2]^{\alpha/2}} \right)$$

When $K = \sqrt{32}$, the spatial distribution of concurrent transmission are shown in Figure 2.23 and the coordinates of interferers are

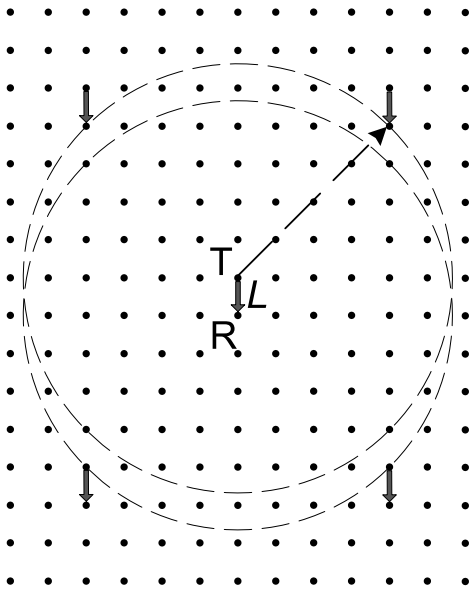

Figure 2.23: Concurrent transmissions when $K = \sqrt{32}$

$$\begin{cases} x = 8n + 4Q \\ y = 10m + 5Q + 1 \end{cases}$$

where $m, n \in \mathbb{Z}$, $Q \in \{0, 1\}$ and $m^2 + n^2 + Q \neq 0$. So the receiver-side interference is

$$I = P_t \times \beta \times \ell^{-\alpha} \times \left(\sum_{\substack{m=-\infty \\ m^2+n^2 \neq 0}}^{\infty} \sum_{n=-\infty}^{\infty} \frac{1}{[(8n)^2+(10m+1)^2]^{\alpha/2}} + \sum_{m=-\infty}^{\infty} \sum_{n=-\infty}^{\infty} \frac{1}{[(8n+4)^2+(10m+6)^2]^{\alpha/2}} \right)$$

When $K = \sqrt{34}$, the spatial distribution of concurrent transmission are shown in Figure 2.24 and the coordinates of interferers are

$$\begin{cases} x = 6n + 3Q \\ y = 12m + 5Q + 1 \end{cases}$$

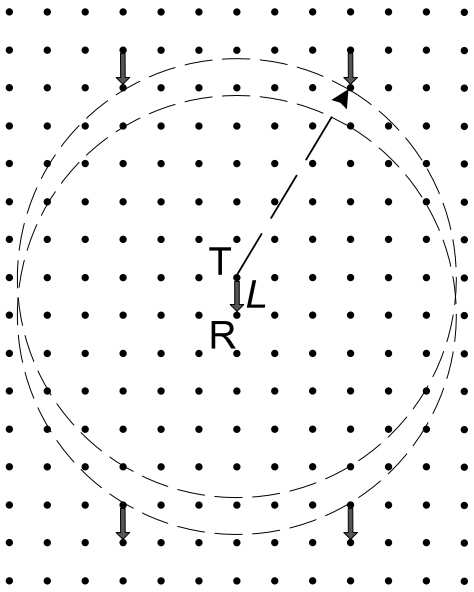

Figure 2.24: Concurrent transmissions when $K = \sqrt{34}$

where $m, n \in \mathbb{Z}$, $Q \in \{0, 1\}$ and $m^2 + n^2 + Q \neq 0$. So the receiver-side interference is

$$I = P_t \times \beta \times \ell^{-\alpha} \times \left(\sum_{\substack{m=-\infty \\ m^2+n^2 \neq 0}}^{\infty} \sum_{n=-\infty}^{\infty} \frac{1}{[(6n)^2+(12m+1)^2]^{\alpha/2}} + \sum_{m=-\infty}^{\infty} \sum_{n=-\infty}^{\infty} \frac{1}{[(6n+3)^2+(12m+6)^2]^{\alpha/2}} \right)$$

When $K = 6$, the spatial distribution of concurrent transmission are shown in Figure 2.25 and the coordinates of interferers are

$$\begin{cases} x = 6n \\ y = 7m + 1 \end{cases}$$

where $m, n \in \mathbb{Z}$ and $m^2 + n^2 \neq 0$. So the receiver-side interference is

$$I = P_t \times \beta \times \ell^{-\alpha} \times \left(\sum_{\substack{m=-\infty \\ m^2+n^2 \neq 0}}^{\infty} \sum_{n=-\infty}^{\infty} \frac{1}{[(6n)^2+(7m+1)^2]^{\alpha/2}} \right)$$

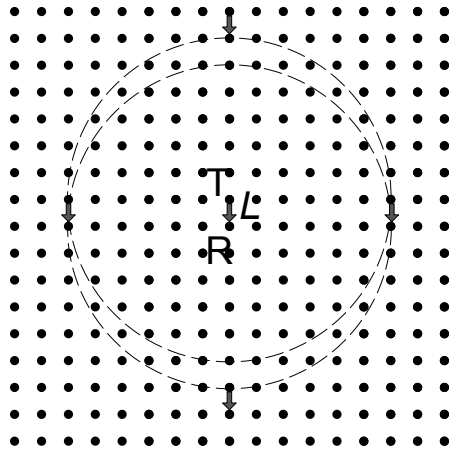

Figure 2.25: Concurrent transmissions when $K = 6$

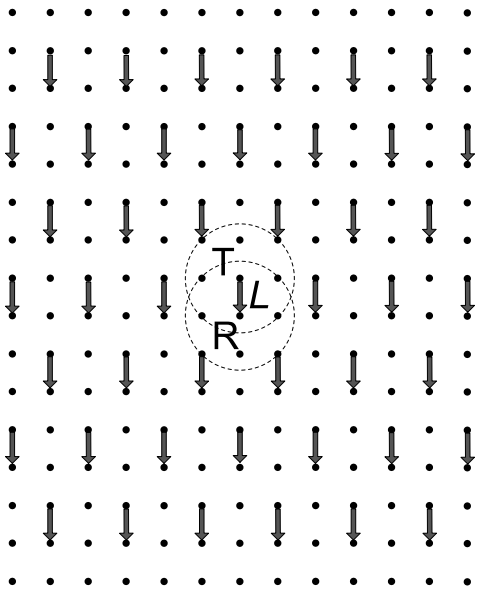

Figure 2.26: $K = \sqrt{2}$

2.4 Optimality of PRK-based scheduling

While detailed study of distributed protocol design using the PRK model is a part of our future work, we analyze in this section the optimality of PRK-based scheduling as compared with SINR-based scheduling to gain insight into the potential effectiveness of PRK-based scheduling.[4] For ensuring data delivery reliability in wireless networked sensing and control, we conduct our comparative analysis on the condition that the link reliability in PRK- and SINR-based scheduling be the same.

2.4.1 Throughput loss in PRK-based scheduling

Similar to Section 2.2, our analysis here considers infinite sized grid and Poisson random networks with uniform traffic patterns. We will verify the analytical insight in Sections 2.7 and 3.6 through testbed-based measurement and simulation where finite networks and non-uniform traffic patterns are considered.

To satisfy a certain link reliability requirement and thus a certain packet-delivery-rate (PDR) for data and acknowledgment (ACK) reception along a link L, we need to make sure that the SINR at the receiver R and the transmitter T is above a certain threshold γ_0 and γ_0' respectively. For a given received signal strength P_r and background noise N_0 at R, this requirement translates into a requirement on controlling the maximum interference I_t at R to be $\frac{P_r}{\gamma_0} - N_0$. Similarly, we can derive the maximum tolerable interference I_t' at T.[5] To control interference, we need to silence the transmission of some nodes in the network, and, to maximize channel spatial reuse (i.e., maximizing the number of concurrent transmitters), we need to minimize the number of silenced transmitters. To this end, we have

Proposition 6. *To minimize the number of nodes silenced for ensuring certain minimum SINR*

[4] Here we do not perform detailed comparative study between PRK- and ratio-K-based scheduling because it is obvious from Section 2.2 that, by adapting to network and environmental conditions as well as application requirements, PRK-based scheduling will perform better than ratio-K-based scheduling.

[5] I_t' may or may not equal to I_t depending on the ACK mechanism and the wireless radios. Accordingly, the exclusion regions around the sender and the receiver of a transmission may or may not be the same in PRK-based scheduling.

at the receiver R (or the transmitter T) in both PRK- and SINR-based scheduling, nodes s-closer to R (or T) rather than those s-farther away should be silenced first. □

Proof. The PRK model silences the nodes within an exclusion region around the receiver (or the transmitter), so the proposition holds for the PRK model. For the SINR model, we prove the proposition by contradiction. Suppose the receiver R has two potential interferers A and B nearby. The s-distances from A and B to receiver R are d_A and d_B respectively, with $d_A < d_B$. If not silenced, the interference that node A generates is greater than that generated by B. To ensure that the total interference incurred to R does not exceed the threshold I_t, therefore, the number of nodes that have to be silenced when B but not A is silenced is no less than the number of nodes that have to be silenced when A but not B is silenced. Thus, silencing B instead of A does not ensure the minimization of the number of silenced nodes, which contradicts the objective of minimizing the number of silenced nodes. The same argument applies to the transmitter T. Thus the proposition holds for the SINR-based scheduling. □

Therefore, the set $\mathcal{S}$ of nodes silenced by the data reception at receiver R are the $|\mathcal{S}|$ number of nodes s-closest to R, where $|\mathcal{S}|$ denotes the cardinality of set $\mathcal{S}$. We denote the set of nodes silenced by R in SINR- and PRK-based scheduling as $\mathcal{S}_{sinr}$ and $\mathcal{S}_{prk}$ respectively. For a tolerable interference I_t at R, we let I_{sinr} and I_{prk} be the actual interference incurred at R in SINR- and PRK-based scheduling respectively. Similarly, for correct ACK reception at the transmitter T in SINR- and PRK-based scheduling, we denote the set of silenced nodes as $\mathcal{S}'_{sinr}$ and $\mathcal{S}'_{prk}$ respectively, and, for a tolerable interference I'_t at T, we let I'_{sinr} and I'_{prk} be the actual interference incurred at T respectively. We also define $\mathbb{S}_{sinr} = \mathcal{S}_{sinr} \cup \mathcal{S}'_{sinr}$ and $\mathbb{S}_{prk} = \mathcal{S}_{prk} \cup \mathcal{S}'_{prk}$ to represent the set of silenced nodes around link L in SINR- and PRK-based scheduling respectively. Then,

Proposition 7. *Given the tolerable interference I_t and I'_t at the receiver R and the transmitter T respectively, $\mathbb{S}_{sinr} \subseteq \mathbb{S}_{prk}$, $I_{prk} \leq I_{sinr} \leq I_t$, and $I'_{prk} \leq I'_{sinr} \leq I'_t$.* □

Proof. Let the longest s-distance from a node in $\mathcal{S}_{sinr}$ to R be d_{sinr}. By the definition of the PRK and the SINR models and Proposition 6, all the nodes in $\mathcal{S}_{sinr}$ and $\mathcal{S}_{prk}$ are within d_{sinr} s-distance away from the receiver R. The difference between the PRK model and the SINR model is that, by the definition of the PRK model (see Inequality 2.29), all the nodes that are d_{sinr} s-distance away from R have to be silenced in the PRK model as long as at least one of them has to be silenced; whereas in the SINR model, we only need to silence the minimum number of nodes d_{sinr} s-distance away from R to ensure that the SINR at R is at least γ_0. For example, in Figure 2.27, there are four nodes d_{sinr} s-distance away from R. While the SINR

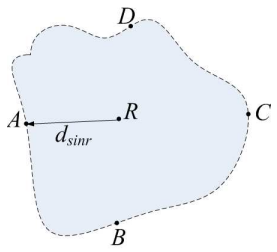

Figure 2.27: Difference in PRK- and SINR-based scheduling: receiver oriented view

model may only need to silence node A to guarantee the SINR threshold I_t, the PRK model will silence all the four nodes d_{sinr} away. Therefore, $\mathcal{S}_{sinr} \subseteq \mathcal{S}_{prk}$. Since $\mathcal{S}_{sinr} \subseteq \mathcal{S}_{prk}$, $I_{prk} \leq I_{sinr}$. SINR-based scheduling will ensure that $I_{sinr} \leq I_t$. Thus, $I_{prk} \leq I_{sinr} \leq I_t$ holds.

Similar argument applies to the transmitter T. Thus, $\mathcal{S}'_{sinr} \subseteq \mathcal{S}'_{prk}$, and $I'_{prk} \leq I'_{sinr} \leq I'_t$. Since $\mathcal{S}_{sinr} \subseteq \mathcal{S}_{prk}$ and $\mathcal{S}'_{sinr} \subseteq \mathcal{S}'_{prk}$, $\mathbb{S}_{sinr} \subseteq \mathbb{S}_{prk}$. □

Now, we are ready to derive the upper bound on the throughput loss in PRK-based scheduling as compared with SINR-based scheduling. By Formulas 2.6 and 2.7, the throughput of PRK- and SINR-based scheduling, denoted by T_{prk} and T_{sinr} respectively, can be computed as follows:

$$T_{prk} = \frac{T_{R,prk}}{|\mathbb{S}_{prk}|} \quad T_{sinr} = \frac{T_{R,sinr}}{|\mathbb{S}_{sinr}|}$$

where $T_{R,prk}$ and $T_{R,sinr}$ are the link throughput to R in PRK- and SINR-based schedul-

ing respectively. From Proposition 7, we know that the average link reliability in SINR-based scheduling is no higher than that in PRK-based scheduling (since the actual interference incurred in SINR-based scheduling is no less than that in PRK-based scheduling). Thus, $T_{R,sinr} \leq T_{R,prk}$. Then, we can define the throughput loss T_{loss} in PRK-based scheduling as

$$\begin{aligned} T_{loss} &= \frac{T_{sinr}-T_{prk}}{T_{sinr}} = \frac{\frac{T_{R,sinr}}{|\mathbb{S}_{sinr}|}-\frac{T_{R,prk}}{|\mathbb{S}_{prk}|}}{\frac{T_{R,sinr}}{|\mathbb{S}_{sinr}|}} \\ &\leq \frac{\frac{T_{R,sinr}}{|\mathbb{S}_{sinr}|}-\frac{T_{R,sinr}}{|\mathbb{S}_{prk}|}}{\frac{T_{R,sinr}}{|\mathbb{S}_{sinr}|}} = \frac{|\mathbb{S}_{prk}|-|\mathbb{S}_{sinr}|}{|\mathbb{S}_{prk}|} \end{aligned} \tag{2.26}$$

Let n_b be the node in $\mathcal{S}_{sinr}$ that is s-farthest away from the receiver R, P_0 be the power of signals that reach R from n_b, and N_b be the number of nodes in the network whose s-distance to R is $sd(n_b, R)$. Similarly, let n'_b be the node in $\mathcal{S}'_{sinr}$ that is s-farthest away from the transmitter T, P'_0 be the power of signals that reach T from n'_b, and N'_b be the number of nodes whose s-distance to T is $sd(n'_b, T)$. Then,

Proposition 8. *The expected T_{loss} is less than or equal to* $\frac{1}{|\mathbb{S}_{prk}|}(\min\{\frac{I_t-I_{prk}}{P_0\times\beta}, N_b\}+\min\{\frac{I'_t-I'_{prk}}{P'_0\times\beta}, N'_b\})$.
□

Proof. Let $dist(n_b, R)$ be the s-distance from n_b to R, and $dist(n'_b, T)$ be the s-distance from n'_b to T. Then from the proof of Proposition 7, we know that the s-distance d from every node in $\mathcal{S}_{prk} \setminus \mathcal{S}_{sinr}$ to R is $dist(n_b, R)$ since the PRK model silences all the nodes on the boundary of the exclusion region around R. Similarly, the s-distance d' from every node in $\mathcal{S}'_{prk} \setminus \mathcal{S}'_{sinr}$ to T is $dist(n'_b, T)$.

Given the interference tolerance I_t and I'_t at R and T respectively, the set of silenced nodes $\mathbb{S}_{prk}$ is fixed for a tightest tessellation of concurrent transmitters in a specific network and environmental setting. To understand the upper bound on T_{loss}, we need to understand the upper bound on $(|\mathbb{S}_{prk}| - |\mathbb{S}_{sinr}|)$ (*see* Inequality 2.26). By the definition of $\mathbb{S}_{prk}$ and $\mathbb{S}_{sinr}$, we know that $|\mathbb{S}_{prk}| - |\mathbb{S}_{sinr}| \leq (|\mathcal{S}_{prk}| - |\mathcal{S}_{sinr}|) + (|\mathcal{S}'_{prk}| - |\mathcal{S}'_{sinr}|)$. To upper bound $(|\mathbb{S}_{prk}| - |\mathbb{S}_{sinr}|)$, we analyze in what follows the upper bound on $(|\mathcal{S}_{prk}| - |\mathcal{S}_{sinr}|)$ and $(|\mathcal{S}'_{prk}| - |\mathcal{S}'_{sinr}|)$.

We first derive the upper bound on $(|\mathcal{S}_{prk}| - |\mathcal{S}_{sinr}|)$. Since all the nodes in $\mathcal{S}_{prk} \setminus \mathcal{S}_{sinr}$ are on the boundary of the exclusion region around R and are $dist(n_b, R)$ s-distance away from R, each such node introduces an expected interference of $P_0 \times \beta$ at receiver R. To ensure that the expected interference at R is no more than I_t (a.k.a., the SINR at R is above γ_0), one necessary condition is that the expected interference introduced by nodes in $\mathcal{S}_{prk} \setminus \mathcal{S}_{sinr}$ should be no more than $I_t - I_{prk}$, that is, the number of nodes in $\mathcal{S}_{prk} \setminus \mathcal{S}_{sinr}$ should be no more than $\frac{I_t - I_{prk}}{P_0 \times \beta}$. Note that this upper bound is usually not tight and not a sufficient condition because the interference at R tends to exceed I_t if the interferences from nodes in $\mathcal{S}_{prk} \setminus \mathcal{S}_{sinr}$ reaches $I_t - I_{prk}$. This is because, if we add, for every area of the same size of the exclusion region around R, $\frac{I_t - I_{prk}}{P_0 \times \beta}$ more transmitters on average in SINR-based scheduling than in PRK-based scheduling, the interference at R will exceed $I_t - I_{prk}$ when the area covered by the network is larger than the exclusion region around R (which is usually the case). Therefore, an upper bound on the number of nodes in $\mathcal{S}_{prk} \setminus \mathcal{S}_{sinr}$ is $\frac{I_t - I_{prk}}{P_0 \times \beta}$. In addition, the number of nodes on the boundary of the exclusion region around R is no more than N_b, thus $(|\mathcal{S}_{prk}| - |\mathcal{S}_{sinr}|) \leq \min\{\frac{I_t - I_{prk}}{P_0 \times \beta}, N_b\}$.

Similarly, we can derive that $(|\mathcal{S}'_{prk}| - |\mathcal{S}'_{sinr}|) \leq \min\{\frac{I'_t - I'_{prk}}{P'_0 \times \beta}, N'_b\}$. Putting the above analysis together, the expected T_{loss} is no more than $\frac{1}{|\mathbb{S}_{prk}|}(\frac{I_t - I_{prk}}{P_0 \times \beta} + \frac{I'_t - I'_{prk}}{P'_0 \times \beta})$. □

Proposition 8 enables us to compute the upper bound, denoted by T_{lb}, on the throughput loss in PRK-based scheduling. For convenience, we let $\Delta X = \min\{\frac{I_t - I_{prk}}{P_0 \times \beta}, N_b\} + \min\{\frac{I'_t - I'_{prk}}{P'_0 \times \beta}, N'_b\}$, and thus $T_{lb} = \frac{\Delta X}{|\mathbb{S}_{prk}|}$. Note that ΔX represents an upper bound on $|\mathbb{S}_{prk} \setminus \mathbb{S}_{sinr}|$, that is, the average number of nodes per exclusion region that are silenced in PRK-based scheduling but not in SINR-based scheduling. In the next subsection, we numerically analyze the properties of ΔX and T_{lb}.

2.5 Numerical analysis

Using Formulas 2.6 and 2.7, the CC2420 radio model described in Section 3.2, and the formulas for computing interference (e.g., Formulas 2.17 and 2.22), we numerically analyze

the impact of parameter K on the network throughput and link reliability in ratio-K-based scheduling, and we analyze the impact that different network and environmental settings have on the effective choice of parameter K.

2.5.1 Methodology

To examine the impact of wireless attenuation in different environments, we consider the set $\{2.1, 2.6, 3, 3.3, 3.6, 3.8, 4, 4.5, 5\}$ of wireless path loss exponents αs, which represent a wide range of real-world environments [57]; we also set the shadowing variance σ^2 based on measurement data from [57]. For the grid networks and Poisson random networks, we vary their parameters such as traffic load, link length, and node distribution density to examine the impact of network properties. Traffic load is controlled by the transmission probability β, and we consider the set $\{0.05, 0.1, 0.15, \ldots, 1\}$ of βs. Link length is chosen so that the link reliability varies from 1% to 100% in the absence of interference. More specifically, for each specific path loss exponent α, we choose a link length ℓ_0 corresponding to an interference-free packet delivery rate (PDR) of 1%, and another link length ℓ_1 corresponding to a signal-to-noise-ratio (SNR) of 5dB more than the minimum SNR for ensuring 100% interference-free PDR; then we take 60 sample link lengths that are uniformly distributed between ℓ_0 and ℓ_1. (Note that the transmission power level is set at -25dBm in our study.) For each average link length ℓ in random networks, we select a set of node distribution densities λs so that the average number of nodes in a circular area of radius ℓ is 5, 10, 15, 20, 30, and 40 respectively.

For convenience, we regard each setting of network and environment parameters as a *system configuration* hereafter. Thus our study examines 75,600 different system configurations, and the boxplots, medians, and distributions to be presented in the rest of the paper are mostly based on the distribution of the corresponding metrics across different system configurations. For each system configuration, we analyze the network performance when the ratio-K model is instantiated with different Ks. The set of Ks we consider are $\{\sqrt{2}, 2, \sqrt{5}, \sqrt{8}, 3, \sqrt{10},$

$\sqrt{13}$, 4, $\sqrt{18}$, $\sqrt{20}$, 5, $\sqrt{26}$, $\sqrt{29}$, $\sqrt{34}$, 6}[6] for grid networks, and $\{1, 1.5, 2, 2.5, \ldots, 10\}$ for Poisson random networks. Using the numerical results on network throughput and link reliability in these 75,600 system configurations, we analyze 1) the impact of different factors on the best ratio-K model instantiation, 2) the sensitivity of model instantiation, and 3) the tradeoff between reliability and throughput in instantiating the ratio-K model.

2.5.2 Impact of different factors on best K

In this section, we analyze how different network and environment properties affect the optimal K that maximizes network throughput and the minimum K for ensuring certain link packet delivery rate (PDR). For random networks, we find that node distribution density λ does not affect the choice of K (even though it has some impact on interfering signal strength and SINR); thus, for the sake of space, here we only present the data for cases where λ is such that the average number of nodes in a circular area of radius ℓ is 15.

Throughput maximization: grid networks. For each system configuration we study, we compute the optimal K that maximizes network throughput. For different path loss exponents α's, Figure 2.28 shows the boxplot (and thus the distribution) of the optimal Ks across different

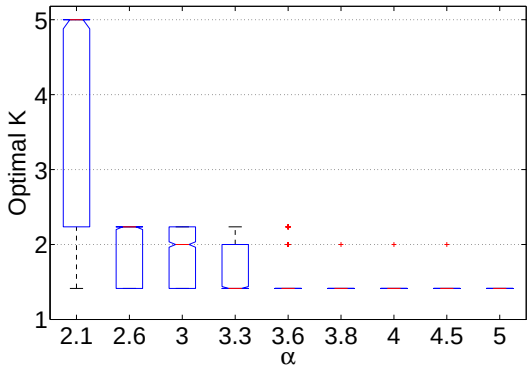

Figure 2.28: Optimal K for different α's: grid network

[6]These Ks are chosen in a *continuous* manner in the sense that, given a receiver, the inner area enclosed by the boundaries of the exclusion regions associated with every two closest Ks does not contain any node.We find that, for ratio-K-based scheduling in grid networks, increasing K after K is already greater than 5 can only increase link reliability but not network throughput. Thus 6 is large enough to serve as the largest K in our study.

system configurations. We see that, in general, the optimal K decreases as α increases. This is because larger α makes interfering signals weaker and thus a transmission can tolerate interference from more concurrent transmitters, which reduces the required K. We also note that $\sqrt{2}$ is the optimal K with high probability when $\alpha \geq 3.3$. Due to the limitation of space, here we only discuss in detail the cases of α being 3.3 and 4.5. Note that 3.3 and 4.5 are typical path loss exponents for indoor and outdoor environments respectively [57].

Figure 2.29 shows the distribution of the optimal K when $\alpha = 3.3$. There are 3 distinct

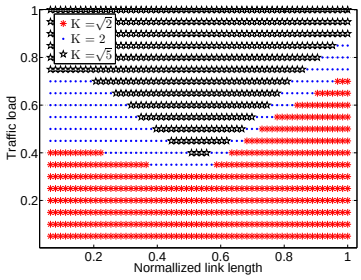

Figure 2.29: Distribution of optimal K when α = 3.3: grid network.

optimal Ks in this case, that is, $\sqrt{2}$, 2, and $\sqrt{5}$. We see that the optimal K tends to increase as traffic load increases. When traffic load is less than 0.35, link length does not affect the optimal K which is $\sqrt{2}$ all the time. When traffic load is greater than 0.4, the pattern is more complex, and both traffic load and link length affect the optimal K. The largest optimal K is $\sqrt{5}$ which occurs when the normalized link length is around 0.6 and the traffic load is high (e.g., ≥ 0.4). The distribution of $K = \sqrt{5}$ has a U-shape. When links are long, the reason why the optimal K can be small (i.e., $\sqrt{2}$) even for high traffic load is because concurrent transmitters are well separated in space due to long link length.

Figure 2.30 shows the distribution of the optimal K when $\alpha = 4.5$. The general patterns are similar to those for $\alpha = 3.3$, but there are only two distinct optimal Ks in this case, i.e., $\sqrt{2}$ and 2. Comparing with the case of α being 3.3, we see that traffic load has less and less impact on the optimal K as α increases. This is because, as α increases, signal power decreases

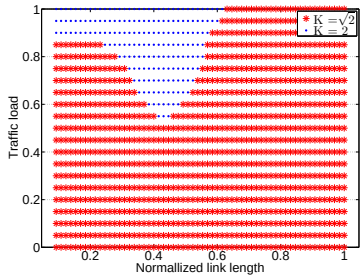

Figure 2.30: Distribution of optimal K when α = 4.5: grid network

significantly, and thus interfering traffic has less and less impact on receiver-side SINR and throughput.

Throughput maximization: random networks. For different path loss exponent α's in random networks, Figure 2.31 shows the boxplot of the optimal Ks across different system

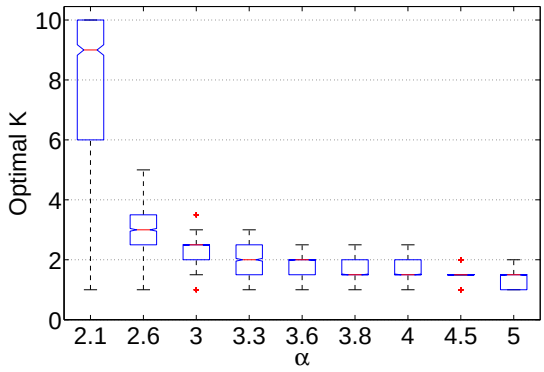

Figure 2.31: Optimal K for different α's: random network

configurations, and Figures 2.32 and 2.33 show the distribution of the optimal Ks for $\alpha = 3.3$ and $\alpha = 4.5$ respectively. We see that, in random networks, the optimal K has a similar distribution pattern as in grid networks. But the optimal Ks in random networks tend to be greater than those in grid networks. This is because, in random networks, the spatial orientations of data transmissions are random (which increases average interference to nodes) instead of in the same direction, and the density of concurrent transmitters tends to be greater than that in grid

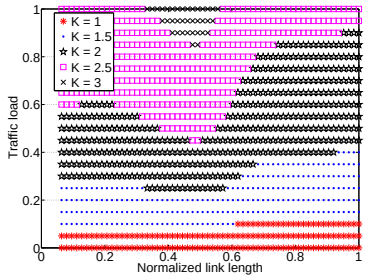

Figure 2.32: Distribution of optimal K when $\alpha = 3.3$: random network

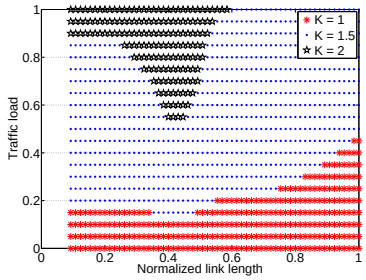

Figure 2.33: Distribution of optimal K when $\alpha = 4.5$: random network

networks.

PDR assurance: grid networks. For each system configuration we study, we compute the minimum K for ensuring certain link packet delivery rate (PDR). For different PDR requirements, Figure 2.34 shows the boxplot of the minimum Ks across different system configurations. We see that, in general, the required minimum K increases as PDR requirement increases, and $\sqrt{2}$ and 2 are two Ks that are used with high probability. For a PDR requirement of 80%, Figure 2.35 shows the distribution of the minimum required K for $\alpha = 3.3$ and $\alpha = 4.5$. We see that the minimum required K tends to increase as traffic load increases, link length increases, and wireless signal attenuation decreases. We also see that the minimum required K changes in a manner different from that for the optimal K of maximizing throughput: when link length increases, the minimum required K for PDR assurance increases monotonically, whereas the optimal K for throughput maximization may decrease or may in-

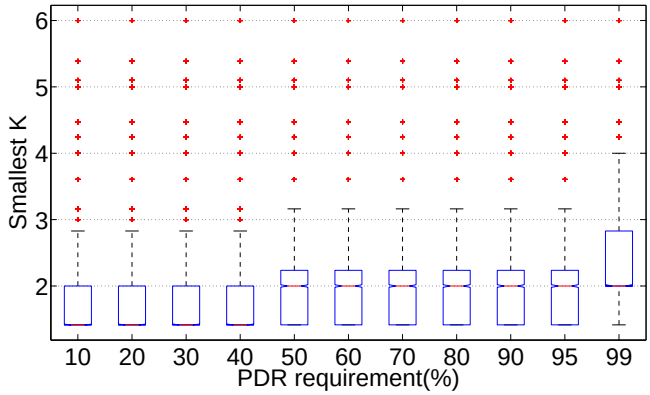

Figure 2.34: Minimum K for ensuring link PDR: grid network

crease depending on network properties as shown in Figures 2.29 and 2.32. This implies that different Ks will be chosen depending on objectives, and we will examine this issue in detail in Section 2.5.4.

PDR assurance: random networks. For random networks, Figure 2.36 shows the minimum Ks for different PDR requirements, and Figure 2.37 shows the distribution of the minimum required K for $\alpha = 3.3$ and $\alpha = 4.5$. We see that the patterns here are similar to those for grid networks. One subtle difference is that the minimum required Ks in random networks tend to be greater than those in grid networks, because, in random networks, the spatial orientations of data transmissions are random (which increases average interference to nodes), and the density of concurrent transmitters tends to be greater than that in grid networks.

2.5.3 Sensitivity of ratio-K-based scheduling

In Section 2.5.2, we see that both the optimal K for maximizing network throughput and the minimum K for satisfying certain link reliability requirement depend on network and environmental characteristics such as traffic load and wireless signal attenuation. To understand the impact of choosing a constant K for the ratio-K model, we analyze in this section the sensitivity of network throughput and link reliability to changing network and environmental

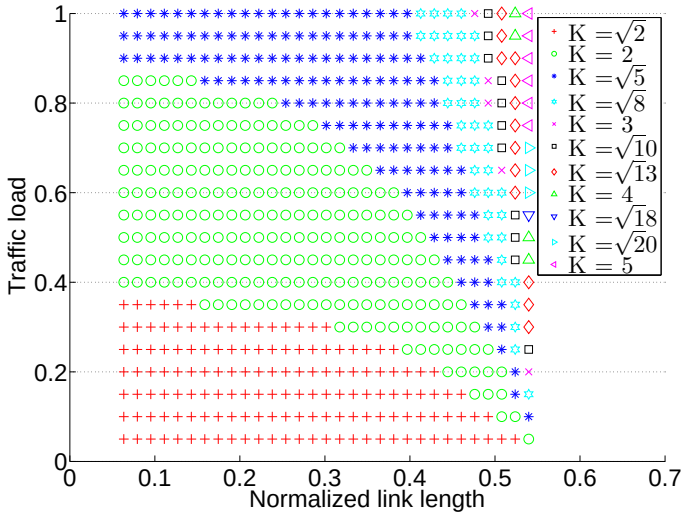

(a) $\alpha = 3.3$

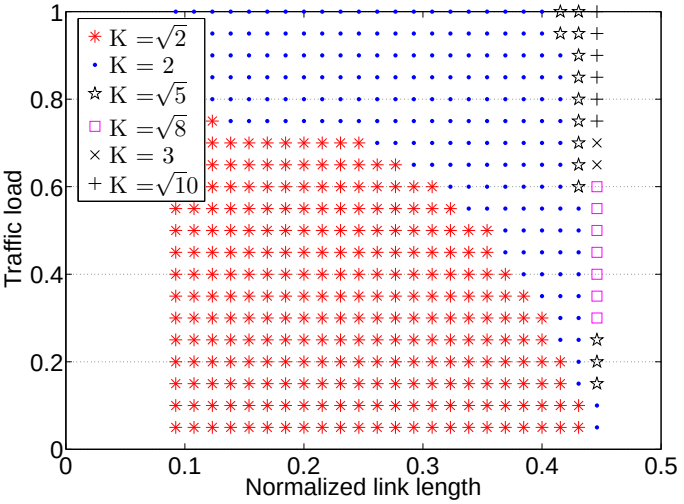

(b) $\alpha = 4.5$

Figure 2.35: Distribution of minimum K in grid network

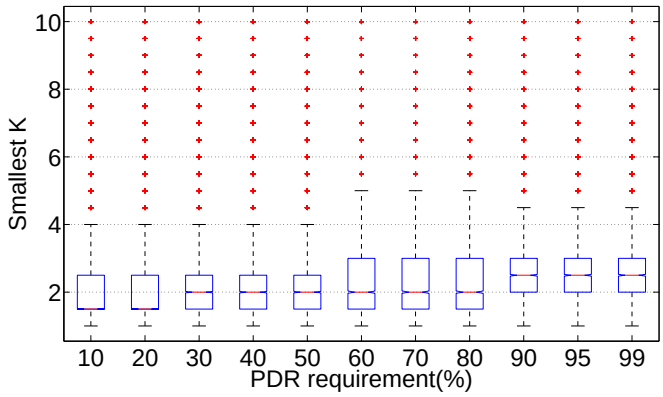

Figure 2.36: Minimum K for ensuring link PDR: random network

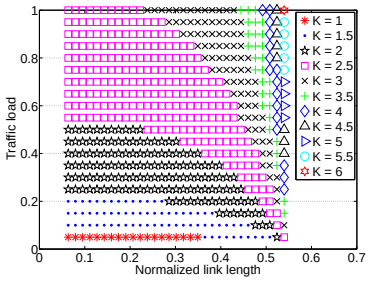

(a) $\alpha = 3.3$

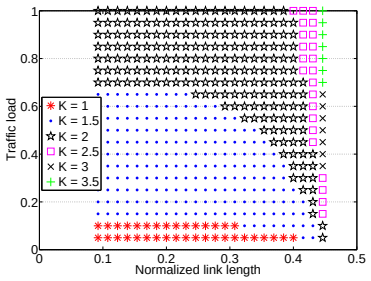

(b) $\alpha = 4.5$

Figure 2.37: Distribution of minimum K in random network

dynamics.

Throughput: grid networks. Given that the optimal K for maximizing network throughput changes with network and environmental properties, using any constant K in ratio-K-based scheduling may lead to throughput loss since the chosen K may not always be optimal. To quantify the impact of not adapting K to network and environmental dynamics, we compute, for each system configuration, the loss in network throughput when using a K that is ΔK away from the optimal K, denoted by K_{opt}, for this system configuration. For different ΔK's, Figure 2.38

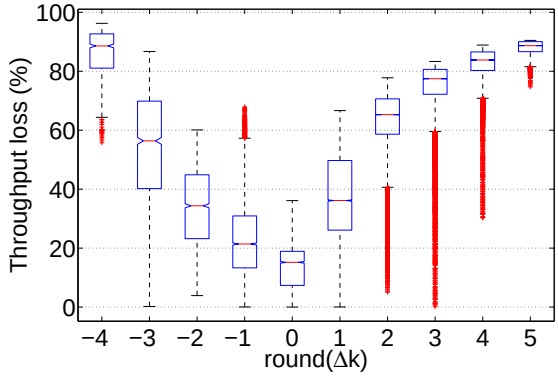

Figure 2.38: Throughput loss in grid networks when using $K = K_{opt} + \Delta K$

shows the boxplot[7] of throughput loss across different system configurations, where the loss is defined as the reduction in throughput divided by the optimal throughput. We see that, in general, throughput loss increases as $|\Delta K|$ increases. If the used K differs from the optimal one by up to 1, throughput loss can be up to 68%, which is non-negligible.

To understand the impact of choosing a fixed K, Figure 2.39(a) shows, for different fixed Ks, the possible throughput loss across different system configurations, and Figure 2.39(b) shows, for K=2, the throughput loss when the optimal K is $K - \Delta K$ (where ΔK is rounded to the precision of 0.1). We see that the throughput loss can be significant. For instance, fixing

[7]Note that, for clarity of presentation, we group data by the rounded ΔK instead of ΔK directly because there are too many ΔK's to present individually in a single figure.

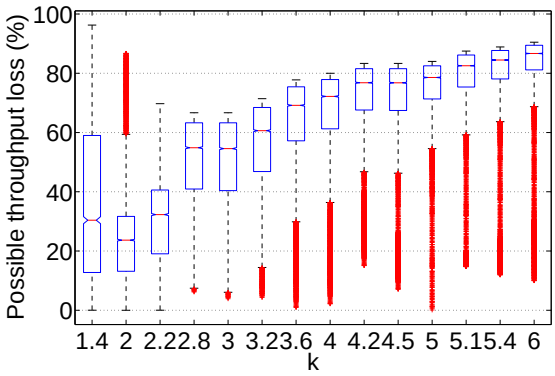

(a) Constant Ks

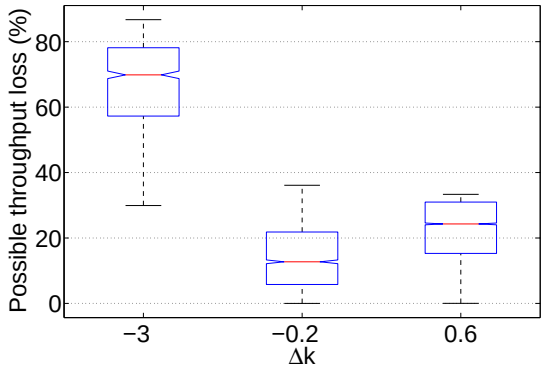

(b) Constant $K = 2$

Figure 2.39: Possible throughput loss by choosing a constant K: grid networks

K to 2 can lead to a throughput loss of up to 86.73% and a median loss of 23.68%.

Therefore, *using a constant K across different network and environmental settings may well lead to significant loss in network throughput*, and, to avoid biased evaluation against ratio-K-based scheduling, we need to take this into account in both protocol design and performance analysis.

Throughput: random networks. Figure 2.40 shows, for different fixed ΔK's, the boxplot of throughput loss across different system configurations. Same as in grid networks, throughput loss increases as $|\Delta K|$ increases. If the used K differs from the optimal one by up to 1, throughput loss can be up to 98%, which is quite large.

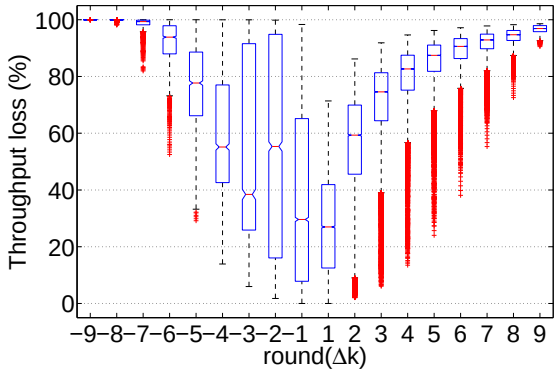

Figure 2.40: Throughput loss in random networks when using $K = K_{opt} + \Delta K$.

To understand the impact of choosing a specific constant K, Figure 2.41(a) shows the pos-

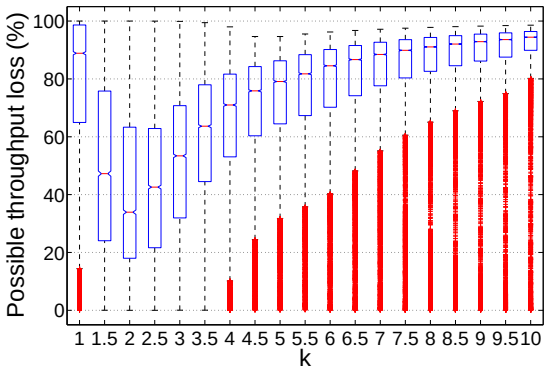

(a) Constant Ks

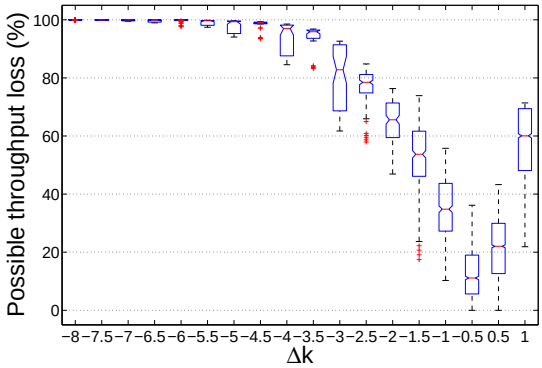

(b) Constant K = 2

Figure 2.41: Possible throughput loss by choosing a constant K: random networks

sible throughput loss for using different Ks, and Figure 2.39(b) shows, for K=2, the throughput loss when the optimal K is $K - \Delta K$ (where ΔK is rounded to the precision of 0.1). Same as in grid networks, using a constant K across different network and environmental settings may well lead to significant loss in network throughput, and we need to take this into account in both protocol design and performance analysis.

Reliability: grid networks. To understand the impact of using a constant K on link reliability, we consider system configurations where a proper choice of K can ensure a link reliability of at least 20%, 40%, 60%, 80%, and 100%. Due to the limitation of space, here we only present the data for configurations where a link reliability of at least 80% can be achieved by choosing a proper K. (Similar phenomena as what we will present have been observed for other configurations too.) Figure 2.42(a) shows, for using different Ks, the boxplot of the PDR (i.e., packet delivery rate) gain across different system configurations, where the PDR gain is defined as $\frac{\text{PDR}_k - 0.8}{0.8}$ and PDR_k is the PDR resulting from using a specific constant K in a system configuration; Figure 2.42(b)-(c) show, for K = 2 and $\sqrt{2}$ respectively, the PDR gain when the optimal K is $K - \Delta K$ (where ΔK is rounded to the precision of 0.1 and 1 respectively).

We see that *Ks less than or equal to 2 tend not to be a good constant number for ensuring reliable data delivery* (e.g., 80% link PDR): a constatnt K of 2 is unable to guarantee 80% link reliability with non-negligible probability; a constant K of $\sqrt{2}$ is mostly unlikely to guarantee 80% reliability, even though $\sqrt{2}$ is the optimal K for maximizing throughput in a wide variety of system configurations we study. On the other hand, *using larger Ks (e.g., 4) can improve link reliability, but this usually comes at the cost of reduced network throughput* due to reduced spatial reuse of channel resources, This can be seen from Figures 2.38 and 2.39(a), and we will study this tradeoff between reliability and throughput in detail next in Section 2.5.4.

Reliability: random networks. Figure 2.43(a) shows, for using different Ks, the boxplot of PDR (i.e., packet delivery rate) gain in different system configurations, where the PDR gain is

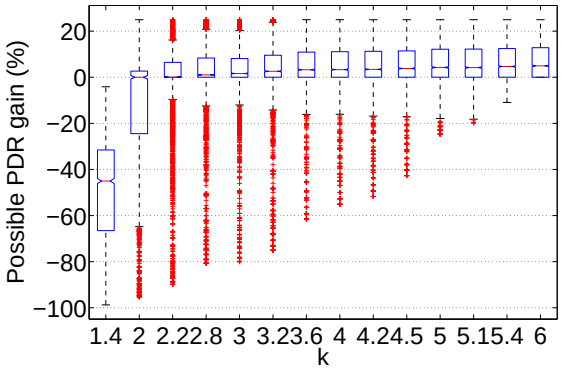

(a) Overall

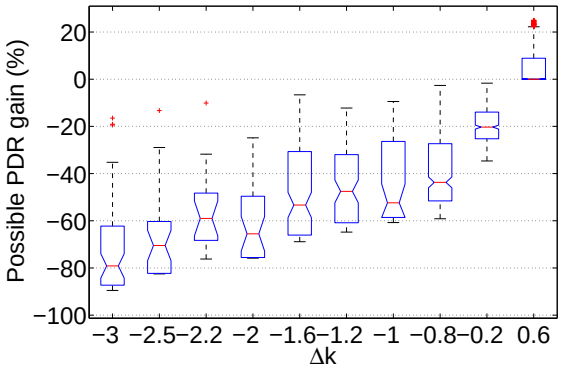

(b) K = 2

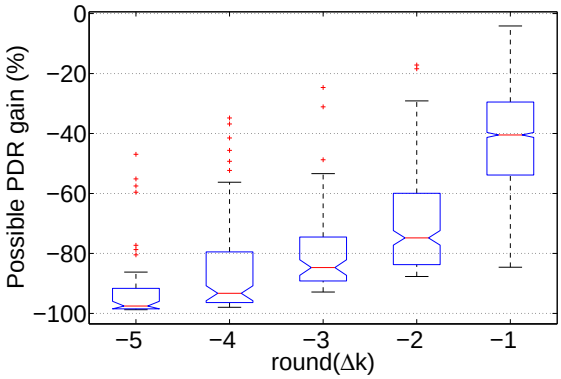

(c) K = $\sqrt{2}$

Figure 2.42: Impact of using a constant K in grid networks

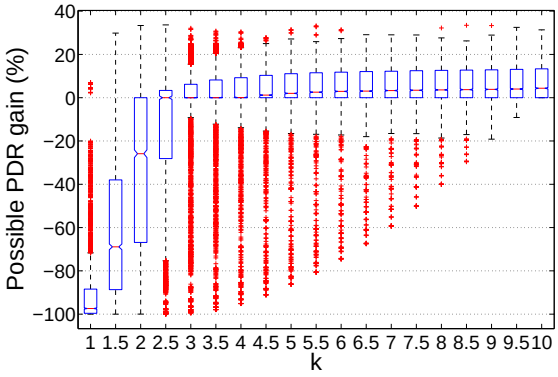

(a) Overall

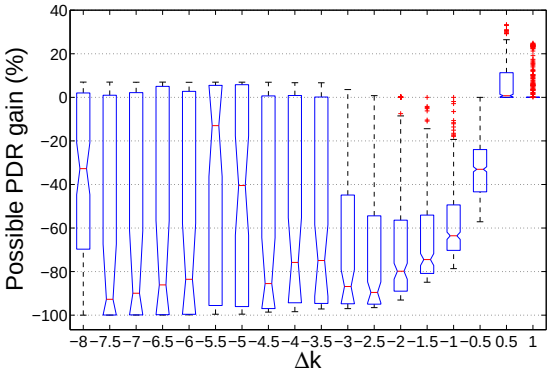

(b) K = 2

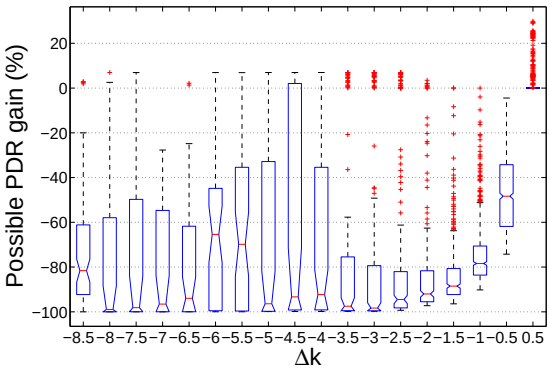

(c) K = $\sqrt{2}$

Figure 2.43: Impact of using a constant K in random networks

defined as $\frac{\text{PDR}_k - 0.8}{0.8}$ and PDR_k is the PDR resulting from using a specific constant K in a system configuration; Figure 2.43(b)-(c) show, for K = 2 and $\sqrt{2}$ respectively, the PDR gain when the optimal K is $K - \Delta K$ (where ΔK is rounded to the precision of 0.1 and 1 respectively). Same as in grid networks, Ks less than or equal to 2 tend not to be a good constant number for ensuring reliable data delivery (e.g., 80% link PDR); using larger Ks (e.g., 4) tend to improve link reliability, but this usually come at the cost of reduced network throughput due to reduced spatial reuse.

2.5.4 Tradeoff between reliability and throughput

Section 2.5.3 has alluded to the inherent tradeoff between link reliability and network throughput in instantiating the ratio-K model. In what follows, we examine the issue in detail for grid and random networks.[8] For each link reliability requirement (e.g., 80%) and each system configuration that can ensure the reliability by using certain minimum K = K_0, we compute the performance gain in packet delivery rate (PDR) and throughput when changing K to $K' = (K_0 + \Delta K)$ for various ΔK's. The performance gain is defined as $\frac{X_{K'} - X_0}{X_0}$, where X_0 is the PDR (or throughput) when $K = K_0$ and $X_{K'}$ is the PDR (or throughput) when $K = K'$.

Grid networks. Figure 2.44 shows the median performance gains for system configurations where a certain minimum PDR can be ensured, and we observe the following: *1) maximum network throughput is usually not achieved at the minimum K for ensuring certain link reliability but at a smaller K; 2) as K increases from the minimum one for ensuring certain link reliability, network throughput tends to decrease with high probability even though link reliability does improve; 3) as PDR requirement increases, moreover, the probability of improving throughput by increasing K from the minimum one of ensuring the PDR requirement further decreases, in addition to being small all the time.*

Random networks. Figure 2.45 shows the median performance gains for system config-

[8] We numerically study the tradeoff because it is difficult to derive the closed-form formula for the relationship between link reliability and network throughput in general.

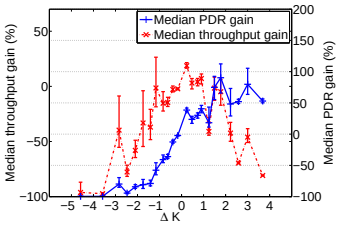

(a) PDR req. = 20%

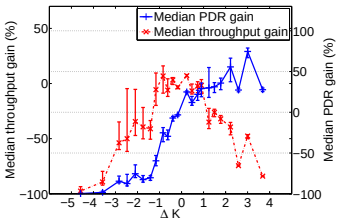

(b) PDR req. = 40%

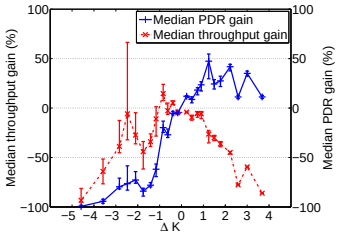

(c) PDR req. = 60%

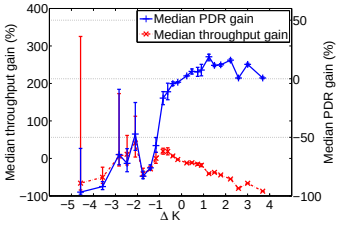

(d) PDR req. = 80%

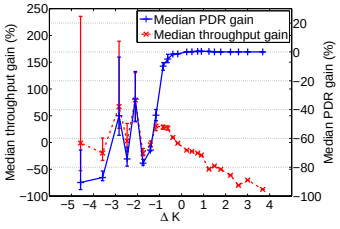

(e) PDR req. = 100%

Figure 2.44: Δk vs. performance gain: grid networks

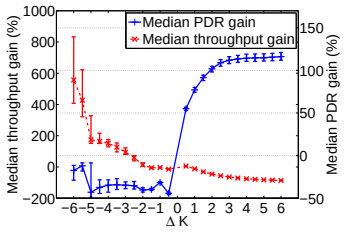

(a) PDR req. = 20%

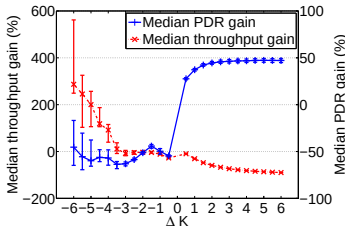

(b) PDR req. = 40%

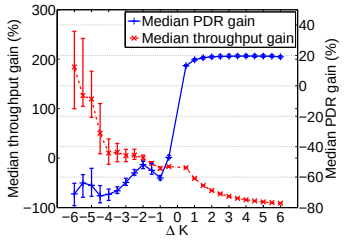

(c) PDR req. = 60%

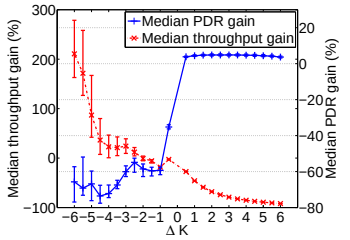

(d) PDR req. = 80%

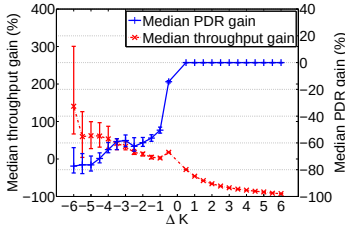

(e) PDR req. = 100%

Figure 2.45: Δk vs. performance gain: random networks

urations where certain minimum PDR can be ensured. Unlike in grid networks, we see that, for scenarios of low PDR requirements (e.g., less than 60%), reduction of K from the minimum one for ensuring certain PDR may lead to reduction in median throughput. This is because, in these scenarios, reduction in K may lead to sharp decrease in PDR as shown in Figure 2.45(a)-(c). For scenarios of high PDR requirements (e.g., 80%), trends similar to those of grid networks have been observed.

Implications. These findings suggest that we should use, in protocol design, the minimum K that ensures the required link reliability, since this helps avoid throughput reduction while ensuring enough reliability at the same time. In general, the minimum link reliability required is application dependent, and it relates to the question of how to balance properties such as throughput, reliability, delay, and energy efficiency. In low-power wireless sensing and control networks such as those for industrial sensing and control, however, it is usually desirable to have high link reliability for the following reasons: 1) reliable data delivery itself is usually important for mission-critical sensing and control; 2) higher reliability implies less variability and better predictability in data delivery performance (e.g., timeliness); this is because, given a link reliability p, the coefficient-of-variation of packet transmission status (i.e., success or failure) is $\sqrt{\frac{1-p}{p}}$ which decreases as p increases; 3) higher reliability implies fewer number of packet retransmissions and thus less energy consumption. Given that, for high reliability requirement, the probability of throughput loss is high when we increase K beyond the minimum one required for ensuring reliability, PDR requirement can serve as a good basis for a node to choose the right K to use.

Choosing the minimum K that ensures the required link reliability also tends to help reduce data delivery delay. Here we analyze the single-hop transmission delays when we need to ensure a link layer data delivery reliability of p_0. To ensure a link layer frame delivery reliability of p_0 when the delivery rate of each transmission is p, a frame may have to be retransmitted.

The maximum number of transmissions, denoted by x_0, can be computed as follows:

$$x_0 = \underset{x \geq 1}{\operatorname{argmin}} (1-p)^x \leq 1 - p_0 < (1-p)^{x-1} \tag{2.27}$$

$$= \begin{cases} 1 & \text{if } p = 1 \\ \lceil \frac{ln(1-p_0)}{ln(1-p)} \rceil & \text{if } 0 < p < 1 \end{cases} \tag{2.28}$$

Then, when a frame is to be delivered by the link layer, the frame will be transmitted/retransmitted until it is successfully received by the receiver or the frame has been transmitted for x_0 number of times.

In what follows, we analyze the expected transmission delay when link scheduling is based on TDMA and CSMA respectively.

TDMA Delay. When TDMA scheme is applied, a node will compete with N_{ex} number of nodes in its exclusive region. We assume that the TDMA scheme is fair to all the nodes within the exclusive region. We also assume that each node will only transmit one packet each time it gains the channel and each packet transmission takes one slot time. Then a transmitter has to wait $\frac{N_{ex}}{2}$ slots for the first transmission attempt on average, and $N_{ex} - 1$ for every retransmission attempt after that. Thus, the expectation of a single packet transmission delay, denoted as $T_{d,tdma}$, is

$$\begin{aligned} & E[T_{d,tdma}] \\ =& E[t_1] \cdot p + E[t_2] \cdot p(1-p) + ... + E[t_{x_0-1}] \cdot p(1-p)^{x_0-1} \\ & + E[t_{x_0}] \cdot (1-p)^{x_0-1} \\ =& \frac{N}{2} + (N-1) \left\{ \frac{1-p}{p} + \left[2x_0 - 1 - \frac{1}{p} \right] \cdot (1-p)^{x_0-1} \right\} \end{aligned}$$

where $E[t_k] = \frac{N_{ex}}{2} + (k-1)(N_{ex}-1), 1 \leq k \leq x_0$

Note that the unit of time is a time slot.

CSMA delay. According to [72], the expected delay between any two transmission can be computed as

$$E[T_n] = \frac{L - (L-1)(1-p_c)^n}{np_c(1-p_c)^{n-1}} \cdot \delta$$

where n is the number of nodes in the exclusive region, L is the length of packet in the number of time slots ($L = 13$ in our study), and δ is the duration of a time slot which is 320 microseconds. p_c is the channel access probability, which is close to the value of $\frac{1}{16.5} = 0.606$ [72]. Notice that $E[T]$ includes the idle time, collision time and the packet transmission time.

So the expected delay D_{csma} when the link quality is p can be computed as

$$\begin{aligned} E[D_{csma}] =& E[T_n] \cdot p + 2E[T_n] \cdot p(1-p) + ... \\ &+ x_0 \cdot E[T_n] \cdot p(1-p)^{x_0-1} + x_0 \cdot E[T_n] \cdot (1-p)^{x_0} \\ =& E[T_n] \cdot \big(\frac{1+(1-p)^{x_0}}{p} + 2x_0(1-p).^{x_0-1}\big) \end{aligned}$$

Simulation Result. Figures 2.46, 2.47, 2.48, and 2.49 show the median delay change and its 95% confidence interval in grid and Poisson networks and when the channel access is through TDMA or CSMA. We see that the transmission delay varies significantly when K varies by ΔK from the minimum K' that ensures a certain link reliability. For Poisson networks with TDMA channel access control (see Figure 2.47(d)), for instance, the median delay gain can be 167% when $\Delta K = -1$. We also observe that choosing the minimum K' that ensures the required link reliability also helps reduce data delivery delay. As K increases from K', the delay increases because the number of nodes in a link's exclusion region increases, which introduces larger contention delay in channel access. As K decreases from K', the contention delay decreases, but the overall delay still increases because retransmissions are required to ensure the

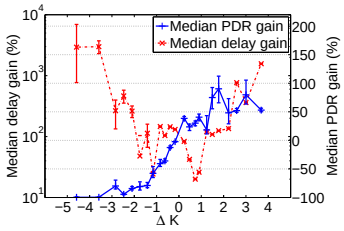

(a) PDR req. = 20%

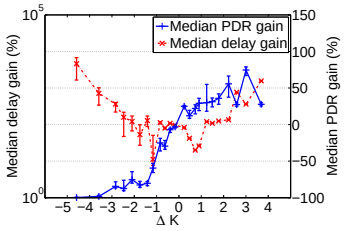

(b) PDR req. = 40%

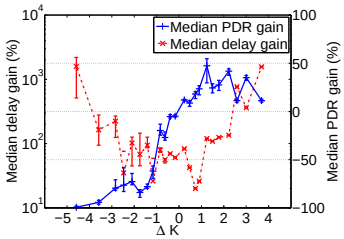

(c) PDR req. = 60%

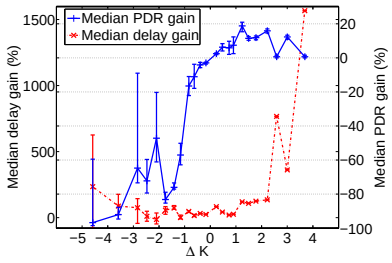

(d) PDR req. = 80%

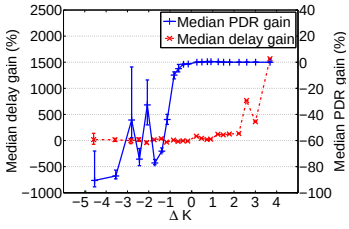

(e) PDR req. = 99%

Figure 2.46: Δk vs. performance gain: TDMA, grid networks

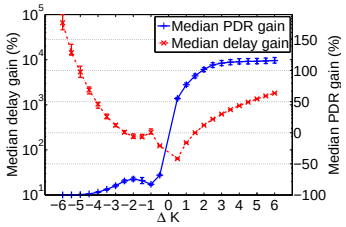

(a) PDR req. = 20%

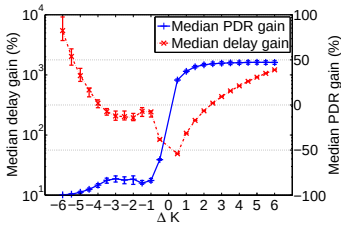

(b) PDR req. = 40%

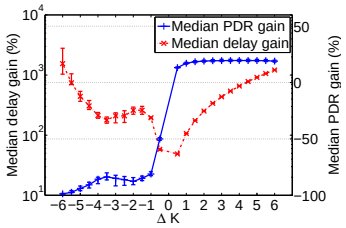

(c) PDR req. = 60%

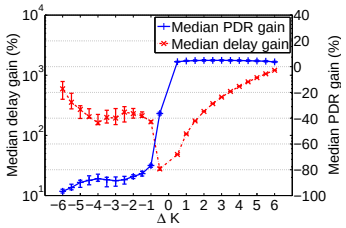

(d) PDR req. = 80%

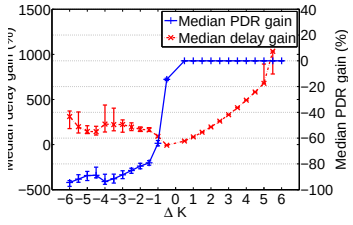

(e) PDR req. = 99%

Figure 2.47: Δk vs. performance gain: TDMA, Poisson networks

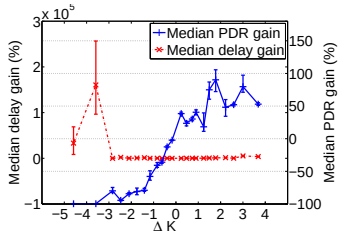

(a) PDR req. = 20%

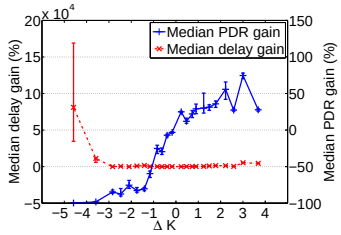

(b) PDR req. = 40%

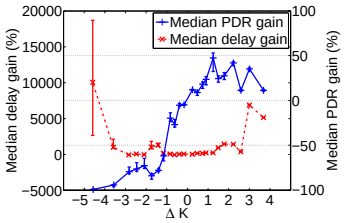

(c) PDR req. = 60%

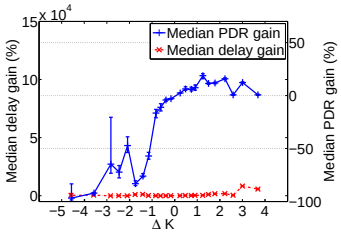

(d) PDR req. = 80%

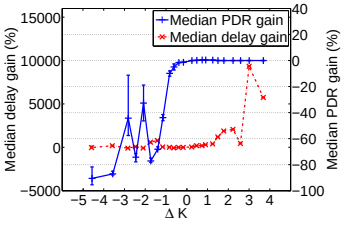

(e) PDR req. = 99%

Figure 2.48: Δk vs. performance gain: CSMA, grid networks

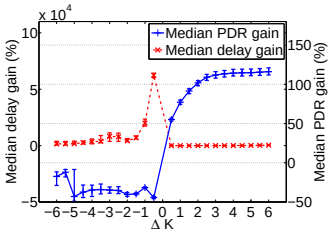

(a) PDR req. = 20%

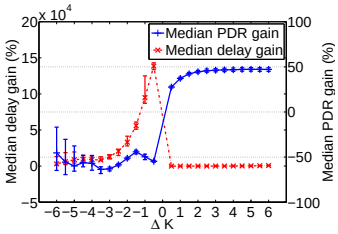

(b) PDR req. = 40%

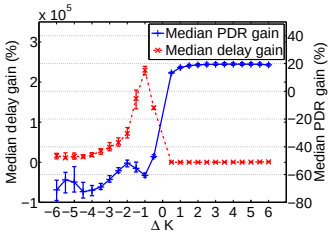

(c) PDR req. = 60%

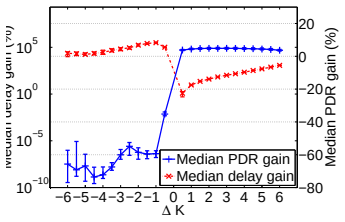

(d) PDR req. = 80%

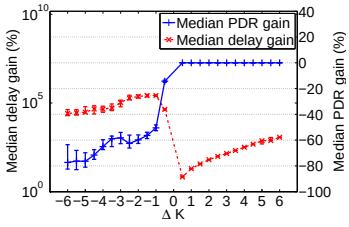

(e) PDR req. = 99%

Figure 2.49: Δk vs. performance gain: CSMA, Poisson networks

same link-layer data delivery reliability as what is enabled by K' without retransmission.

As K increases from K', the delay increases because the number of nodes in a link's exclusion region increases, which introduces larger contention delay in channel access. As K decreases from K', the contention delay decreases, but the overall delay still tends to increase because retransmissions are required to ensure the same link-layer data delivery reliability as what is enabled by K' without retransmission. Similar phenomena are observed for random networks and contention-based channel access control mechanisms [17]. Given that the performance (e.g., convergence rate) of networked control usually decreases dramatically with increasing network delay, it is important to ensure small network delay in mission-critical sensing and control, which further emphasizes the need for high link reliability.

2.6 Summary and the PRK interference model

Through detailed study with different configurations of grid and random networks, we find that both network throughput and link reliability are sensitive to the choice of K in instantiating the ratio-K model. Thus it is important to take this into account in protocol design, for instance, by adapting K to network and environmental dynamics.

We also observe that there is inherent tradeoff between link reliability and network throughput. In ratio-K-based scheduling, therefore, it is desirable to use the minimum K that ensures the required link reliability, since this tends to avoid throughput loss caused by using any unnecessarily large K. This observation suggests that link reliability requirement can serve as a good basis for each node to choose the right K to use in ratio-K-based scheduling. Accordingly, we propose the *physical-ratio-K* (PRK) interference model as a link-reliability-based instantiation of the ratio-K model as follows: "Given a transmission from node n_s to node n_r, a concurrent transmitter n_i does not interfere with the reception at n_r if and only if the following holds:

$$P(n_i, n_r) < \frac{P(n_s, n_r)}{K_{n_s, n_r, T_{pdr}}} \tag{2.29}$$

where $P(n_i, n_r)$ and $P(n_s, n_r)$ is the strength of signals reaching n_r from n_i and n_s respectively, and $K_{n_s,n_r,T_{pdr}}$ is chosen such that the probability of n_r successfully receiving packets from n_s is at least T_{pdr} in the presence of interference from all concurrent transmitters." It is usually difficult to derive closed-form formula for computing the parameter $K_{n_s,n_r,T_{pdr}}$ in general. But K is amenable to online, distributed instantiation, because link reliability is a locally measurable metric and can even be identified through real-time, data-driven, passive measurement [77]. In particular, the problem of identifying parameter $K_{n_s,n_r,T_{pdr}}$ can be modeled as a classical "regulation control" problem [28], where the "reference input" is the required link reliability T_{pdr}, the "control input" is the parameter $K_{n_s,n_r,T_{pdr}}$, and the "feedback" is the current link reliability from n_s to n_r. Because the adaptation of K is local and the signal strength between nearby nodes is a pairwise, locally measurable metric too, we expect the PRK model to be a good basis for designing distributed MAC protocols. Since our focus in this paper is understanding the behavior of ratio-K-based scheduling instead of protocol design, we relegate the study of distributed, PRK-based medium access control to our future work. But we will study the potential performance of PRK-based medium access control in Section 2.4.

Based on the above discussion, we see that the PRK model has the locality of the ratio-K model. The PRK model also has the high fidelity of the SINR model, since it is based on link reliability which captures the properties and constraints of wireless communication. Even though the parameter $K_{n_s,n_r,T_{pdr}}$ of the PRK model depends on interference from all concurrent transmitters in the network as in the SINR model, the PRK model is simpler than the SINR model in terms of distributed protocol design. This is because, unlike the SINR model which *explicitly* characterizes interference from each concurrent transmitter in the whole network, interference is modeled *implicitly* in the PRK model through locally measurable link reliability without worrying about who the concurrent transmitters are. Thus, the PRK model enables a receiver to locally adapt the parameter K for satisfying its local link reliability requirement without explicit network-wide coordination.

We define the PRK model based on signal strength instead of geographic distance so that the model is more generically applicable, for instance, to scenarios where transmission power varies across nodes [44] or signal attenuation is non-uniform such as in our measurement study of Section 2.7. Note that the selection of $K_{n_s,n_r,T_{pdr}}$ is based on each link of a receiver n_r such that the model can also be applied to cases where different links of a receiver vary significantly, for instance, in their senders' transmission powers. To relate the PRK model to the ratio-K model and to facilitate discussions in Sections 2.4 and 2.7, we define the concept *s-distance* as follows: the s-distance from a node T to another node R, denoted by $sd(T,R)$, is $\frac{1}{P(T,R)}$ where $P(T,R)$ is the strength of signals reaching R from T. If $sd(T_1,R) > sd(T_2,R)$, then T_1 is regarded as *s-farther* away from R than T_2 is, and T_2 is regarded as *s-closer* to R than T_1 is. Given a $K' = K_{n_s,n_r,T_{pdr}}$, the PRK model defines an exclusion region $\mathbb{ER}(n_r,K')$ around the receiver n_r such that a node n_j is in $\mathbb{ER}(n_r,K')$ if and only if $sd(n_j,n_r) < \mathbb{R}(n_s,n_r,K')$, where $\mathbb{R}(n_s,n_r,K') = \frac{K'}{P(n_s,n_r)}$ is called the *s-radius* of the exclusion region $\mathbb{ER}(n_r,K')$.

2.7 Measurement study of PRK- and SINR-based scheduling

Our analytical results show that the PRK model serves well as the basis of instantiating the ratio-K model in different network and environmental settings and that PRK-based scheduling achieves a spatial throughput close to what is possible in SINR-based scheduling. To corroborate these results, we experimentally compare the performance of PRK- and SINR-based scheduling using the *NetEye* wireless sensor network testbed [1] at Wayne State University and the *MoteLab* testbed [69] at Harvard University, and we also experimentally verify the tradeoff between reliability and throughput in both PRK- and SINR-based scheduling. To reflect the impact of link-layer behavior on network-wide behavior, we also consider end-to-end throughput in this section. The purposes of this measurement evaluation are to verify the analytical insight and to correct the misconceptions about the potential performance of ratio-K-based scheduling,

thus our evaluation will be based on the centralized scheduling algorithm Longest-Queue-First (LQF) that has been used to compare different wireless interference models by Maheshwari et al. [40]. Distributed protocol design via the PRK model is a part of our future work.

2.7.1 Methodology

We use both the NetEye and the MoteLab testbeds so that we can evaluate PRK- and SINR-based scheduling in different network and environmental settings. In what follows, we first describe properties of the two testbeds, then we discuss the traffic patterns and the scheduling objectives studies here.

NetEye testbed. NetEye [1] is deployed in an indoor office as shown in Figure 2.50. We

Figure 2.50: *NetEye* wireless sensor network testbed

use a 10×12 grid of TelosB motes in NetEye, where every two closest neighboring motes are separated by 2 feet. Each of these TelosB motes is equipped with a 3dB signal attenuator and a 2.45GHz monopole antenna. In our measurement study, we set the radio transmission power to be -25dBm (a.k.a. power level 3 in TinyOS) such that multihop networks can be created. In addition to grid networks, the 10×12 grid enables us to experiment with random networks, where a random network is generated out of the 10×12 grid by removing each mote of the grid with certain probability.

Part of the input to PRK- and SINR-based scheduling algorithms (to be discussed in Sec-

tion 2.7.2) are radio model, background noise at every node, and strength of signals from any one node to every other node. To collect these information about the 10×12 grid in NetEye, we perform the following experiment: let the 120 motes take turns to be a transmitter one at a time; when a mote is a transmitter, it broadcasts 600 128-byte packets with a transmission power of -25dBm and an inter-packet interval of 100ms (note: each packet transmission takes $\sim$4ms); while a mote is transmitting packets, every other mote keeps sampling its radio RSSI once every 2ms whether or not it can receive packets from the transmitter, and, if a mote can receive packets from the transmitter, it logs the received packets. Using the data collected in this experiment, we can derive the background noise power at each node,[9] the strength of signals from any node to every other node, and the packet delivery rate (PDR) from any node to every other node as well as the associated SINR. These data also enable us to derive the empirical radio model for the TelosB motes in NetEye, and the radio model shows the relation between PDR and SINR. We will use this radio model in our scheduling algorithms for two purposes: 1) to choose the SINR threshold for satisfying certain link reliability, and 2) to compute the expected PDR for a given SINR at a receiver. For the transmission power of -25dBm, Figure 2.51 shows the boxplot of PDR for links of different length, and Figure 2.52 shows the histogram of background noise power in NetEye. We see that there is a high degree of variability in PDR for links of equal length and in background noise power. Thus the testbed enables us to do experiments in non-uniform settings.

MoteLab testbed. MoteLab is deployed at three floors of the EECS building of Harvard as shown in Figure 3.13. Our experiments use all of the 101 operational Tmote Sky motes, with 32, 39, and 30 motes distributed at the first, second, and third floors respectively. We use a transmission power of $-1dBm$ (a.k.a. power level 27) to generate a well-connected multi-hop networks.

Using a method similar to that for NetEye, we have characterized the empirical radio model,

[9] It is derived from RSSI readings in the absence of packet transmission.

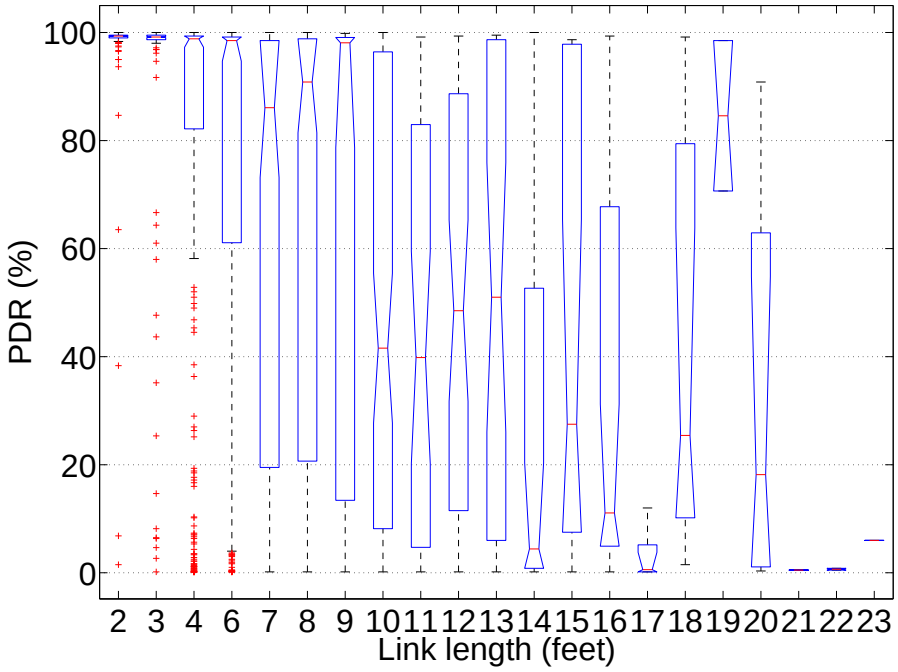

Figure 2.51: PDR vs. link length in NetEye when transmission power is -25dBm

background noise at every node, and strength of signals from any node to every other node in MoteLab. Figure 2.54 shows the histograms of the PDRs of all the wireless links, and Figure 2.55 shows the histogram of background noise power in MoteLab. We see that there is a high degree of variability in link PDRs and background noise power. Thus the testbed enables us to do experiments in non-uniform settings too.

Traffic patterns. To generate the traffic load for scheduling, we consider convergecast in wireless sensor networks where data packets generated by all the nodes need to be delivered to a base station node.

For NetEye, we consider convergecast in both grid and random networks. For grid network, we let the node at one corner serve as the base station to which the remaining nodes of the 10×12 grid deliver their packets (mostly via multi-hop paths); we generate the random network out of the 10×12 grid by removing a mote in the grid with 30% probability, and then we let a

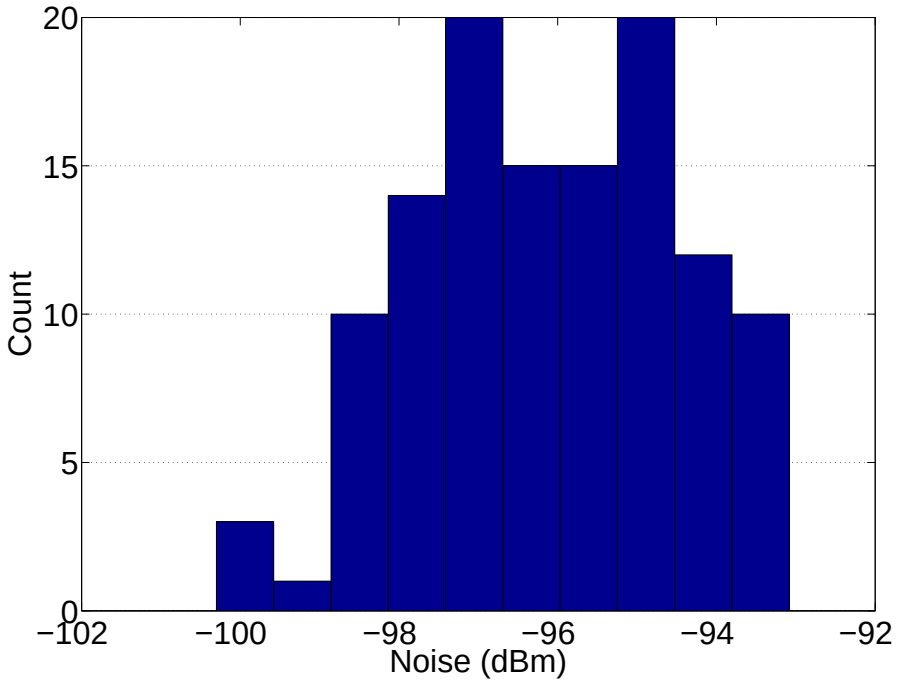

Figure 2.52: Histogram of background noise power in NetEye

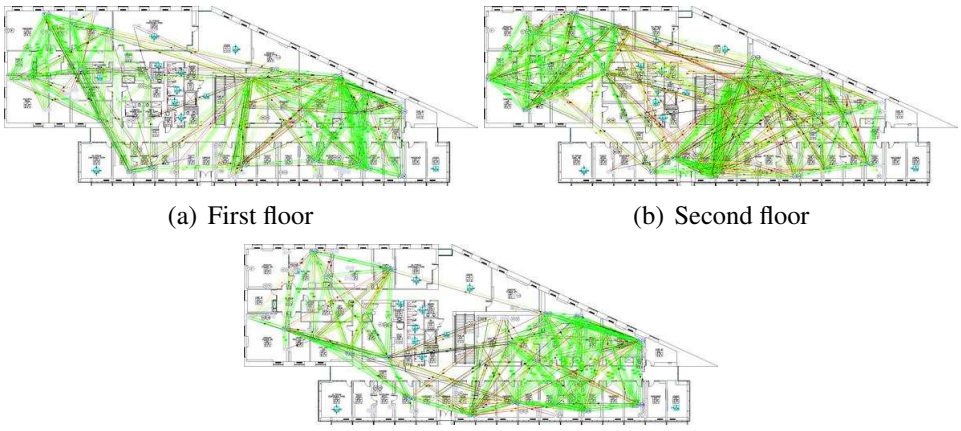

(a) First floor

(b) Second floor

(c) Third floor

Figure 2.53: *MoteLab* testbed

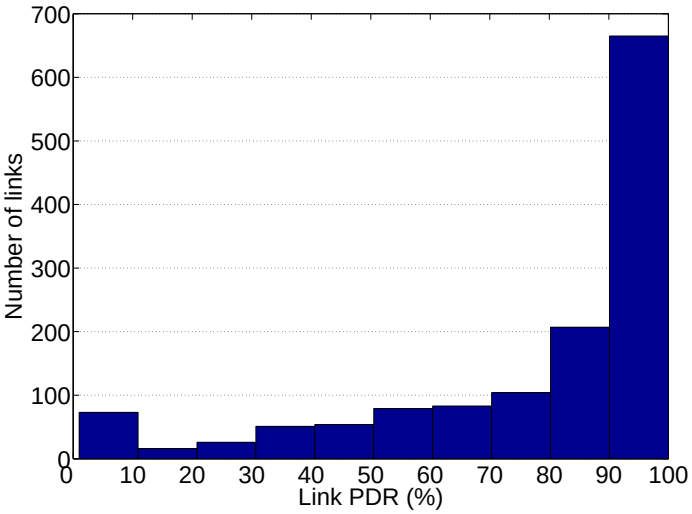

Figure 2.54: Histogram of link PDRs in MoteLab

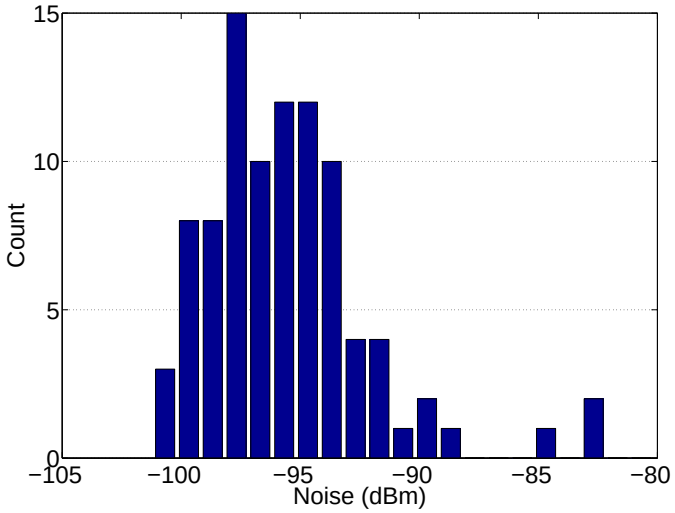

Figure 2.55: Histogram of background noise power in MoteLab

mote closest to a corner of the original grid be the base station (with ties broken randomly). In both the grid and random networks, an approximate routing tree is built by letting each mote choose as its parent the mote having the minimum ETX (i.e., expected transmission count) value to the base station among all the motes within 6 feet distance. Given a routing tree, we generate the traffic load as follows: each node generates a packet with 50% probability, and then the number of packets that need to be delivered across a link is the number of packets generated in the subtree rooted at the transmitter of the link. Then the traffic load is used as the input to PRK- and SINR-based scheduling. (Note that this traffic load can simulate event detection and may also be repeated to simulate periodic data collection in sensor networks.)

For MoteLab, we let mote #115 at the center of the second floor be the base station to which the remaining 100 motes deliver their packets (mostly via multi-hop paths). Then the routing tree and network traffic are generated in the same manner as in NetEye.

Scheduling objectives. When scheduling the aforementioned traffic load, we consider three different scheduling objectives: 1) *Obj-5*: to guarantee a 5dB minimum SINR at transmitters and receivers (with throughput maximization as a second-order objective), which corresponds to a link PDR of $\sim$88% and $\sim$97% in NetEye and MoteLab respectively; 2) *Obj-8*: to guarantee an 8dB minimum SINR at transmitters and receivers, which corresponds to a link PDR of $\sim$95% and $\sim$98% in NetEye and MoteLab respectively; and 3) *Obj-T*: to maximize network throughput. When comparing PRK- and SINR-based scheduling for different objectives and networks, we consider both link PDR and network throughput.

Overall, we have 12 different experiment configurations, where each configuration specifies a scheduling objective, a topology, and an interference model. A schedule is generated by our scheduling algorithms for each system configuration, where the schedule $S = \{S_1, S_2, \ldots, S_\tau\}$, with S_j being a set of links scheduled in j-th time slot and τ being the schedule length. Experiment with each schedule is repeated 10 times to gain statistical insight. To experiment with a schedule in NetEye, we select a mote not in the 10×12 grid to be the com-

mander that broadcasts the schedule, slot by slot, to the motes involved (as either a transmitter or a receiver) in each slot such that the links in the same lot are synchronized to transmit at the same time; each slot is repeated 30 times before moving onto the next slot so that we can get 30 samples on the transmission status (i.e., success or failure) along each link of the slot to understand the behavior of each slot.

In the next subsection, we describe the scheduling algorithms used in our evaluation.

2.7.2 Scheduling algorithms

Optimal SINR- and ratio-K-based scheduling are NP-complete in general [14, 54], thus we use the greedy, approximate scheduling framework, denoted by Longest-Queue-First (LQF) [30, 35, 9],[10] that has been used to compare different wireless interference models in literature [40]. In addition to interference model, LQF takes as input the link demand vector $f = (f_1, f_2, \ldots, f_L)$ for L number of links, where the demand f_i for the i-th link is the number of packets to be transmitted across the link. The output of LQF is a schedule $S = \{S_1, S_2, \ldots, S_\tau\}$, where S_j is a set of links scheduled in the j-th time slot. LQF works as follows to generate the output schedule:

1. Order and rename links such that $f_1 \geq f_2 \geq \ldots \geq f_L$.

2. Set $i = 1, S = \emptyset, \tau = 0$. (Note: initial schedule is empty.)

3. Schedule link i in the very first available time slot to which link i can be added based on certain scheduling objective (e.g., guaranteeing certain minimum link reliability or maximizing network throughput) and interference model. If no such slot exists, increment τ and schedule link i in the newly created slot. (Note: incrementing τ is equivalent to creating a new empty slot at the end of the current schedule.)

[10]Note that the LQF scheduling framework has been shown to achieve close-to-optimal throughput in many practical scenarios [30, 35] and has been a research focus in recent years. Besides LQF, we have also experimented with other scheduling algorithms such as the commonly-used GreedyPhysical [10, 66] and the recently proposed iOrder [15] algorithm. Similar phenomena have been observed for different algorithms, and here we only present the results based on LQF for conciseness; interested readers can find the results based on GreedyPhysical and iOrder in Appendix IV.

4. Repeat step 3 f_i times.

5. Increment i. Go back to step 3 until $i > L$.

For scheduling based on the SINR model, we can use LQF without any modification [40, 39], and we only need to instantiate LQF in the following manner: at step 3, link i can be added to a slot j if 1) the SINR at all the receivers and senders of the slot is above certain threshold γ_0 when the scheduling objective is to guarantee certain minimum link reliability, or 2) if adding link i can increase the expected throughput in slot j when the scheduling objective is to maximize network throughput only. For convenience, we denote this SINR-based scheduling algorithm LQF$_{sinr}$.

For PRK-based scheduling, we need to extend LQF to accommodate the special properties of the PRK model. Given two links l and l', we define the s-distance from l to l', denoted by $sd(l, l')$, as $\min_{n\in\{l.t,l.r\},n'\in\{l'.t,l'.r\}} sd(n, n')$ where $l.t$ and $l'.t$ are the transmitter of l and l' respectively and $l.r$ and $l'.r$ are the receiver of l and l' respectively. Accordingly, for any three links l, l', and l'', l'' is regarded s-closer to l' than l is if $sd(l'', l') < sd(l, l')$. Then, for every link i' in a slot S_j in PRK-based scheduling, the s-radius of the exclusion region of i' in S_j is less than $\min_{l\in S_j, l\neq i'} sd(l, i')$. When link i cannot be added to any of the existing slots in step 3 of LQF, link i (more precisely, the transmitter and/or the receiver of i) may be within the exclusion region of another link already scheduled. When the scheduling objective is to ensure certain minimum link reliability, link i is within the exclusion region of another link i' in a slot S_j if 1) there is no other link $i'' \in S_j$ that is s-closer to i' than i is, and 2) the SINR at the transmitter or receiver of i' becomes less than certain threshold γ_0 (to violate the link reliability requirement) if we add i to S_j. When the scheduling objective is to maximize network throughput, link i is regarded as within the exclusion region of link i' in S_j if 1) there is no other link $i'' \in S_j$ that is s-closer to i' than i is, and 2) the local throughput of i' decreases if we add i to S_j, where the local throughput of i' is defined as $T_{i'}$ (see Formula 2.7) divided by the number of nodes in the exclusion region of i'. If i is within the exclusion region of i', we

say that the exclusion region of i' covers i.

Let S' be the set of existing slots when link i is being scheduled in step 3 of LQF but cannot be added into any one of S'. Had S' only include one slot S_j ($j = 1, 2, \ldots, |S'|$), then according to the definition of the PRK model, for every link $i' \in S_j$ whose exclusion region covers i, we should remove from S_j every link $i'' \in S_j$, if any, with $sd(i'', i') = sd(i, i')$ so that the exclusion region of i' is well defined in S_j according to the PRK model; this is because, in the PRK model, all the concurrent transmitters of certain s-distance to a transmitter or receiver R, denoted by $\mathcal{S}_0$, are regarded as interferers to R and need to be silenced as long as any node in $\mathcal{S}_0$ has to be silenced for ensuring certain ACK or packet reception reliability at R; we denote all such removed links as $\mathbb{L}(S_j, i)$, and note that $\mathbb{L}(S_j, i)$ may be empty. To make the exclusion region of every link in every slot of S' well defined while minimizing the number of links that have to be removed from the existing slots (for the purpose of high throughput), we need to find the slot $S_{j'}$ such that $|\mathbb{L}(S_{j'}, i)| \leq |\mathbb{L}(S_j, i)|$ for all $j = 1, 2, \ldots, |S'|$; then we regard link i as being silenced by some link $i' \in S_{j'}$, which entails the generation of a new slot for i. We denote $\mathbb{L}(S_{j'}, i)$ as $\mathbb{L}(i)$; to conform to the PRK model, we need to reschedule every link in $\mathbb{L}(i)$, if non-empty, in step 3 of LQF. Therefore, the PRK-based instantiation of LQF becomes as follows, which is the same as LQF$_{sinr}$ except for the italicized part of step 3:

1. Order and rename links such that $f_1 \geq f_2 \geq \ldots \geq f_L$.
2. Set $i = 1, S = \emptyset, \tau = 0$.
3. Schedule link i in the very first available time slot to which link i can be added based on certain scheduling objective and PRK interference model. If no such slot exists, increment τ and schedule link i in the newly created slot; *additionally, remove $\mathbb{L}(i)$, if non-empty, from an existing slot and reschedule them using step 3.*
4. Repeat step 3 f_i times.
5. Increment i. Go back to step 3 until $i > L$.

For convenience, we denote this algorithm as LQF$_{prk}$.

2.7.3 Experimental results

In what follows, we present the measurement results for NetEye and MoteLab respectively.

NetEye testbed. Using the scheduling algorithms LQF$_{prk}$ and LQF$_{sinr}$, we have measured the performance of PRK- and SINR-based scheduling using the methodology discussed in Section 2.7.1. Figures 2.56 and 2.57 show the PDR and end-to-end throughput of PRK- and SINR-based scheduling in the grid network and the random network respectively, with the error bars representing the 95% confidence intervals (which are very small) of the corresponding metrics. The PDR is defined as the number of successfully delivered packets divided by the number of packets transmitted in a schedule; the end-to-end throughput is defined as the number of successfully delivered packets divided by the schedule length (i.e., number of slots used in a schedule).[11] Note that the throughput is not that high because of the limited concurrency allowed in the testbed which is in turn due to the wide transitional region of wireless communication as can be seen from Figure 2.51. For instance, Table 2.3 shows the probability of

# of Concurrent Links	1	2	3
Probability	0.46	0.51	0.03

Table 2.3: Probability of concurrent links in a slot: random network, PRK, *Obj-8*

having different number of concurrent links in a slot in PRK-based scheduling for the random network and the *Obj-8* objective.

We see that, in agreement with our analytical insight, there is inherent tradeoff between reliability and throughput in both PRK- and SINR-based scheduling. As the scheduling objective moves from *Obj-8* to *Obj-5* and to *Obj-T*, for instance, the throughput in PRK- and SINR-based scheduling keeps increasing, but the PDR keeps decreasing accordingly.

We also see that the performance of PRK-based scheduling is very close to that of SINR-

[11] We have also comparatively studied the PDRs of individual links as well as the spatial throughput in PRK- and SINR-based scheduling, and we observe similar phenomena as shown in Figures 2.56(a) and 2.57(a). Thus we only present data on end-to-end behavior here.

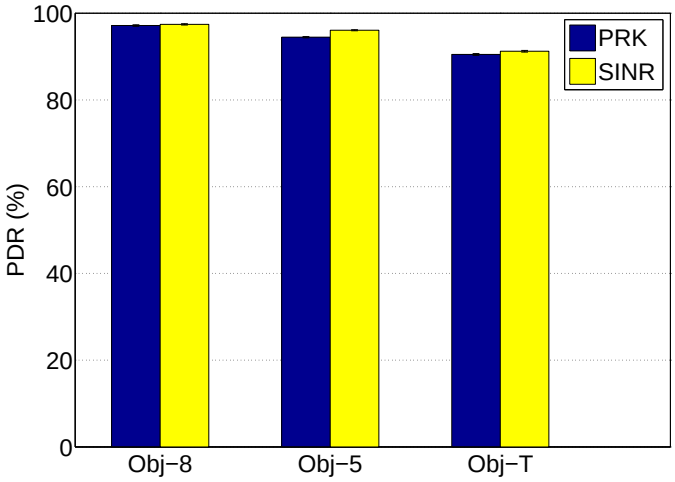

(a) PDR

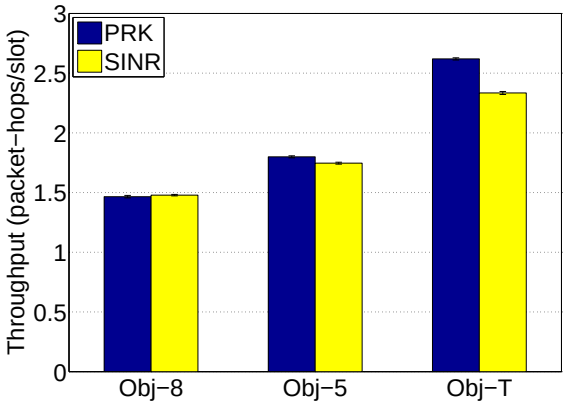

(b) Spatial throughput

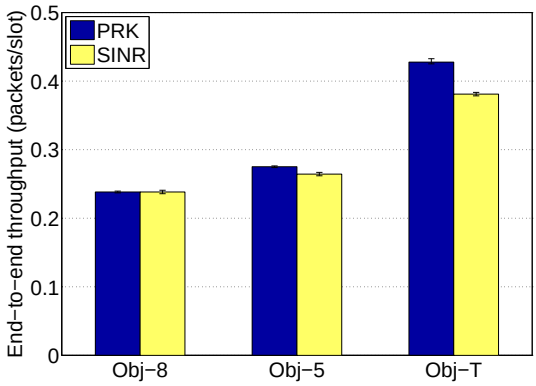

(c) End-to-end throughput

Figure 2.56: PDR and throughput in the grid network

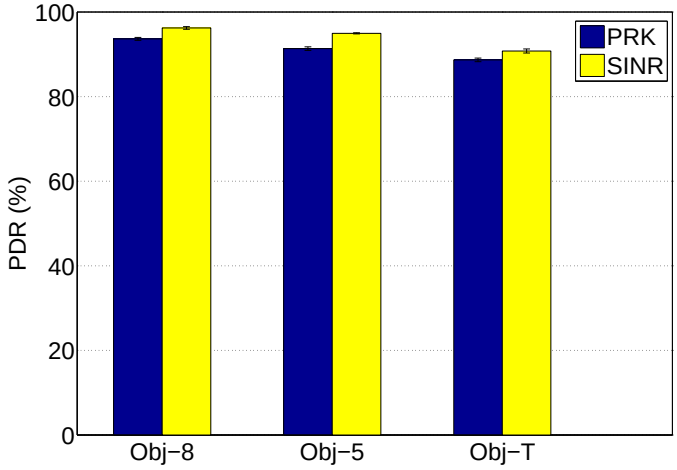

(a) PDR

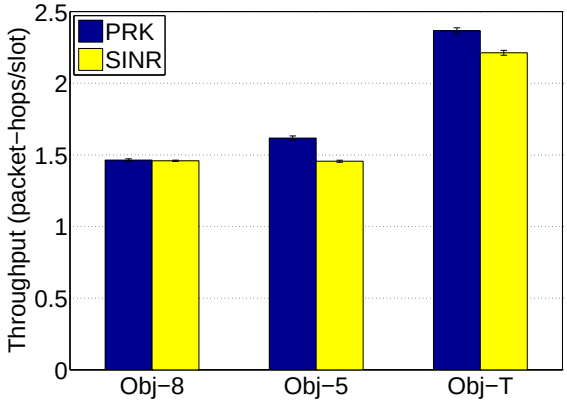

(b) Spatial throughput

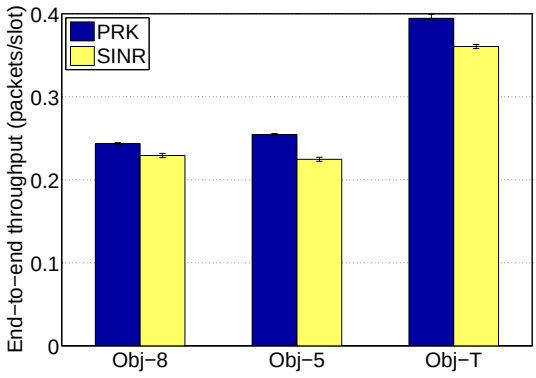

(c) End-to-end throughput

Figure 2.57: PDR and throughput in the random network

based scheduling, thus the PRK model is able to address the drawbacks of the ratio-K model as observed in [40]. The PDRs of PRK- and SINR-based scheduling are above the required link reliability for objectives *Obj-8* and *Obj-5* except for cases that we will discuss in the next paragraph. The PDR in PRK-based scheduling is slightly lower than that in SINR-based scheduling, and, due to reliability-throughput tradeoff, the throughput tends to be slightly higher in PRK-based scheduling. The reason why PRK-based scheduling tends to have slightly lower PDR and higher throughput is because PRK schedules are slightly shorter (e.g., by 3-4 slots less) than SINR schedules, and this is enabled by the fact that silencing/removing links closer-by in the PRK model allows more concurrently transmitting remote links (as discussed in Proposition 6). Note that LQF is one of the best known algorithms for SINR-based scheduling [30, 35]; the reason why SINR-based scheduling has slightly lower throughput than PRK-based scheduling is because of the reliability-throughput tradeoff in interference-oriented scheduling and not because of the bad performance of LQF itself.

Note that the measured PDRs of the PRK and SINR schedules slightly differ, sometimes higher and sometimes lower, from the PDRs predicted via the radio model and the required SINR threshold when we run the scheduling algorithms LQF$_{prk}$ and LQF$_{sinr}$. This is because 1) wireless link properties (e.g., attenuation) change over time, and the schedule generated based on historical trace data may well behave differently as network condition changes, 2) the radio model itself evolves over time [53], and 3) the generated schedule may not be the tightest tessellation of concurrent transmitters, and the SINR at receivers of a schedule may well be greater than the required minimum SINR threshold as shown in Figure 2.58. Therefore, it is important to adapt to in-situ network and environment conditions in scheduling. It is expected that the locality and high fidelity of the PRK model will enable new approaches to distributed, interference-oriented MAC protocol design, and we will study this issue in our future work.

Together with the above factors, the fact that LQF$_{sinr}$ and LQF$_{prk}$ are approximate algorithms and do not guarantee the optimality of the resulting schedules also explains why PRK

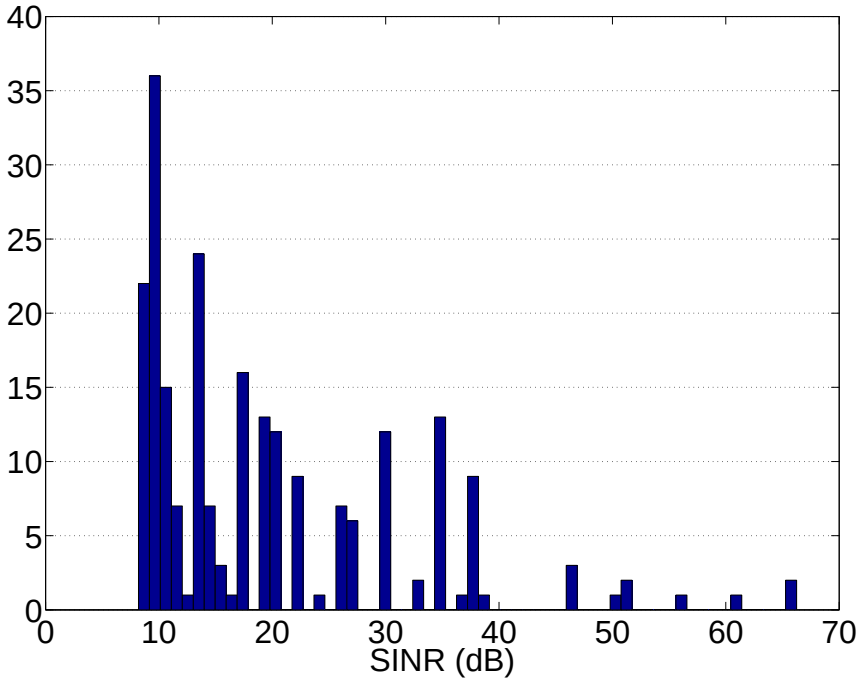

Figure 2.58: Histogram of receiver-side SINRs in a PRK schedule

schedules have slightly lower PDRs and higher throughput than SINR schedules even though the latter should have higher PDRs based on the analysis of Section 2.4. For instance, both PRK and SINR schedules ensure the minimum SINR threshold at receivers, but the actual SINRs at the receivers of SINR schedules are higher than those in PRK schedules; thus PDRs are higher in SINR schedules, and the reliability-throughput tradeoff leads to slightly lower throughput in SINR-based scheduling.

MoteLab testbed. Even though the network, traffic, and environmental settings are different for NetEye- and MoteLab-based measurement studies, we observe similar phenomena in MoteLab as those in NetEye. For instance, Figure 2.59 shows the PDR and throughput for PRK- and SINR-based scheduling in MoteLab. The figure shows the tradeoff between link reliability and network throughput in scheduling; it also shows that PRK-based scheduling enables a throughput similar to what is feasible in SINR-based scheduling while ensuring the

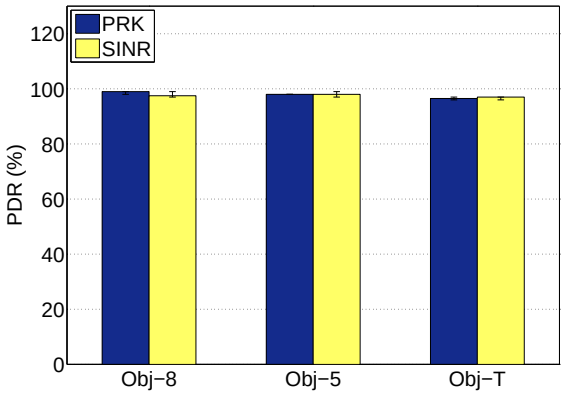

(a) PDR

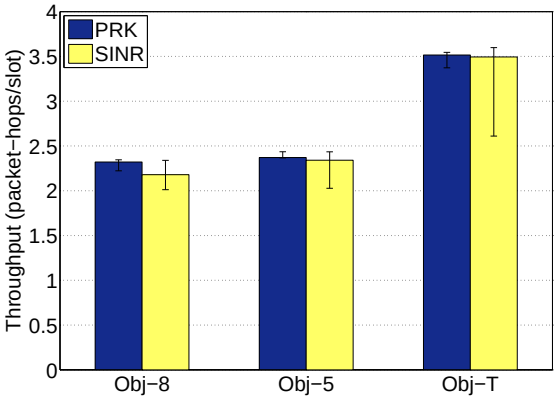

(b) Spatial throughput

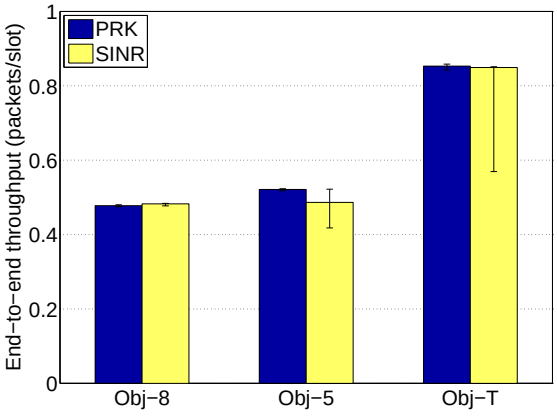

(c) End-to-end throughput

Figure 2.59: PDR and throughput in MoteLab

required link reliability.

2.8 Discussion

In this section, we examine the ratio-K and the PRK models via simulation with finite TelosB networks. We also analyze the interference modeling issues for UWB networks.

2.8.1 Simulation with finite networks

Given a set of concurrent transmissions in a finite network, the interference at different receivers may be different depending on their positions in the network. Therefore, the link reliability tends to vary across different links, and the throughput defined by Formula 2.6 becomes a local metric representing only the local spatial throughput around the neighborhood of a link. Accordingly, the minimum K required to satisfy certain link reliability, denoted by K_{min}, and the optimal K to maximize the local spatial throughput, denoted by K_{opt}, tends to vary across different links of the network. Usually, interference at the center of a network tends to be greater than that at network boundary, thus K_{min} and K_{opt} for links at network center tend to be different from those for links at network boundary. For convenience, we call this phenomenon the *boundary effect*, which does not exist in the uniform, infinite networks studied in Sections 2.2 and 2.4. To understand whether the observations in Sections 2.2 and 2.4 apply to finite networks, we study the issues of boundary effect, ratio-K instantiation, and the optimality of the PRK model in finite networks using Matlab simulation.

We consider the same system configurations studied in Section 2.5.1 except for the following changes: 1) to understand boundary effect, we add another network parameter N to denote network size (i.e., number of nodes in a network), and the set of Ns we consider are $\{64, 144, 256, 400, 576, 784, 1024, 12961600, 1936, 2304, 2704, 3136, 3600, 4096, 4624, 5184, 5776, 6400, 7056\}$; 2) to reduce simulation time, we only consider the 5 link lengths of $\{1m, 2m, 6m, 10m, 14m\}$ and the 10 node transmission probabilities (i.e., β) of $\{0.1, 0.2, 0.3, 0.4, 0.5, 0.6, 0.7, 0.8, 0.9, 1\}$. Given a link L in a system configuration and the parameter K of the ratio-K model, we simulate ratio-K-based scheduling by starting at L, and gradually add concurrent

transmission links, one at a time, that are s-closest to the set of already scheduled links and whose addition does not violate the ratio-K model; this process continues until no more concurrent transmission link can be added without violating the ratio-K model, then we compute the reliability and local spatial throughput around L based on the resulting schedule. In our simulation study, we focus on the reliability and the local spatial throughput of a link L_c at the center of the network and another link L_b that is s-farthest away from L_c. We use the same set of Ks as in Section 2.5.1 to examine the impact of different ratio-K instantiations. The observations in grid and random networks are similar, thus we only present the data for grid networks here.

Boundary effect. Let K_{min} and K'_{min} be the minimum K for satisfying certain link reliability at link L_c and L_b respectively, and let K_{opt} and K'_{opt} be the optimal K for maximizing the local spatial throughput of L_c and L_b respectively. Then we characterize the boundary effect with $\Delta K_{min} = K_{min} - K'_{min}$ and $\Delta K_{opt} = K_{opt} - K'_{opt}$.

In general, ΔK_{min} is non-negligible, but it tends to decrease as path loss exponent α increases and node transmission probability β decreases. For instance, Tables 2.4 and 2.5 show

β	[0.1, 0.2]	0.3	0.4	[0.5,0.7]	0.8	[0.9, 1]
$N = 64$	0	0	0	0.59	0.59	0.59
$N = 144$	0	0	0.59	0.59	0.59	0.82
$N = 256$	0	0	0.59	0.59	0.82	0.82
$N = 400$	0	0	0.59	0.59	0.82	0.82
$N \geq 576$	0	0.59	0.59	0.59	0.82	0.82

Table 2.4: Median ΔK_{min} in grid networks when $\alpha = 3.3$ and PDR req. = 80%

β	[0.1, 0.6]	[0.7, 1]
$N = 64$	0	0
$N \geq 144$	0	0.59

Table 2.5: Median ΔK_{min} in grid networks when $\alpha = 4.5$ and PDR req. = 80%

the median ΔK_{min}s for different configurations of grid networks when PDR req. = 80%, $\alpha =$ 3.3 or 4.5 respectively. We see that when node transmission probability is not too high (e.g.,

<0.3), ΔK_{min} is almost always 0.

Compared with ΔK_{min}, ΔK_{opt} tends to be smaller since the Ks used for maximizing throughput tends to be small (e.g., $\sqrt{2}$). For instance, ΔK_{opt} is 0 for $\sim$99% of the scenarios we study when $\alpha \geq 3.3$; When $\alpha < 3.3$, ΔK_{opt} may not be 0, but the throughput difference between using K_{opt} and K'_{opt} is very small and tends to be negligible.

Therefore, while boundary effect does affect how the ratio-K model should be instantiated in different parts of a network, its severity depends on traffic load. When traffic is not too heavy (such as in low-rate, real-time sensing and control), the boundary effect may be negligible; when traffic load is high, the locality of the PRK model may help find the right K to use through distributed, local coordination among nodes. Detailed study of this issue is a part of our future work.

Verification of analytical results. Figures 2.60 and 2.61 show the sensitivity of network

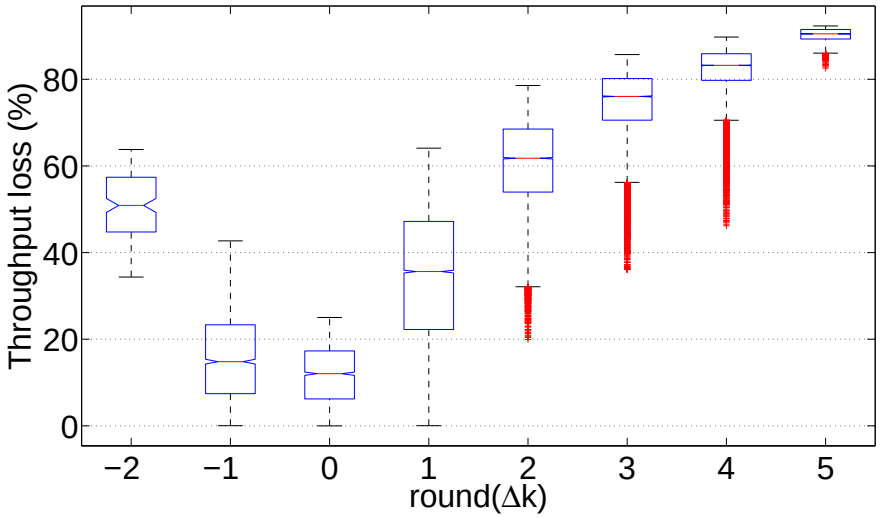

Figure 2.60: Throughput loss in finite grid networks when using $K = K_{opt} + \Delta K$

throughput and PDR to ratio-K instantiation, Figure 2.62 shows the tradeoff between reliability and throughput in ratio-K-based scheduling, and Figure 2.63 shows the throughput loss in PRK-based scheduling as compared with SINR-based scheduling. We see that observations

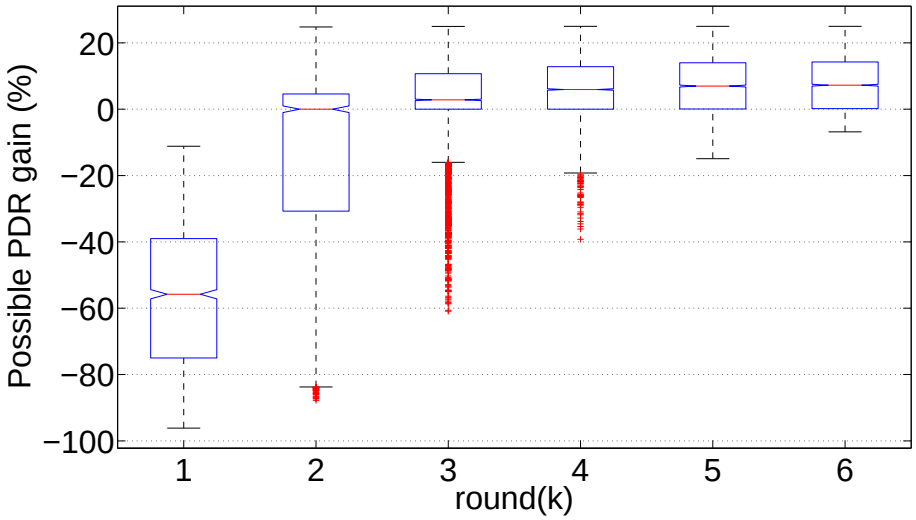

Figure 2.61: Impact of using a constant K in finite grid networks

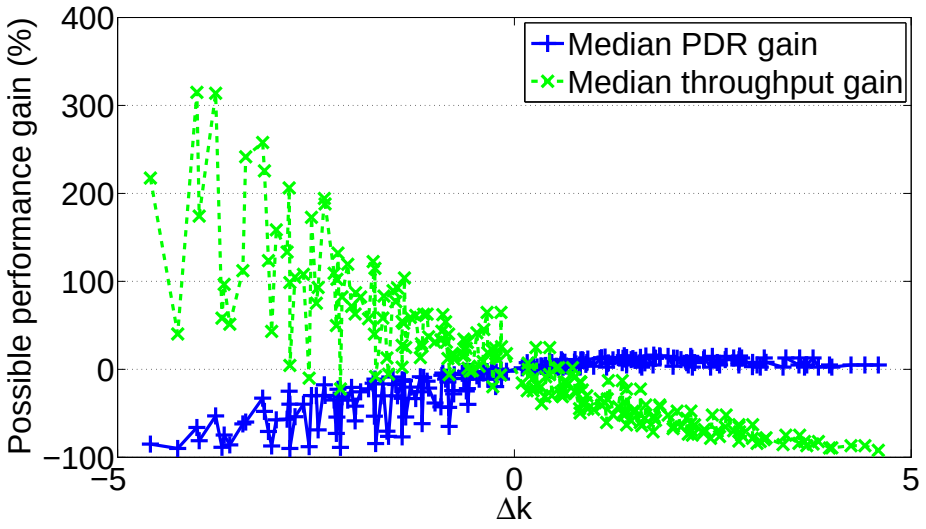

Figure 2.62: ΔK vs. performance gain in finite grid networks: PDR req. = 80%

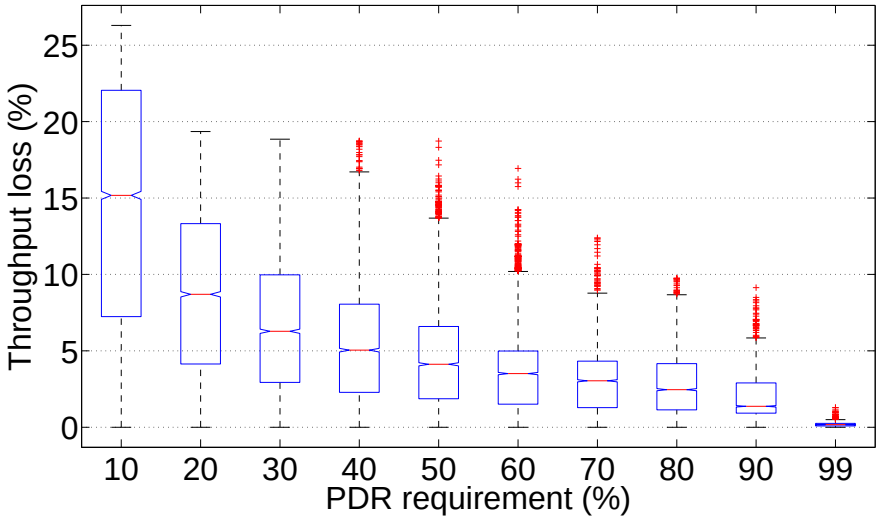

Figure 2.63: Throughput loss in the PRK model: finite grid networks

in infinite networks carry over to finite networks despite the potential boundary effect in finite networks.

2.8.2 Ultra-wideband networks

To understand whether the observations for IEEE 802.15.4 networks carry over to other wireless networks. We analyze the interference modeling issues in IEEE 802.15.4a-based ultra-wideband (UWB) networks. When analyzing UWB networks, we use the same methods as those in Sections 2.2 and 2.4, and we consider the same set of system configurations as in Section 2.5.1 except for the following: 1) we replace the CC2420 radio model with the IEEE 802.15.4a DS-UWB radio model used in [78], 2) we use the typical channel models for UWB networks as specified in [3]. The observations in grid and random networks are similar, thus we only present the data for grid networks here.

Figures 2.64 and 2.65 show the sensitivity of network throughput and PDR to ratio-K instantiation, Figure 2.66 shows the tradeoff between reliability and throughput in ratio-K-based scheduling, and Figure 2.67 shows the throughput loss in PRK-based scheduling as compared with SINR-based scheduling. We see that the observations for TelosB networks

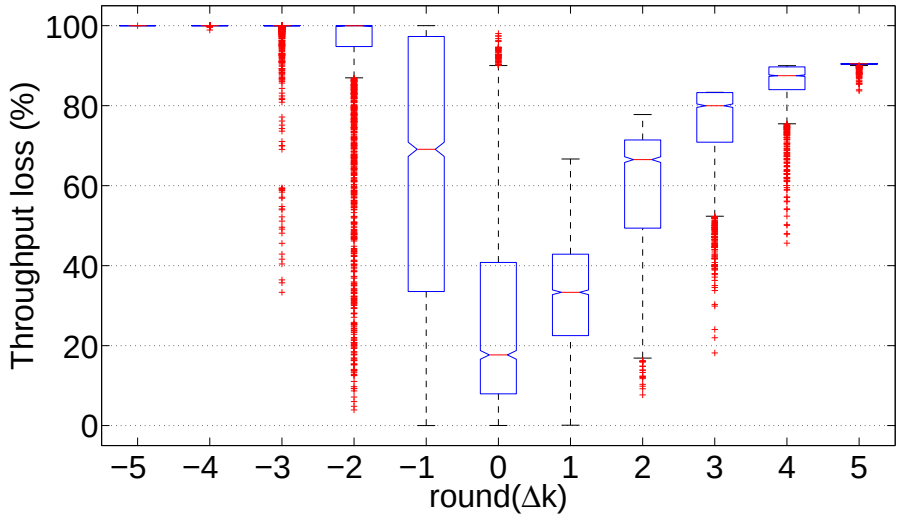

Figure 2.64: Throughput loss in UWB grid networks when using $K = K_{opt} + \Delta K$

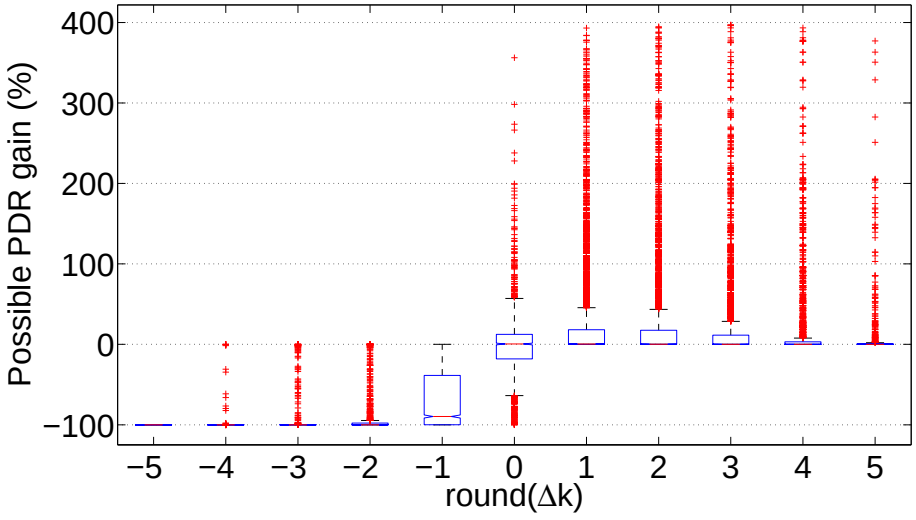

Figure 2.65: Impact of using a constant K in UWB grid networks

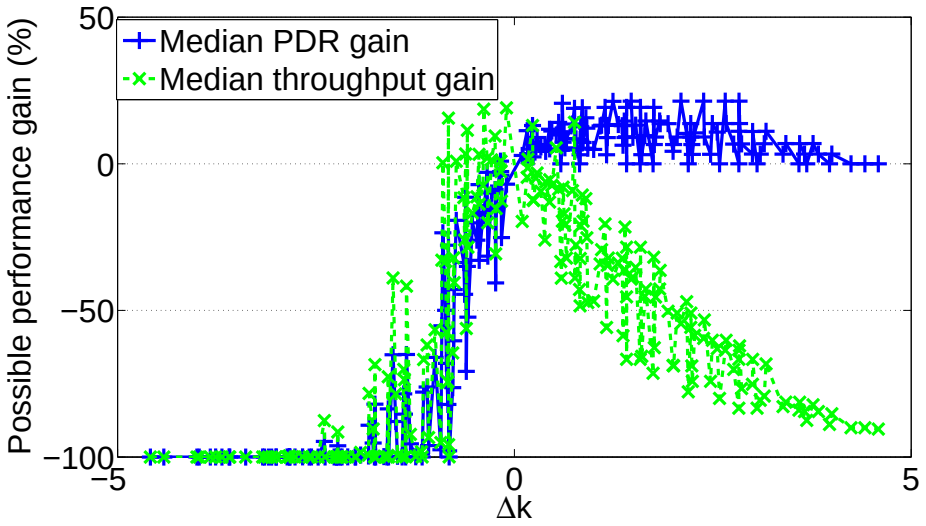

Figure 2.66: ΔK vs. performance gain in UWB grid networks: PDR req. = 80%

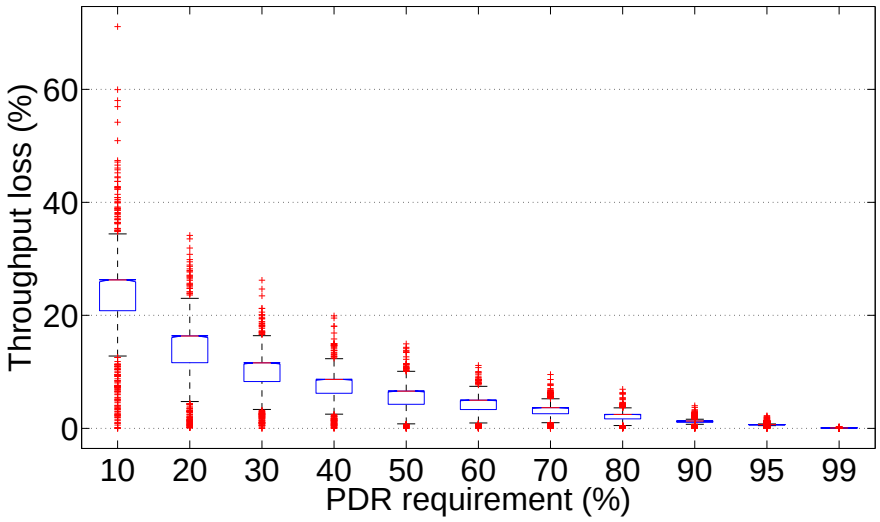

Figure 2.67: Throughput loss in the PRK model: UWB grid networks

apply to UWB networks too, even though the specific optimal K for maximizing throughput and the minimum K for satisfying certain link reliability in UWB networks tend to be less than those in TelosB networks due to the higher interference tolerance capability of UWB radios.

2.9 Related work

The seminal work of Gupta and Kumar [25] used both the ratio-K and the SINR models in analyzing the capacity of wireless networks. Since the paper did not focus on MAC protocol design, it did not study the impacts of different factors on the optimal ratio-K model, the tradeoff between reliability and throughput, and the optimality of the correctly instantiated ratio-K model.

Maheshwari et al. [40] and Moscibroda et al. [44] have studied the benefits of SINR-based scheduling as compared with ratio-K-based scheduling. Without studying the impact of different factors and the tradeoff between reliability and throughput in ratio-K-based scheduling, however, these work did not study how to best use the ratio-K model. Focusing on wireless sensing and control networks and based on comprehensive study of the behavior of ratio-K-based scheduling (in particular, the tradeoff between reliability and throughput), we propose the PRK interference model as a basis of adapting K to network and environmental dynamics in ratio-K-based scheduling. We have also studied the optimality of PRK-based scheduling through analysis, simulation, and testbed-based measurement.

Most closely related to our work is Shi et al. [56] who, in parallel with our study, examined the effectiveness of the protocol interference model for frequency scheduling (together with routing and power control). Having not focused on distributed protocol design, however, Shi et al. left it as a challenging open problem on how to efficiently choose optimal K in instantiating the ratio-K model, and the optimal K was searched by solving a series of centralized optimization problems in [56]. Through detailed study on the sensitivity of and the inherent tradeoff between throughput and reliability in ratio-K-based scheduling, we discover the simple, distributed, link reliability-based approach to instantiating the ratio-K model, and

we propose the PRK model which has both the locality of the ratio-K model and the high fidelity of the SINR model. Orthogonal to the focus of Shi et al. [56], our work also examines the effectiveness of ratio-K-based scheduling from the perspective of time scheduling and distributed protocol design, studies why PRK/ratio-K-based scheduling can be very close to the performance of SINR-based scheduling, examines the issue in wireless sensing and control networks with a wide range of system configurations (on factors such as traffic load, link length, and wireless signal attenuation), and corroborates the analytical and simulation results with testbed-based measurement.

Other approximate interference models such as hop-based model [51] and range-based model [66] have also been used in the literature, but they are either similar or inferior to the ratio-K model [40]. Therefore, we did not study those approximate models in this paper. Katz et al. [33] studied the feasibility of local interference model, where only nodes in a local neighborhood (with diameter ρ) need to coordinate with one another to ensure minimum SINR at each receiver. But they did not study the impact of various factors on the optimal ρ, nor did they study how to correctly instantiate ρ in dynamic, potentially unpredictable network and environmental settings. Sharma et al. [54] and Wang et al. [66] studied TDMA scheduling based on the ratio-K model. But Wang et al. [66] only considered the case where K is 1, and Sharma et al. [54] did not exam the impact of traffic load and node distribution on the optimal K. The simulation study of optimal K in [54] is also based on approximate instead of optimal scheduling.

Spatial reuse control based on the concept of exclusion region has been studied too [43, 67, 34, 38, 21, 49]. Nonetheless, the issue of the optimal Ks in different scenarios and the comparison between ratio-K- and SINR-based scheduling were not studied in these work. Menon et al. [43] also used the Matern Hard-core Process to analyze the distribution of interferers in a random field; but their work did not consider the impact of traffic load on optimal spatial reuse, only focused on the exclusion region around the receiver (but not the sender), and did

not study how the tradeoff between reliability and throughput affects optimal spatial reuse. The analysis in [67] and [34] used the honey-grid model which assumes the existence of a node at every point in space. The impact of traffic load on optimal spatial reuse was not studied in [67], only the exclusion region around the receiver (and not the sender) is considered in [34] for controlling transmission power and carrier sensing threshold. Only the case of single interferer is considered in [38] and [49] for controlling parameters such as carrier sensing range and transmission power. Only the case of K = 1 is considered in [21] for transmission power control.

Das et al. [20] showed that additive interference from multiple interferers significantly affect link properties, especially for links of medium-to-high quality. Maheshwari et al. [41] and Son et al. [58] studied the additivity of interfering signals (i.e., whether the aggregate signal strength of multiple interfering signals is the sum of the strength of the individual signals) for TelosB and MICA2 motes respectively, and it was found that measurement errors may affect the conclusions.

Several studies [22, 27] recently proposed mechanisms for interference cancellation where a single receiver could simultaneously receive packets from multiple senders. These results challenge the traditional paradigm where a receiver can only receive one packet at a time, and they suggest new ways of interference management. Nonetheless, interference still needs to be controlled due to the constraints of these interference cancellation mechanisms [37]. For instance, ZigZag decoding [22] works the best when the number of interferers is small (e.g., less than 6). How to schedule transmissions to take advantage of interference cancellation is an interesting problem to study, and there has been some recent effort on this [37]. But the detailed study of this issue is beyond the scope of this paper.

2.10 Concluding remarks

Through detailed analysis of how different network and environmental factors, such as traffic load and wireless signal attenuation, affect the optimal instantiation of the ratio-K model,

we showed that the performance of ratio-K-based scheduling is highly sensitive to the choice of K and that it is important to take this into account in both protocol design and performance evaluation. We then comparatively studied the performance of PRK- and SINR-based scheduling and showed that, if correctly instantiated via the PRK model, ratio-K-based scheduling can achieve a close-to-optimal performance. Our findings on PRK-based scheduling and the inherent tradeoff between reliability and throughput suggest that the ratio-K model can be effectively instantiated through link-reliability-based adaptation of K, which is amenable to distributed, local implementation too. These findings showed the feasibility of integrating the high fidelity of the SINR model with the locality of the ratio-K model, and suggested new approaches to MAC protocol design in dynamic, unpredictable network and environmental settings. Thus these findings opened up new opportunities and perspectives on interference-oriented protocol design and analysis in wireless sensing and control networks

In the immediate following chapter, we studied the benefits of the interference control in network link scheduling, based on the insight of the *PRK model* that it always silenced the ”close” node. The effort of this study leads to the result of *iOrder*.

CHAPTER 3

IORDER SCHEDULING

3.1 Background

With the development of networked embedded sensing and control, wireless networks are increasingly applied to mission-critical applications such as industrial monitoring and control [18]. This is evidenced by the recent industry standards such as WirelessHART [70] and ISA SP100.11a [63] which target wireless networked sensing and instrumentation. In supporting real-time, mission-critical tasks, these wireless networks are required to ensure real-time, reliable data delivery. In data-intensive sensing such as in camera sensor networks, it is also necessary to enable high-throughput data delivery. Nonetheless, wireless communication is subject to various dynamics and uncertainties. Due to the broadcast nature of wireless communication, in particular, concurrent transmissions may interfere with one another and introduce co-channel interference. Co-channel interference not only reduces the reliability and throughput of wireless networks, it also increases the variability and uncertainty in data communication [77]. Therefore, effectively scheduling concurrent transmissions to control co-channel interference has become critical for enabling reliable, predictable wireless communication.

Optimal interference-oriented scheduling in wireless networks has been shown to be NP-complete in general [23, 54], and the research community has proposed different polynomial-time approximation algorithms accordingly. Most approximation algorithms are greedy in nature, and two representatives are Longest-Queue-First (LQF) [35, 30, 9] and GreedyPhysical [10, 66]. When scheduling concurrent transmissions for a time slot, LQF greedily adds to the slot non-interfering links in a decreasing order of their senders' queue lengths; GreedyPhysical selects non-interfering links for the slot in a decreasing order of their interference numbers, where the interference number of a link ℓ is defined as the number of other links that

do not share any end-node with ℓ but can be interfered by ℓ. Different from the greedy algorithms, Goussevskaia et al. proposed the algorithm LengthDiversity [23]. In LengthDiversity, the links of a network are grouped into different classes based on their lengths. Links in different classes are scheduled independent of one another, and links in the same class are scheduled using virtual-grid-based coloring. LengthDiversity chooses the link lengths and the size of virtual-grids so that the resulting schedule ensures a certain minimum signal-to-interference-plus-noise-ratio (SINR) at each receiver.

When scheduling transmissions for a time slot, it is usually the interference among the transmissions that limits the number of concurrent transmissions in the slot. In approximation algorithms where links are added to a time slot in a sequential manner until reaching the interference limit,[1] the order in which links are added determines the accumulation of interference at the receivers and thus affects the number of concurrent links schedulable in the slot (see Section 3.3 for an example). Nonetheless, existing scheduling algorithms either do not take this ordering effect into account (e.g., in LQF) or do not explicitly optimize for the ordering effect (e.g., in GreedyPhysical and LengthDiversity). Thus the *open questions* are: 1) how to explicitly optimize the ordering of link addition in wireless scheduling? and 2) how does link ordering affect the throughput and delay of data delivery?

To address these open questions for insight into wireless scheduling, we formulate the concept of *interference budget* that, given a set of scheduled transmissions in a time slot, characterizes the additional interference power that can be tolerated by all the receivers without violating the application requirement on link reliability. Then, by modeling the scheduling problem as a knapsack problem, we propose the scheduling algorithm *iOrder* that optimizes link ordering by considering both interference budget and queue length in scheduling. When constructing the schedule for a time slot, iOrder first picks a link with the maximum number of queued packets; then iOrder adds links to the slot one at a time in a way that maximizes the

[1] For example, the SINR at some receiver falls below a minimum threshold.

interference budget at each step; this process repeats until no additional link can be added to the slot without violating the application requirement on link reliability.

To understand the impact of link ordering on scheduling, we first analytically prove the approximation ratio of iOrder in Poisson random networks, then we comparatively study the performance of iOrder and existing algorithms via simulation and testbed-based measurement. We observe that optimizing link ordering can improve the performance of existing algorithms by a significant margin in the case of both backlogged and online traffic, for instance, doubling the throughput and reducing the latency of LQF by a factor up to 24, and improving the throughput of LengthDiversity by a factor up to 19.6. Thus our study demonstrates the importance of explicitly optimizing link ordering in wireless scheduling, which opens up new avenues for future research and for optimizing wireless network performance. Our detailed simulation study also discover the surprisingly low performance of LengthDiversity despite its good asymptotic approximation ratio. We find that this is due to the large constant factor hidden in the analysis of LengthDiversity [23]. Therefore, it is important to examine the constant factors when analyzing wireless scheduling algorithms.

As a first step towards addressing the limiting impact of interference on wireless scheduling, our objective in this paper is to characterize the benefits of optimizing link ordering in TDMA scheduling, and we do not focus on distributed algorithm design. Nonetheless, our scheduling algorithm iOrder is amenable to distributed implementation, and we discuss potential approaches in Section 3.6; we also discuss in Section 3.6 the scenarios when centralized TDMA scheduling is also applicable without having to resort to distributed implementation.

The rest of the paper is organized as follows. We present the system models and problem definition in Section 3.2. We present algorithm iOrder in Section 3.3. Then we perform detailed simulation and measurement study of iOrder and existing algorithms in Sections 3.4 and 3.5 respectively. We discuss potential distributed approaches to implementing iOrder in Section 3.6. We present related work in Section 3.7 and concluding remarks in Section 5.

3.2 Preliminaries

Here we present the wireless channel and radio models used in the analytical and simulation parts of this paper, and we define the problem of wireless TDMA scheduling.

3.2.1 Wireless channel and radio models

Channel model. To characterize signal attenuation in wireless networks, we use the log-normal path loss model [50] which is widely adopted in protocol design and analysis. By this model, the power P_r (in dBm) of the received signal at a node distance d away from the transmitter is computed as

$$P_r = P_{tx} - PL(d_0) - 10\alpha log_{10}\frac{d}{d_0} + N(0, \sigma^2) \tag{3.1}$$

where P_{tx} is the transmission power, $PL(d_0)$ is the power decay at the reference distance d_0, α is the path loss exponent, $N(0, \sigma)$ is a Gaussian random variable with mean 0 and variance σ. In our study, we assume that all the nodes use the same transmission power, and we use different instantiations of α and σ to represent different wireless environments.

Radio model. The reception capability of a radio can be characterized by the bit error rate (BER) and the packet delivery rate (PDR) in decoding signals with specific signal-to-interference-plus-noise-ratios (SINR). Our study considers the CC2420 radios [61], which are compatible with the IEEE 802.15.4 standard and are widely used in wireless sensor network platforms such as TelosB and Tmote Sky motes. For CC2420 radio, the BER for a SINR of γ is computed as follows [2]:

$$\text{BER}(\gamma) = \frac{8}{15} \times \frac{1}{16} \times \sum_{k=2}^{16}(-1)^k \binom{k}{16} e^{(20\times\gamma\times(\frac{1}{k}-1))} \tag{3.2}$$

Accordingly, the PDR for a SINR of γ is computed as follows:

$$\text{PDR}(\gamma, f) = (1 - \text{BER}(\gamma))^{8f} \tag{3.3}$$

where f is the packet length (in units of bytes) including overhead such as packet header.

Remarks. The aforementioned models are among the most general models commonly used in the literature, even though they do not capture all the real-world phenomena such as the irregularity of wireless communication [79]. We use these models in our analysis and simulation to gain insight into wireless scheduling, and then we verify the analytical and simulation results through testbed-based measurement which captures complex real-world phenomena as we discuss in Section 3.5.

3.2.2 Problem definition

We consider wireless networks where, for the purpose of reliable data delivery, the scheduling is required to ensure a minimum signal-to-interference-plus-noise-ratio (SINR) γ_t for all the receivers involved in any transmission. Note that reliable data delivery is important not only for reliability but also for predictable data delivery latency in mission-critical networks [16].

We consider a network $G(V, E)$ where V is the set of nodes, and E is the set of directed links $\{\langle T_i, R_i\rangle : i = 1, 2, \ldots, |E|\}$; each link $\ell_i = \langle T_i, R_i\rangle$ is such that, when node T_i transmits, the signal-to-noise-ratio (SNR) at receiver R_i is no less than γ_t in the absence of interference. We assume a time-slotted system where a node can finish transmitting a packet in each time slot. We define a *slot-schedule* $\mathcal{S}_j$ for a time slot j as the set of concurrent transmitting links in slot j. Given a link ℓ_i and a slot-schedule $\mathcal{S}_j$, we define the indicator variable $I(\ell_i \in \mathcal{S}_j)$ whose value is 1 if $\ell_i \in \mathcal{S}_j$, and 0 otherwise. A slot-schedule $\mathcal{S}_j$ is *valid* if, in the presence of the concurrent transmissions of the schedule, the SINRs at all the receivers of the schedule is no less than γ_t and there is no primary interference between the concurrent transmissions.[2] γ_t can be chosen based on the desired packet delivery rate (PDR) and formula (3.3). To ensure a high PDR (e.g., close to 100%), we use a SINR threshold $\gamma_t = 5dB$ in most places of this paper unless specified otherwise. A *schedule* $\mathbb{S}$ consists of a sequence of slot-schedules

[2]There is primary interference between two links ℓ_i and ℓ_j if ℓ_i and ℓ_j share any common end-node.

$\mathcal{S}_j, j = 1, 2, \ldots$, and $\mathbb{S}$ is valid if $\mathcal{S}_j$ is valid for every time slot j.

We consider two types of traffic models: backlogged traffic and online traffic. In the case of backlogged traffic, every transmitter T_i has L_i ($L_i \geq 0$) number of queued packets to be delivered to the receiver R_i. In the case of online traffic, packets arrive at each transmitter T_i over time and need to be delivered to the receiver R_i.

For backlogged traffic, we define the following *backlog-scheduling* problem:

Problem $\mathbb{P}_{bl}$: Given L_i queued packets at each transmitter T_i ($i = 1, \ldots, |E|$), find a valid schedule $\mathbb{S}_{bl} = \{\mathcal{S}_1, \mathcal{S}_2, \ldots\}$ such that $\sum_{\mathcal{S}_j \in \mathbb{S}_{bl}} I(\ell_i \in \mathcal{S}_j) = L_i$ for every i and that $|\mathbb{S}_{bl}| \leq |\mathbb{S}'|$ for every other valid schedule $\mathbb{S}'$ with $\sum_{\mathcal{S}_{j'} \in \mathbb{S}'} I(\ell_i \in \mathcal{S}_{j'}) = L_i$ for every i.

For online traffic, we define the following *slot-scheduling* problem such that scheduling online traffic becomes solving the slot scheduling problem for each time slot:

Problem $\mathbb{P}_s$: Given a link $\ell_i \in E$, find a valid slot-schedule $\mathcal{S}_{\ell_i}$ such that $\ell_i \in \mathcal{S}_{\ell_i}$, and $|\mathcal{S}_{\ell_i}| \geq |\mathcal{S}'|$ for every other valid slot-schedule $\mathcal{S}'$ with $\ell_i \in \mathcal{S}'$.

Note that, by combining the backlog and online traffic models, we can model hybrid traffic patterns where there is both backlog and online traffic; but, to be concise, we skip the detailed discussion on hybrid traffic models in this paper.

3.3 Algorithm iOrder

In what follows, we first demonstrate the drawbacks of existing scheduling algorithms by examining their behavior in solving an example slot-scheduling problem, then we present our algorithm iOrder and analyze its approximation ratio and time complexity.

3.3.1 A motivating example

We consider a simple convergecast network as shown in Figure 3.1, where every node has a CC2420 radio and uses a transmission power of $-25dBm$ (a.k.a. power level 3 [61]), and each link is 3.06 meters long. The environment is a typical indoor environment with path loss exponent $\alpha = 3.5$, reference distance $d_0 = 1$ meter, and $PL(d_0) = 55dBm$; the mean back-

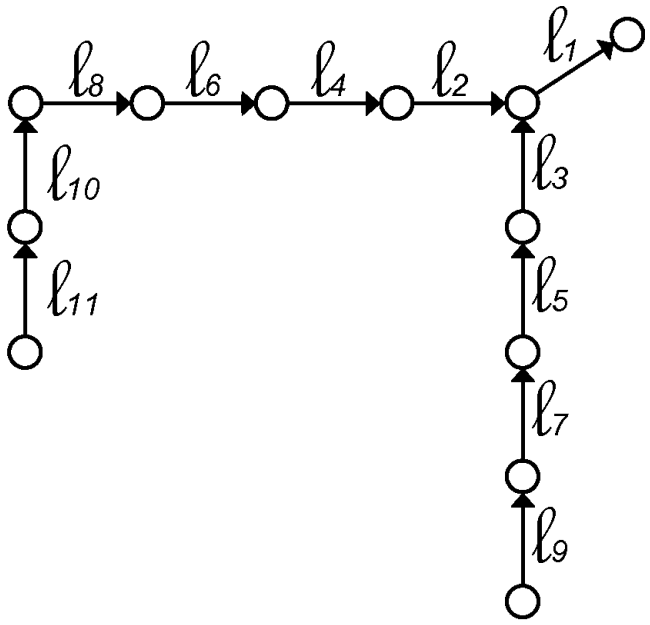

Figure 3.1: A simple network

ground noise power is $-105dBm$. This network setup ensures, in the absence of concurrent transmissions, a signal-to-noise ratio (SNR) of $8dB$ for every receiver of a transmitting link. We consider a state of the network where the number of queued packets, denoted by L_i, for each link ℓ_i $(i = 1, 2, \ldots, 11)$ satisfies the following:

$$\begin{aligned} &L_1 > L_k, && 2 \leq k \leq 11 \\ &L_{2k} > L_{2k+2}, && 1 \leq k \leq 3 \\ &L_{2k} = L_{2k+1}, && 1 \leq k \leq 4 \\ &L_8 > L_{10} > L_{11} \end{aligned}$$

We consider the slot-scheduling problem $\mathbb{P}'_s$ where we want to find a largest valid schedule that includes link ℓ_1 and ensures a minimum SINR γ_t of $6dB$ at all the receivers. For convenience, we define the *hop distance* between two links ℓ_i and ℓ_j $(i \neq j)$ as the number of links in the shortest path connecting any end-node of ℓ_i to any end-node of ℓ_j. With the network setup and minimum SINR requirement of $6dB$, any two links whose hop distance is 0 or 1 can

interfere with each other, but any two links whose hop distance is no less than 2 do not interfere with each other in the absence of other concurrent transmissions. For instance, if links ℓ_1 and ℓ_4 transmit together, the SINR at the receiver of ℓ_4 is $0.64dB$ which is below the SINR threshold of $6dB$; on the other hand, if ℓ_1 and ℓ_6 transmit together in the absence of other transmissions, the SINR at the receiver of ℓ_1 and ℓ_6 is 7.75dB and 6.08dB respectively, thus ℓ_1 and ℓ_6 do not interfere with each other in this case.

For problem $\mathbb{P}'_s$, an optimal solution $\mathcal{S}_{opt}$ is $\{\ell_1, \ell_{11}, \ell_9\}$ where the SINR at the receiver of ℓ_1, ℓ_{11}, and ℓ_9 is $7.81dB$, $7.71dB$, and $7.28dB$ respectively. That is, three concurrent links can be scheduled together for $\mathbb{P}'_s$. In what follows, we examine how the existing algorithms LQF [35], GreedyPhysical [10], and LengthDiversity [23] will behave for problem $\mathbb{P}'_s$.

LQF. When constructing a slot-schedule $\mathcal{S}_{gms}$, LQF selects links in a decreasing order of the number of packets queued at their senders. Therefore, LQF will consider links ℓ_6 or ℓ_7 first. Without loss of generality, we assume that LQF picks ℓ_6 at random. As discussed earlier, ℓ_1 and ℓ_6 can transmit concurrently in the absence of other transmitters. Once ℓ_6 is added into the slot-schedule, however, no other link can be added without making the SINR at the receiver of ℓ_6 lower than $6dB$ (which is the minimum SINR allowed by problem $\mathbb{P}'_s$). For instance, if we also add ℓ_9 to the slot-schedule $\{\ell_1, \ell_6\}$, the SINR for the receiver of ℓ_6 will become $5.98dB$. Therefore, LQF will generate the slot-schedule $\mathcal{S}_{gms} = \{\ell_1, \ell_6\}$, which is one link less than the optimal slot-schedule $\mathcal{S}_{opt} = \{\ell_1, \ell_{11}, \ell_9\}$ in concurrency.

GreedyPhysical. When constructing a slot-schedule $\mathcal{S}_{gp}$, GreedyPhysical selects links in a decreasing order of their interference number. Among all the links at least 2-hop away from ℓ_1, ℓ_6 has the largest interference number. Thus GreedyPhysical first selects ℓ_6 to add to the partial slot-schedule $\{\ell_1\}$, after which no more links can be added (similar to the case in LQF). Therefore, $\mathcal{S}_{gp} = \{\ell_1, \ell_6\}$, which is one link less than the optimal slot-schedule $\mathcal{S}_{opt}$ in concurrency.

LengthDiversity. LengthDiversity divides the network links into different classes and then

schedule the individual link classes independent of one another. The k-th class $\mathcal{C}_k$ $(k = 0, 1, ...)$ consists of links whose length is in the range $[2^k, 2^{k+1})$. When scheduling links of a class $\mathcal{C}_k$, LengthDiversity first partitions the deployment area of those links into a square grid where each cell has a side length $\mu 2^k$, with $\mu = 4\left(8\gamma_t \cdot \frac{\alpha-1}{\alpha-2}\right)^{\frac{1}{\alpha}}$; it then 4-color the cells so that no neighboring cells have the same color and only the links whose receivers are inside the cells of the same color can transmit concurrently. For the example problem $\mathbb{P}'_s$, $\mu = 12.4$ meters. Therefore, only one link is allowed to transmit at a time in LengthDiversity, and the slot-schedule for $\mathbb{P}'_s$ is $\mathcal{S}_{ld} = \{\ell_1\}$, which is two links less than the optimal slot-schedule $\mathcal{S}_{opt}$ in concurrency.

Goussevskaia et al. [23] proved an approximation ratio $\delta_{ld} = C_{ld}g(L) = O(g(L))$ for LengthDiversity, where $g(L)$ is the logarithm of the largest ratio between the lengths of any two links in the network, and the constant factor $C_{ld} = \frac{4(2(\sqrt{2}\mu+1))^\alpha}{\gamma_t}$. Note that LengthDiversity does not consider the inner structure within cells in scheduling and the constants μ and C_{ld} are usually large (see Table 3.1), which lead to its low performance as shown in the above example and in Section 3.4.

	μ		C_{ld}	
α	$\gamma_t = 5dB$	$\gamma_t = 8dB$	$\gamma_t = 5dB$	$\gamma_t = 8dB$
2.5	22.6	29.8	4.5e+4	4.4e+4
3.5	11.7	14.1	3.2e+5	3.1e+5
4.5	8.8	10.3	3.5e+6	3.3e+6

Table 3.1: Constants μ and C_{ld} in LengthDiversity

3.3.2 Scheduling for maximal interference budget

From Section 3.3.1, we see that interference is a major factor for limiting the number of concurrent transmissions in a time slot. Existing algorithms LQF, GreedyPhysical, and LengthDiversity do not explicitly consider or minimize interference accumulation during scheduling, thus leading to performance loss. To understand the impact of considering interference accumulation in scheduling, we propose the algorithm *iOrder* that tries to minimize interference accumulation and maximize the additional interference that can be tolerated by all the receivers

of a time slot without violating application requirement on link reliability. To this end, we first define the *interference budget of a valid slot-schedule* $\mathcal{S}_{\ell_i}$, denoted by $I_b(\mathcal{S}_{\ell_i})$, as the maximum extra interference that can be tolerated by all the receivers of $\mathcal{S}_{\ell_i}$ without invalidating $\mathcal{S}_{\ell_i}$. Formally, let P_{ℓ_j} be the strength of the signal from the sender to the receiver of link ℓ_j, P_{noise,ℓ_j} be the background noise power at the receiver of ℓ_j, and I_{ℓ_k,ℓ_j} be the strength of the signal reaching the receiver of ℓ_j from the sender of ℓ_k. Then the maximum extra interference that can be tolerated by the receiver of a link $\ell_j \in \mathcal{S}_{\ell_i}$, denoted by $I_b(\ell_j)$, satisfies

$$\frac{P_{\ell_j}}{P_{noise,\ell_j} + \sum_{\ell_k \in \mathcal{S}_{\ell_i}, \ell_k \neq \ell_j} I_{\ell_k,\ell_j} + I_b(\ell_j)} = \gamma_t.$$

Thus

$$I_b(\ell_j) = \frac{P_{\ell_j}}{\gamma_t} - P_{noise,\ell_j} - \sum_{\ell_k \in \mathcal{S}_{\ell_i}, \ell_k \neq \ell_j} I_{\ell_k,\ell_j}.$$

Therefore,

$$\begin{aligned} I_b(\mathcal{S}_{\ell_i}) &= min_{\ell_j \in \mathcal{S}_{\ell_i}} I_b(\ell_j) \\ &= min_{\ell_j \in \mathcal{S}_{\ell_i}} (\tfrac{P_{\ell_j}}{\gamma_t} - P_{noise,\ell_j} - \textstyle\sum_{\ell_k \in \mathcal{S}_{\ell_i}, \ell_k \neq \ell_j} I_{\ell_k,\ell_j}). \end{aligned} \tag{3.4}$$

Then, for the slot-scheduling problem $\mathbb{P}_s$, we can add to the schedule $\mathcal{S}_{\ell_i}$ one link at a time, and pick the link that maximizes the interference budget of the extended schedule each time a link is to be added. We denote this algorithm as *iOrder-slot* and present it in Algorithm 1. This

Algorithm 1 iOrder-slot(ℓ_i, E)

Require: starting link ℓ_i, a set E of links where $\ell_i \notin E$
Ensure: a valid slot-schedule $\mathcal{S}_{\ell_i}$ such that $\ell_i \in \mathcal{S}_{\ell_i}$

```
S_{ℓ_i} = {ℓ_i}, E' = E;
Compute the set of schedulable links: E_c = {ℓ_k : ℓ_k ∈ E', S_{ℓ_i} ∪ {ℓ_k} is a valid schedule};
while E_c ≠ ∅ do
    ℓ_j = argmax_{ℓ_k ∈ E_c} I_b(S_{ℓ_i} ∪ ℓ_k);
    S_{ℓ_i} = S_{ℓ_i} ∪ ℓ_j, E' = E' \ {ℓ_j};
    E_c = {ℓ_k : ℓ_k ∈ E', S_{ℓ_i} ∪ {ℓ_k} is a valid schedule};
end while
Return schedule S_{ℓ_i}.
```

algorithm design is similar to approximation algorithms to the knapsack problem [29] in the sense that the interference budget serves as the constraint on the total amount of interference and thus the total number of links allowed for a time slot.

For online traffic, we can apply iOrder-slot to generate a schedule for every time slot. As we will show in Section 3.4, the choice of the starting link ℓ_i does not significantly affect the size/optimality of the resulting schedule $\mathcal{S}_{\ell_i}$. For the purpose of stabilizing queueing in the network, therefore, we can choose a link with the maximum number of queued packets as the starting link. We denote this algorithm for online traffic as *iOrder-ol* and present it in Algorithm 2.

Algorithm 2 iOrder-ol(m, E_m)

Require: a set E_m of non-empty links where each link ℓ_i has L_i queued packets at the beginning of the m-th time slot

Ensure: a valid slot-schedule $\mathcal{S}_m$ for the m-th time slot

1: $\ell_j = \text{argmax}_{\ell_k \in E_m} L_k$;
2: Return iOrder-slot($\ell_j, E_m \setminus \{\ell_j\}$).

For backlogged traffic, we can also apply iOrder-slot to generate the schedule for each time slot in an iterative manner until all the packet transmissions are scheduled. For stabilizing packet queues, we select the link with the maximum number of remaining packets to be scheduled as the starting link for each time slot. We denote this algorithm for backlogged traffic as *iOrder-bl* and present it in Algorithm 3.

In what follows, we use the general term *iOrder* to refer to any of the algorithms iOrder-slot, iOrder-ol, or iOrder-bl; the context will clarify which one we refer to exactly.

Now let's revisit the example problem $\mathbb{P}'_s$ discussed in Section 3.3.1. iOrder will first select link ℓ_{11} to add to the schedule $\{\ell_1\}$, and the resulting SINR at the receiver of ℓ_1 and ℓ_{11} is $7.93dB$ and $7.81dB$ respectively, both of which are more than $1dB$ above the required $\gamma_t = 6dB$. Accordingly, iOrder can add a third link ℓ_9 to the slot-schedule $\{\ell_1, \ell_{11}\}$ while still maintaining its validity. In the end, iOrder generates an optimal schedule $\{\ell_1, \ell_{11}, \ell_9\}$ for problem $\mathbb{P}'_s$, and the resulting SINR at the receiver of ℓ_1, ℓ_{11}, and ℓ_9 is $7.81dB$, $7.71dB$, and

Algorithm 3 iOrder-bl(E)

Require: a set E of non-empty links where each link ℓ_i has L_i queued packets
Ensure: a valid schedule $\mathbb{S}_E$ for transmitting all the queued packets

$\mathbb{S}_E = \emptyset$, $E' = E$;
while $E' \neq \emptyset$ **do**
  $\ell_j = \text{argmax}_{\ell_k \in E'} L_k$;
  $\mathcal{S}_{\ell_j}$ = iOrder-slot($\ell_j, E' \setminus \{\ell_j\}$);
  $\mathbb{S}_E = \mathbb{S}_E \cup \{\mathcal{S}_{\ell_j}\}$;
  for all $\ell_k \in \mathcal{S}_{\ell_j}$ **do**
    $L_k = L_k - 1$;
    if $L_k = 0$ **then**
      $E' = E' \setminus \{\ell_k\}$;
    end if
  end for
end while
Return $\mathbb{S}_E$.

$7.28dB$ respectively. Thus iOrder outperforms existing algorithms for this example problem $\mathbb{P}'_s$.

Approximation ratio. Given that iOrder-slot is a basic element of the iOrder algorithm family (i.e., iOrder-slot, iOrder-ol, iOrder-bl), we analyze the optimality of iOrder-slot in solving the slot-scheduling problem $\mathbb{P}_s$, which will also shed light on the potential effectiveness of iOrder-ol and iOrder-bl. As in the literature [10], we consider the following Poisson network $\mathbb{G}$: n nodes are uniformly distributed on a 2D plane at random with a density of λ nodes per unit area; for connectivity of the network, the transmission range $r_0(n) = 2\sqrt{\frac{log(n)}{\pi\lambda}}$ for every node, and that the transmission power $P_{tx}(n) = \frac{(\gamma_t+\gamma_b)P_{noise}(r_0(n))^\alpha}{G_0}$ such that the signal-to-noise-ratio (SNR) is $\gamma_t + \gamma_b$ at receivers in the absence of interference, where P_{noise} is the background noise power, α is the path loss exponent of the wireless channel, and G_0 is the signal power gain at a reference distance d_0. Then we have

Theorem 1. *For network $\mathbb{G}$, the approximation ratio $\delta(n)$ of algorithm iOrder is no more than*

$$\frac{P_{tx}G_0(\pi + \frac{2\pi}{\alpha-2}(1 - (\frac{n}{\pi\lambda})^{\frac{2-\alpha}{2}}))U_{opt}}{I_b\pi(r_{ci}(n))^2}, \tag{3.5}$$

where $U_{opt} = min\{1 + \frac{I_b(r_{ci}(n))^\alpha}{P_{tx}G_0}, \pi(r_{ci}(n))^2\lambda\}$, $I_b = \frac{\gamma_b}{\gamma_t}P_{noise}$, $r_{ci}(n) = r_0(n)(\frac{n}{lnn})^{\frac{1}{2}-\frac{1}{\Gamma(\alpha)+\epsilon}}$, $\Gamma(\alpha) = \frac{1}{2} + \frac{\sqrt{9\alpha^2-20\alpha+4}}{2(\alpha-2)}$, *and* ϵ *is any arbitrarily small positive number.*

Proof. For convenience, we denote the optimal scheduling algorithm as OPT. To characterize the approximation ratio of iOrder, we consider an arbitrary link $\langle n_t, n_r\rangle$ (with n_r being the receiver) in a large network $\mathbb{G}$, and compare the maximum single-slot schedule that includes $\langle n_t, n_r\rangle$ in iOrder and OPT. According to [10], there exists a "close-in" region $\mathbb{R}_{ci}$ of radius $r_{ci}(n)$ that is centered at n_r such that interference outside the region converges to 0 as $n \to 0$. Thus we focus on the number of concurrent transmitters in $\mathbb{R}_{ci}$ that are allowed in the schedules of iOrder and OPT.

In the schedule $\mathcal{S}_o$ that is generated by OPT, let I_b be the largest interference power that can be introduced to receiver n_r by all the transmitters other than n_t such that the SINR at n_r is no less than the required threshold γ_t. Then

$$\frac{P_{tx}G_0(r_0(n))^{-\alpha}}{P_{noise} + I_b} = \gamma_t$$

Thus

$$I_b = \frac{P_{tx}G_0(r_0(n))^{-\alpha}}{\gamma_t} - P_{noise}$$

Since $P_{tx}(n) = \frac{(\gamma_t+\gamma_b)P_{noise}(r_0(n))^\alpha}{G_0}$,

$$I_b = \frac{\gamma_b}{\gamma_t}P_{noise} \tag{3.6}$$

The expected number of concurrent transmitters in $\mathcal{S}_o$, denoted by N_{opt}, is maximized if all the transmitters except n_t (called *interferers* hereafter) is on the boundary of the close-in region $\mathbb{R}_{ci}$. In this case, the interference power P_{ci} introduced by each of the interferer is such that

$$P_{ci} = \frac{P_{tx}G_0}{(r_{ci}(n))^\alpha}$$

Thus the total number of interferers N'_{opt} is such that

$$N'_{opt} \leq \frac{I_b}{P_{ci}} = \frac{I_b(r_{ci}(n))^\alpha}{P_{tx}G_0}$$

Thus $N_{opt} = 1 + N'_{opt} \leq 1 + \frac{I_b(r_{ci}(n))^\alpha}{P_{tx}G_0}$. Since the total expected number of nodes in region $\mathbb{R}_{ci}$ is $\pi(r_{ci}(n))^2\lambda$, thus $N_{opt} \leq \pi(r_{ci}(n))^2\lambda$. Therefore,

$$N_{opt} \leq min\{1 + \frac{I_b(r_{ci}(n))^\alpha}{P_{tx}G_0}, \pi(r_{ci}(n))^2\lambda\} \tag{3.7}$$

In the schedule $\mathcal{S}'_i$ generated by iOrder for the Poisson network $\mathbb{G}$, concurrent transmitters are uniformly distributed in region $\mathbb{R}_{ci}$. This is because, in the process of generating $\mathcal{S}'_i$ in a uniform geometric network $\mathbb{G}$, iOrder will pick a transmitter that is of the maximum minimum distance to the receivers of all the links already scheduled in $\mathcal{S}'_i$. In a large network, this selection process will lead to a set of statistically uniformly distributed transmitters. From the results of Che et al. [16] on the spatial distribution of concurrent transmitters, the spatial process of transmitters in $\mathcal{S}'_i$ can be approximated by a thinning process Φ of $\mathbb{G}$ [59] where a typical node in $\mathbb{G}$ is retained in Φ with some probability p, and the set of transmitters in region $\mathbb{R}_{ci}$ are the nodes of Φ that lie in $\mathbb{R}_{ci}$. That is, the set of transmitters in schedule $\mathcal{S}'_i$ can be approximated as a spatial Poisson process Φ with density $p\lambda$, and the schedule $\mathcal{S}_i$ that iOrder generates for region $\mathbb{R}_{ci}$ consists of the nodes of Φ that lie in $\mathbb{R}_{ci}$. According to [26] and given that the radius of $\mathbb{G}$ is $\sqrt{\frac{n}{\pi\lambda}}$, the interference I'_b that is incurred to receiver n_r can be calculated as

$$I'_b = P_{tx}G_0p\lambda(\pi + \frac{2\pi}{\alpha - 2}(1 - (\frac{n}{\pi\lambda})^{\frac{2-\alpha}{2}}))$$

Since network $\mathbb{G}$ is large, $I'_b \approx I_b$. Thus

$$p \approx \frac{I_b}{P_{tx}G_0\lambda(\pi + \frac{2\pi}{\alpha-2}(1 - (\frac{n}{\pi\lambda})^{\frac{2-\alpha}{2}}))}$$

$\widehat{\delta}(n)$	n=50	n=100	n=200
α=2.5	6.6	6.3	11.2
α=3.5	11.1	11.7	11.5
α=4.5	15	16.9	18.1

Table 3.2: $\widehat{\delta}(n)$: upper bound on the approximation ratio of iOrder

$\widehat{\delta}(n)$	n=50	n=100	n=200
α=2.5	50	79.2	118.4
α=3.5	32.8	45	60.8
α=4.5	27.4	36.2	47

Table 3.3: $\tilde{\delta}(n)$: approximation ratio of GreedyPhysical

(Note that the path loss exponent $\alpha \geq 2$, thus $0 \leq p \leq 1$.) Therefore, the expected number of transmitters, denoted by N_{iOrder}, in the schedule $\mathcal{S}_i$ of iOrder for region $\mathbb{R}_{ci}$ is calculated as follows:

$$N_{iOrder} \approx p\lambda\pi(r_{ci}(n))^2 = \frac{I_b\pi(r_{ci}(n))^2}{P_{tx}G_0(\pi + \frac{2\pi}{\alpha-2}(1-(\frac{n}{\pi\lambda})^{\frac{2-\alpha}{2}}))} \tag{3.8}$$

Therefore, the approximation ratio $\delta(n)$ of iOrder calculates as follows:

$$\begin{aligned} \delta(n) &= \frac{N_{opt}}{N_{iOrder}} \\ &\leq \frac{P_{tx}G_0(\pi+\frac{2\pi}{\alpha-2}(1-(\frac{n}{\pi\lambda})^{\frac{2-\alpha}{2}}))min\{1+\frac{I_b(r_{ci}(n))^\alpha}{P_{tx}G_0},\pi(r_{ci}(n))^2\lambda\}}{I_b\pi(r_{ci}(n))^2} \end{aligned} \tag{3.9}$$

□

We use $\widehat{\delta}(n)$ to denote the upper bound of $\delta(n)$ as shown in Formula (3.5). For a setting of $\lambda = 3$, $\gamma_t = 5dB$, $\gamma_b = 3dB$, $P_{noise} = -95dBm$, $G_0 = 1$, and $\epsilon = 0.1$, Table 3.2 shows the upper bounds for the approximation ratios of iOrder with different network size n and wireless path loss exponent α. We see that the approximation ratio of iOrder tends to be small, especially in small networks. Note also that our approved approximation ratio of iOrder is orders-of-magnitude smaller than the proved approximation ratio of LengthDiversity as shown in Table 3.1. The proved approximation ratio of GreedyPhysical [10] in the SINR model is $\tilde{\delta}(n) = \min\{\pi\lambda(r_{ci}(n))^2, n\}$ (with $r_{ci}(n)$ defined in Theorem 1); Table 3.3 shows $\tilde{\delta}(n)$, from which we see that the approximation ratio of GreedyPhysical is significantly greater than that

of iOrder too. The approximation ratio of LQF also tends to be large because, in the worst case, only two concurrent transmissions are allowed in the whole network when the two most queued transmitters are close to one another and can transmit concurrently. To corroborate these analytical results in a wide range of scenarios, we next study the performance of iOrder and the existing algorithms through simulation and testbed-based measurement in Section 3.4 and Section 3.5 respectively.

Time complexity. Assuming the basic operation in computing time complexity is computing the SINR at a receiver in the presence of concurrent transmissions, it is not difficult to find that the time complexity for algorithm iOrder-slot is $O(|E|^3)$. Accordingly, the time complexity for iOrder-ol is $O(|E_m|^3)$, similar to that of iOrder-slot. To compute the time complexity for iOrder-bl, we can replace each link ℓ_i (having L_i queued packets) with L_i virtual links $\ell_{i,1}, \ldots, \ell_{i,L_i}$, each of which has only one queued packet. Then the system will consist of $\sum_{\ell_i \in E} L_i$ number of virtual links. The time complexity for the lines 3-11 of iOrder-bl is dominated by that of line 4 (i.e., iOrder-slot), thus their time complexity is $O((\sum_{\ell_i \in E} L_i)^3)$. Accordingly, it is easy to see that the time complexity for iOrder-bl is $O((\sum_{\ell_i \in E} L_i)^4)$.

3.4 Simulation

To gain insight into the impact of link ordering on wireless scheduling, we comparatively study different scheduling algorithms via simulation. We first discuss the simulation methodology and then the simulation results. The insight gained through this simulation study will be verified via testbed-based measurement in Section 3.5.

3.4.1 Simulation methodology

We have built a custom simulation package using Matlab. To understand the potential impact that the environmental and network settings have on the behavior of different algorithms, we use networks of different scales and different wireless channel parameters. More specifically, we consider the set $\{2.5, 3, 3.5, 4, 4.5, 5, 5.5, 6\}$ of wireless path loss exponents αs, which

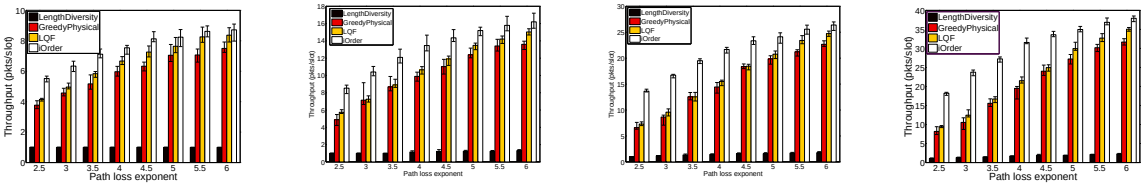

(a) 5×5 networks (b) 7×7 networks (c) 9×9 networks (d) 11×11 networks

Figure 3.2: Network throughput in different algorithms

represent a wide range of real-world environments [57]; we also set the shadowing variance σ based on measurement data from [57]. We consider 2D Poisson networks with the node distribution density $\lambda = 1$ node$/m^2$ and the background noise power $P_{noise} = -95dBm$. Given an environmental setting (i.e., specific values for α and σ), we set the transmission power P_{tx} of all the nodes such that every node has, on average, 10 neighbors to which the signal-to-noise-ratio (SNR) is above the threshold $\gamma_t = 5dB$ in the absence of interference. Then we choose the average link length r_0 such that receivers r_0 distant from their transmitters have a SNR of $\gamma_t + \gamma_b$. We set γ_t as $5dB$ to ensure 100% link reliability during scheduling. We call γ_b the *starting SINR budget*, and $\gamma_b = 1dB$ in this paper unless mentioned otherwise;

We consider networks that are deployed in squares with side lengths kr_0, where $k = 5, 7, 9, 11$. For convenience, we denote the network deployed in a square of side length kr_0 as a $k \times k$ network. For $k = 5, 7, 9, 11$, the average number of nodes in a $k \times k$ network is $70, 140, 237$, and 346 respectively in our simulation.

Given an average link length r_0, we consider one-hop unicast where the receiver n_r of a node n_t is the node whose distance to n_t is the closest to r_0, with ties broken at random. (We will study multi-hop convergecast in Section 3.5.) For each node, we consider the case of backlogged traffic as well as online traffic. In the backlogged traffic pattern, each node has m number of packets queued for transmission, where m is a Poisson random variable with mean being 30. In the online traffic pattern, packets arrive at each node in a Poisson manner with an average rate of 0.15 packet/time-slot,[3] and we assume packet arrivals happen at the

[3]The average arrive rate of 0.15 packet/slot is chosen so that it does not exceed the capacity of many of the

very beginning of the individual time slots. Backlogged traffic represents the case where nodes need to upload stored data, and network throughput (i.e., total number of packets delivered per time slot in the network) is an important performance metric. Online traffic can represent the case of real-time sensing and control, and packet delivery latency as well as queue length are important performance metrics. When simulating online traffic, we assume that packet queues are managed in a FIFO manner. We set the queue size to be large enough (e.g., 20) to avoid queue overflow.

Using the above experiment design, we evaluate the performance of LengthDiversity, Greedy-Physical, LQF, and iOrder.For each scheduling algorithm and each configuration of environmental, network, and traffic parameters, we repeat the experiment 20 times such that we can analyze the variability and confidence intervals of performance metrics. (Note that, since we have analyzed the approximation ratios of the above algorithms in Section 3.3, here we do not numerically compute the performance of optimal scheduling due to its NP-completeness [23] and the intractable computation time for large networks.)

3.4.2 Simulation results

In what follows, we first discuss the results for backlogged traffic and then for online traffic. The data presented in most of the figures include the medians and their 95%confidence intervals of the corresponding metrics (e.g., throughput and delay).

3.4.3 Backlogged traffic

For networks of different scales and different wireless path losses, Figure 3.2 shows the network throughput of different scheduling algorithms. We see that, except for LengthDiversity, there is a clear throughput increase in all the algorithms as network size or path loss exponent increases. This is because larger network size or path loss exponent implies higher degree of spatial reuse possible in scheduling. Among all the algorithms, iOrder always performs better than the other algorithms. For instance, iOrder may double the throughput of LQF in large

networks we study.

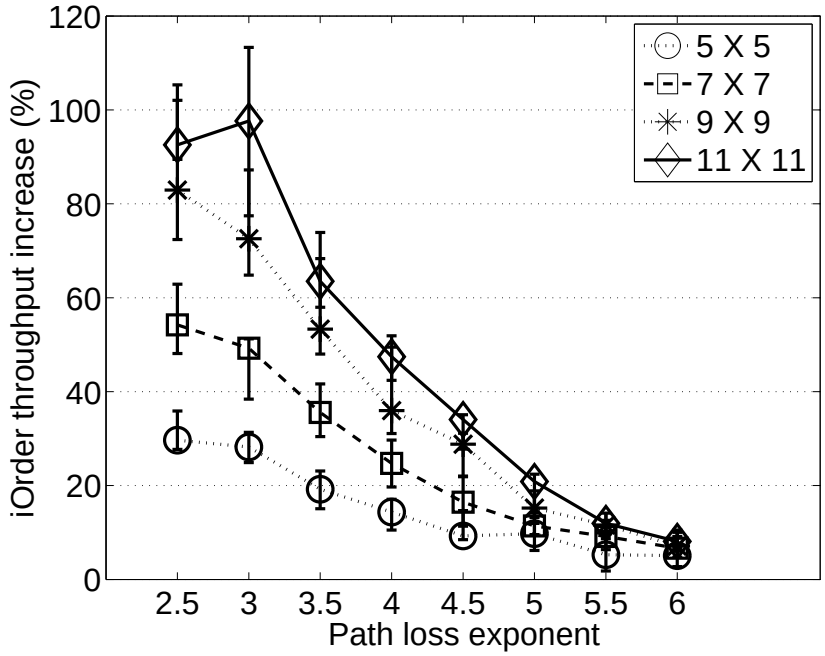

Figure 3.3: Throughput increase in iOrder

networks (e.g., 11×11 network) with small path loss exponents (e.g., 2.5 or 3), and iOrder may improve the throughput of LengthDiversity by a factor up to 19.6. Among the existing algorithms, LQF performs better than GreedyPhysical and LengthDiversity. One reason for this is because LQF is based on queue length whose stochastic temporal behavior prevents LQF from getting stuck at low-performance slot-schedules. Surprisingly, the throughput of LengthDiversity is very low (even compared with other existing protocols) despite its good asymptotic approximation ratio. For instance, LengthDiversity only allows for one transmission per slot in 5×5 networks and at most 3 concurrent transmissions per slot in 11×11 networks. As discussed in Section 3.3.1, this is due to the large μ value in LengthDiversity that schedules transmissions based on virtual grids of cell side lengths $\mu 2^k$ ($k = 0, 1, \ldots$).

Since LQF performs better than GreedyPhysical and LengthDiversity, we only focus on the comparative study of iOrder and LQF hereafter. To gain insight into the impact of link ordering on wireless scheduling in different settings, Figure 3.3 shows the throughput increase in iOrder, as compared with LQF, in networks of different scales and different path loss exponents. We

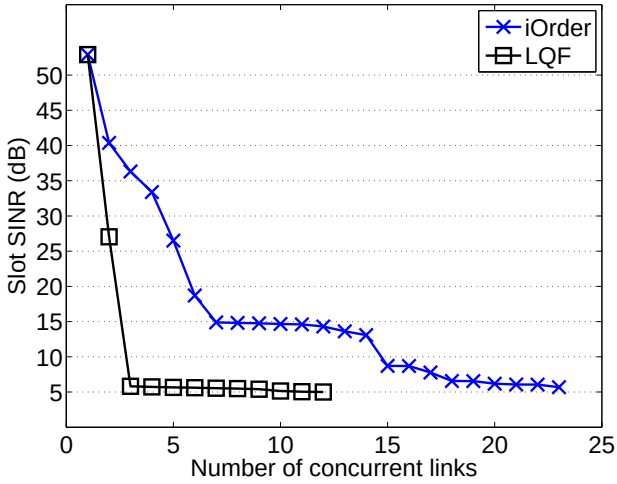

(a) 11×11 networks, $\alpha = 2.5$

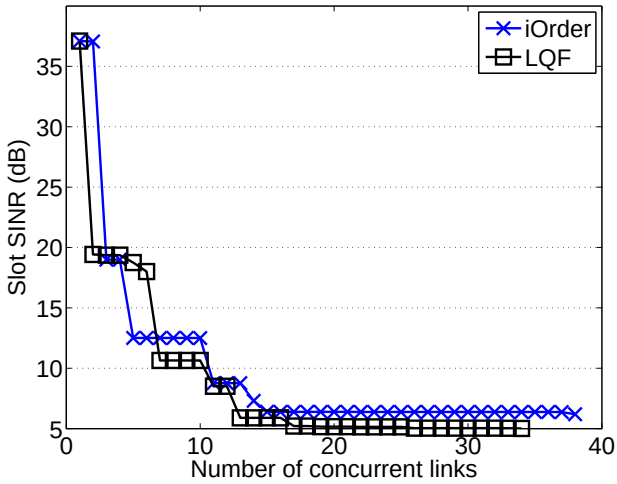

(b) 11×11 networks, $\alpha = 6$

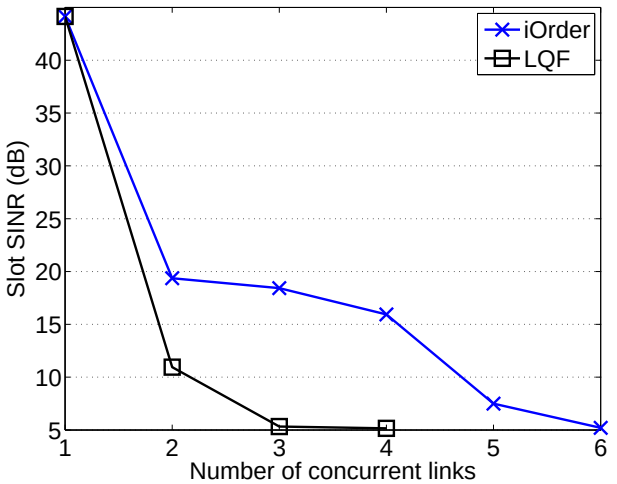

(c) 5×5 networks, $\alpha = 2.5$

Figure 3.4: Time series of slot SINR

see that the throughput increase (and thus the importance of optimal link ordering) drops as the path loss exponent α increases. This is because, when adding a new link to a partial slot-schedule, the interference between the new link and the existing links of the slot-schedule decreases as α increases, which makes the interference budget less sensitive to the different choices of new link addition and thus the benefit of optimal ordering/choice of link addition less significant. For a typical 11×11 network with $\alpha = 2.5$ and $\alpha = 6$ respectively, for instance, Figures 3.4(a) and 3.4(b) show how the *slot SINR* evolves in LQF and iOrder as new links are added to the schedule of a typical slot, where the slot SINR is defined as the minimum SINR at all the receivers of a slot. We see that, with smaller α, the slot SINR in iOrder decreases much slower than that in LQF. Despite the impact of α, we observe that the throughput enhancement as a result of optimized link ordering in iOrder is still significant (e.g., up to 115%) for typical indoor and outdoor environments where α is usually less than 4.5 [57]. We also see that the throughput enhancement in iOrder increases with network size. This is because larger networks give more opportunity of spatial reuse and thus more room for optimization. For instance, Figures 3.4(a) and 3.4(c) show that, for the same extra SINR budget in iOrder, more concurrent links can be scheduled in larger networks since they provide more schedulable candidates.

Figures 3.2 and 3.3 show that the trend how network size affect algorithm performance is monotonic. For conciseness, therefore, we only present data for 5×5 and 11×11 networks hereafter.

SINR budget. The starting SINR budget γ_b determines the interference that can be tolerated during scheduling without violating application requirement on link reliability. Thus it tends to affect allowable concurrent transmissions. In general, we can control γ_b in two ways: 1) control the link length r_0 (e.g., in routing), and 2) control the transmission power P_{tx} (e.g., in power control). To increase γ_b, for instance, we can decrease r_0 or increase P_{tx}. To understand the potential impact that γ_b may have on the relative goodness between LQF and iOrder as well

as the importance of link ordering, we comparatively study the performance of LQF and iOrder when $\gamma_b = 1dB, 3dB$, and $5dB$ respectively.

Figure 3.5 shows, when γ_b is controlled by changing r_0, the throughput increase in iOrder as compared with LQF. We see that the enhancement in iOrder does not change much at the 95% confidence level. After examining the scheduling data in LQF and iOrder, we find that this is mostly due to the fact that controlling γ_b by changing r_0 does not have statistically significant impact on the throughput of LQF and iOrder (as shown in Figure 3.6), which is due to the

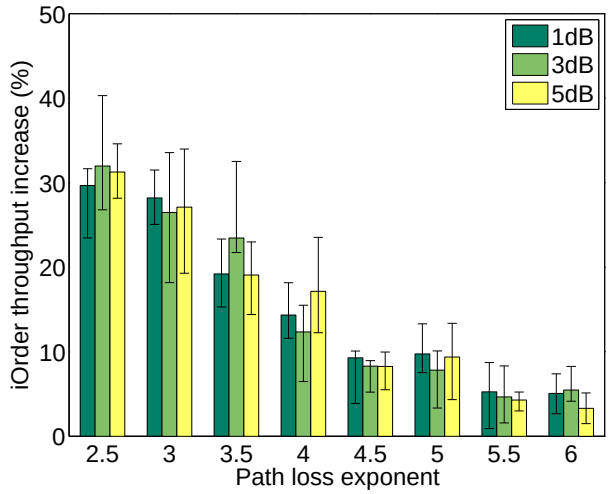

(a) 5×5 networks

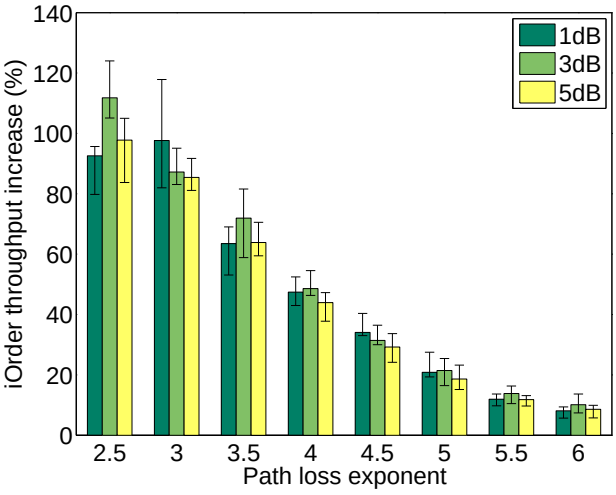

(b) 11×11 networks

Figure 3.5: Impact of SINR budget γ_b: control by r_0

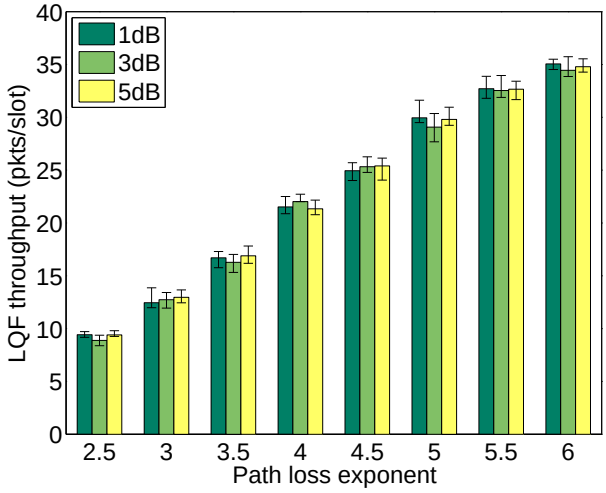

(a) LQF

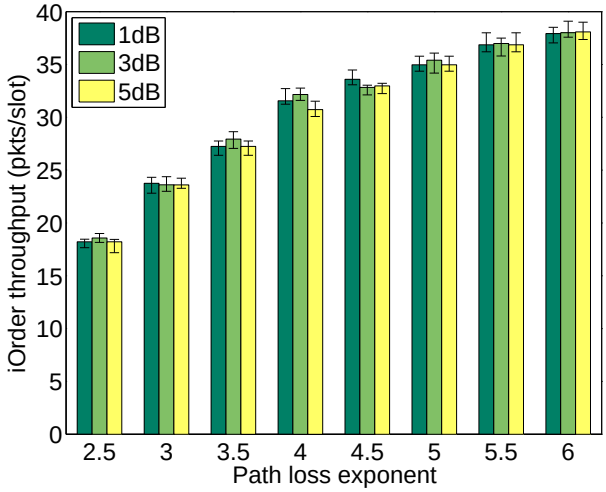

(b) iOrder

Figure 3.6: Network throughput in 11×11 networks when γ_b is controlled by r_0

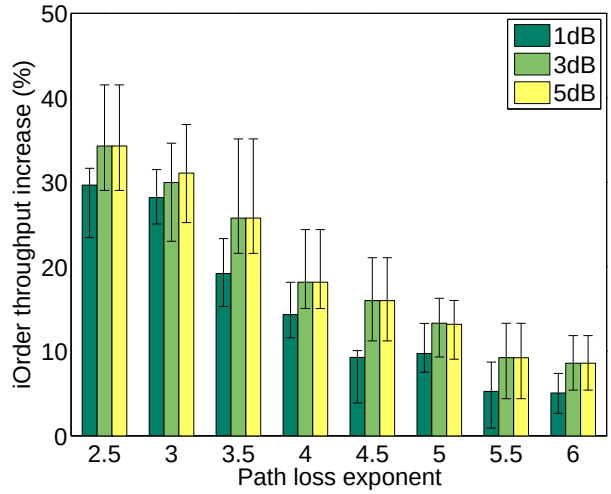

(a) 5×5 networks

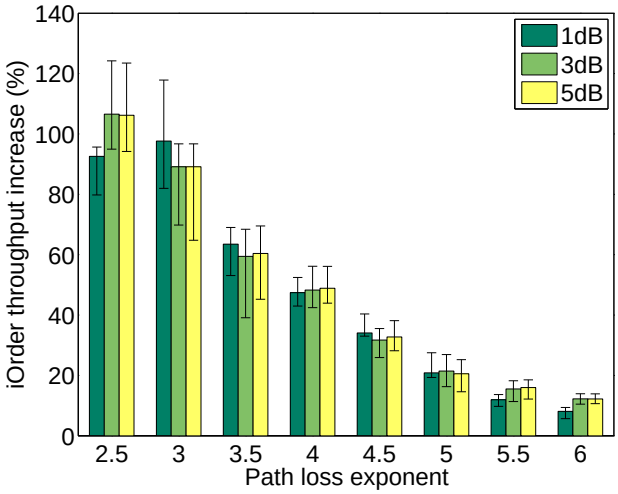

(b) 11×11 networks

Figure 3.7: Impact of SINR budget γ_b: control by P_{tx}

fact that nodes' transmission power P_{tx} do not change and thus the interference field does not change significantly. One implication of this fact is that, in routing, a node does not need to intentionally choose shorter links for the purpose of controlling transmission concurrency.

Figure 3.7 shows, when γ_b is controlled by changing P_{tx}, the throughput increase in iOrder as compared with LQF. We see that, as γ_b increases, the throughput increase in iOrder does not change much at the 95% confidence level. This is again due to the fact that the actual throughput does not change with statistical significance in PRK and iOrder (as shown in Figure 3.8).

Note that this result holds even for very large γ_b's (e.g., 10dB and 100dB). The reason for

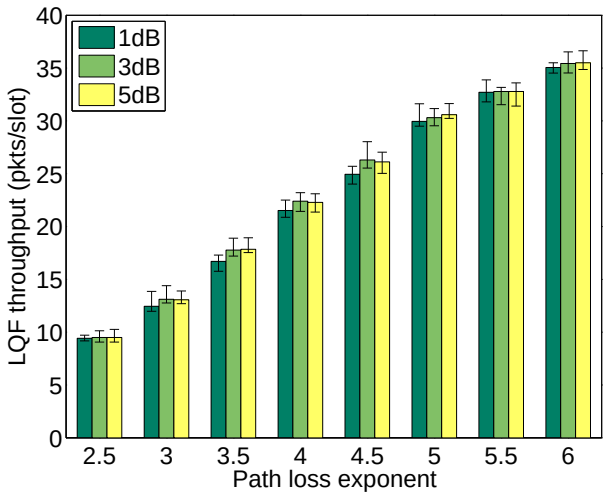

(a) LQF

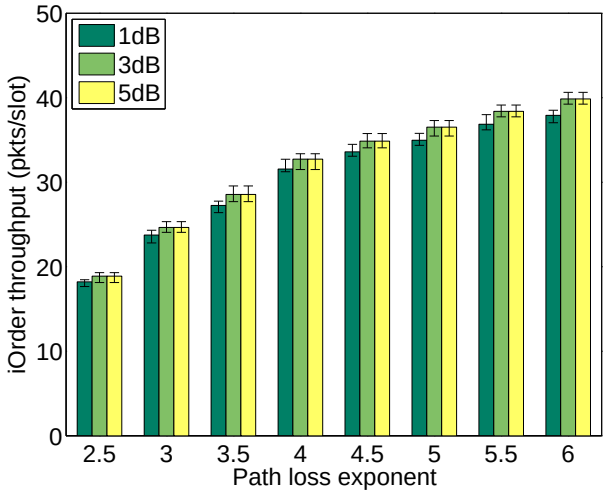

(b) iOrder

Figure 3.8: Network throughput in 11×11 network when γ_b is controlled by P_{tx}

this is that, given the same set of concurrent transmitters, increasing their transmission power by the same factor does not lead to significant change of the SINR at the receivers (since the background noise power is usually small compared with the power of the data and interference signal). One implication of this fact is that, in power control, a node does not need to intentionally use higher power level for the purpose of controlling transmission concurrency.

iOrder & starting link location. For the purpose of stabilizing packet queueing, iOrder

chooses the link with the highest queue length as the first link of a slot-schedule. It is possible that this is not optimal since the location of the starting link of a slot-schedule may affect the total number of the links that can be scheduled for the slot. To characterize the potential impact of starting link location, we study the performance of three variants of iOrder with different strategies on choosing the starting link of a slot-schedule: *iOrder-C* that chooses the link closest to the geometric center of the network deployment area as the starting link, *iOrder-B* that chooses the link farthest away from the network geometric center as the starting link, and *iOrder-M* that chooses as the starting link the link closest to the middle point between the network geometric center and the point in the deployment area that is farthest from the center. Figure 3.9 shows the performance of these variants of iOrder. We see that iOrder-C tends to enable the lowest throughput, and iOrder-B tends to enable the highest throughput. But the differences between the throughput of these algorithms tend to be small and, in many cases, not statistically significant. This observation can help facilitate distributed implementation of iOrder since we may choose not to worry about starting link location in iOrder scheduling. We will explore this direction in our future work.

3.4.4 Online traffic

For online traffic, we measure the delivery latency of a packet as the interval between the packet arrival time at a node and the moment when the node finishes transmitting the packet. Figure 3.10 shows the delivery latency in LQF and iOrder for different network and wireless path loss settings. We see that, in both LQF and iOrder, the median latency decreases with increasing path loss exponent α. This is because, when α increases, the network throughput increases as a result of increased spatial reuse, and thus the median waiting/queueing time for each packet decreases. Compared with LQF, iOrder reduces packet delivery latency significantly, for instance, by a factor up to 24 in 11×11 networks with $\alpha = 3.5$ (as in some typical indoor environments [57]). This shows that iOrder can better support applications such as real-time sensing and control.

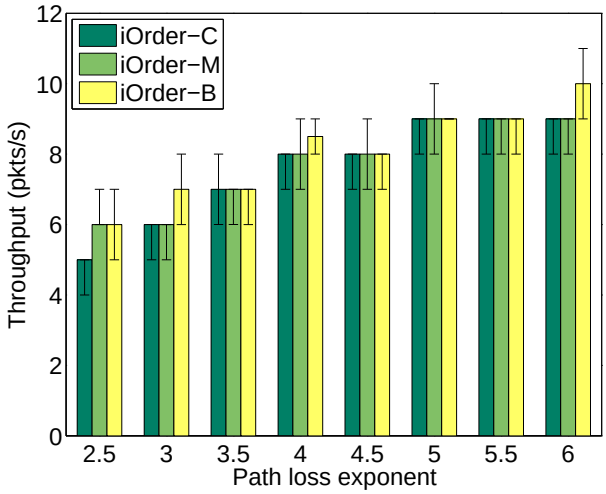

(a) 5×5 network

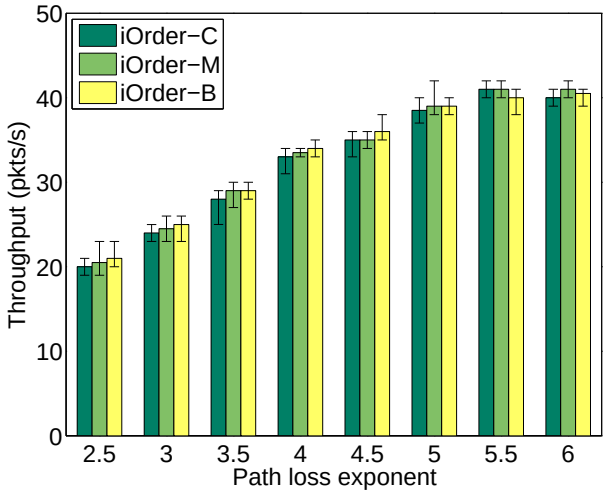

(b) 11×11 network

Figure 3.9: Impact of starting link location on the throughput of iOrder

To gain insight into the queueing behavior which will also help explain packet delivery latency in LQF and iOrder, we examine the evolution of queue length (i.e., number of queued packets at nodes) in LQF and iOrder. Figures 3.11 and 3.12 show, for a typical indoor and outdoor environment respectively, how the queue length evolves over time (measured in time slot number) in LQF and iOrder. We see that iOrder usually has much smaller queue length than LQF does, which, together with the fact that iOrder has higher throughput than LQF, explains why the packet delivery latency is much smaller in iOrder (as shown in Figure 3.10).

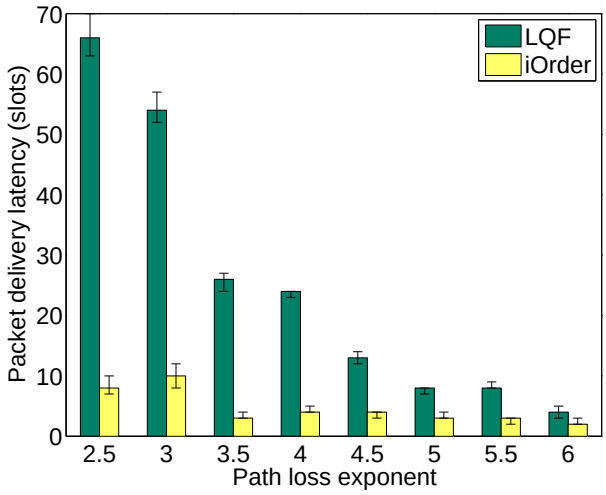

(a) 5×5 networks

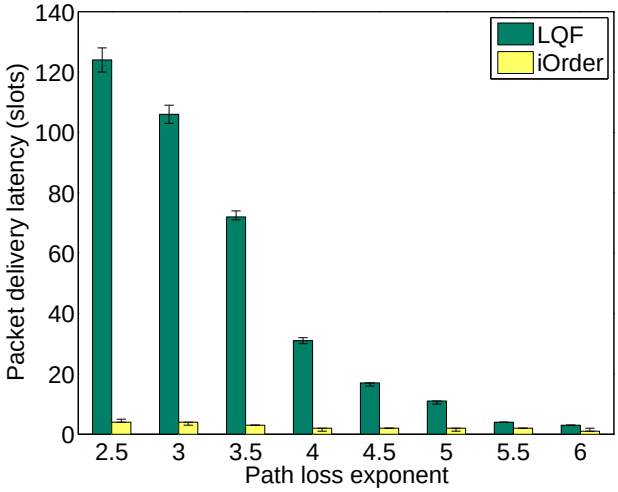

(b) 11×11 networks

Figure 3.10: Packet delivery latency

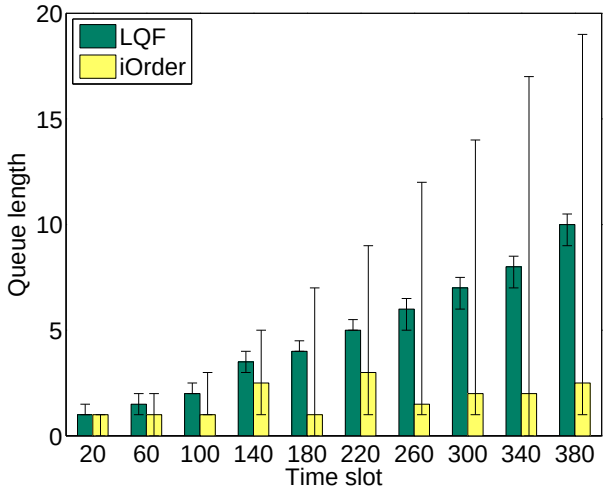

(a) 5×5 network

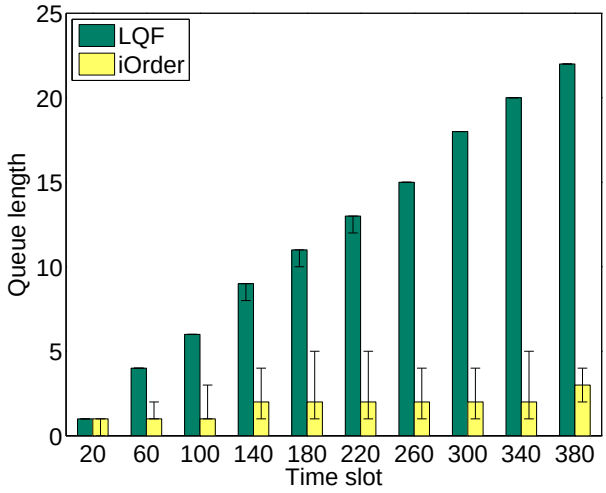

(b) 11×11 network

Figure 3.11: Time series of queue length: $\alpha = 3.5$

We also see that the average arrival rate of 0.15 packets/per-node/time-slot is below nodes' service rate in iOrder, thus the queue length of iOrder is bounded and small; on the other hand, 0.15 packet/per-node/time-slot is above nodes' service rate in LQF for most cases except the 5×5 networks with $\alpha = 4.5$, which leads to the ever increasing queue length and thus long packet delivery latency. Note that, for 5×5 networks, the cross-node variation in queue length tends to be more in iOrder than in LQF. This is expected since, unlike LQF which focuses on balancing queue length across nodes, iOrder focuses more on improving spatial reuse and

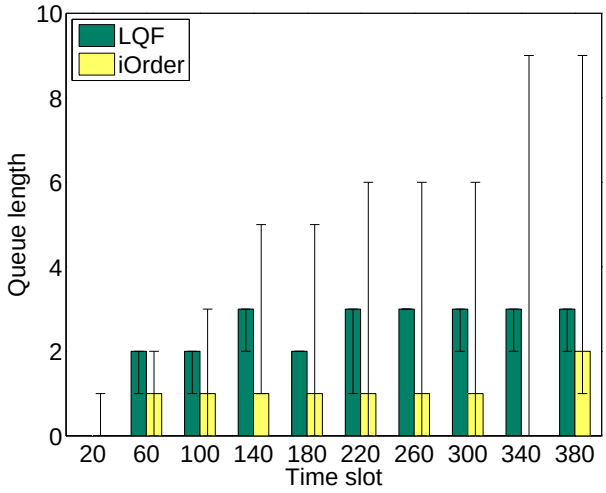

(a) 5×5 network

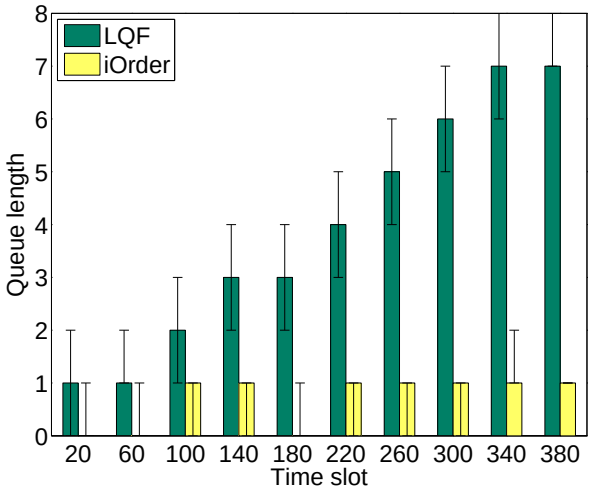

(b) 11×11 network

Figure 3.12: Time series of queue length: $\alpha = 4.5$

concurrency in scheduling. Nonetheless, the maximum queue length in iOrder is still small (e.g., less than 20) and can be implemented even in resource constrained platforms such as TelosB motes.

3.5 Testbed measurement

Our simulation results show that, by optimizing link ordering in scheduling, iOrder outperforms existing scheduling algorithms. To corroborate these results, we experimentally compare the performance of iOrder and LQF using the *MoteLab* testbed [69].

3.5.1 Measurement methodology

We use the MoteLab wireless sensor network testbed at Harvard University [69]. MoteLab is deployed at three floors of the EECS building of Harvard as shown in Figure 3.13. In our experiments, we use all of the 101 operational Tmote Sky motes, with 32, 39, and 30 motes distributed at the first, second, and third floors respectively. We use two radio transmission powers $0dBm$ and $-3dBm$ (a.k.a. power level 31 and 23 respectively) to generate networks of different connectivity.

Part of the input to iOrder and LQF are the radio model, background noise at every node, and strength of signals from any node to every other node. To collect these information for

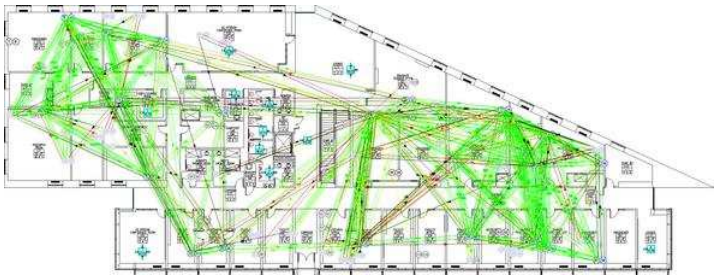

(a) First floor

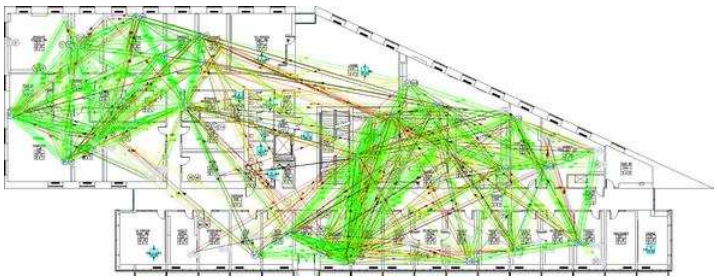

(b) Second floor

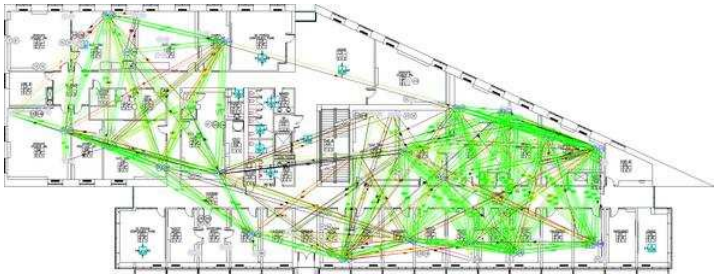

(c) Third floor

Figure 3.13: *MoteLab* testbed

MoteLab, we perform the following experiment: let the 101 motes take turns to be a transmitter one at a time; when a mote is a transmitter, it broadcasts 600 128-byte packets with an inter-packet interval of 100ms (note: each packet transmission takes $\sim$4ms); while a mote is transmitting packets, every other mote keeps sampling its radio RSSI once every 2ms whether or not it can receive packets from the transmitter, and, if a mote can receive packets from the transmitter, it logs the received packets. We execute the above experiment for both the transmission power of $0dBm$ and $-3dBm$. Using the data collected in these experiments, we can derive the background noise power at each node, the strength of signals from any node to every other node when the transmission power is $0dBm$ or $-3dBm$, and the packet delivery rate (PDR) from any node to every other node as well as the associated SINR. These data also enable us to derive the empirical radio model for the Tmote Sky motes in MoteLab. Figure 3.14 shows the measured radio model, as represented by the relation between packet delivery rate (PDR) and SINR at a receiver, for a typical mote in MoteLab. We will use this radio model in our scheduling algorithms for two purposes: 1) to choose the SINR threshold for satisfying a certain link reliability, and 2) to compute the expected PDR for a given SINR at a receiver.

Figure 3.15 shows the histograms of the PDRs of all the wireless links in MoteLab when the

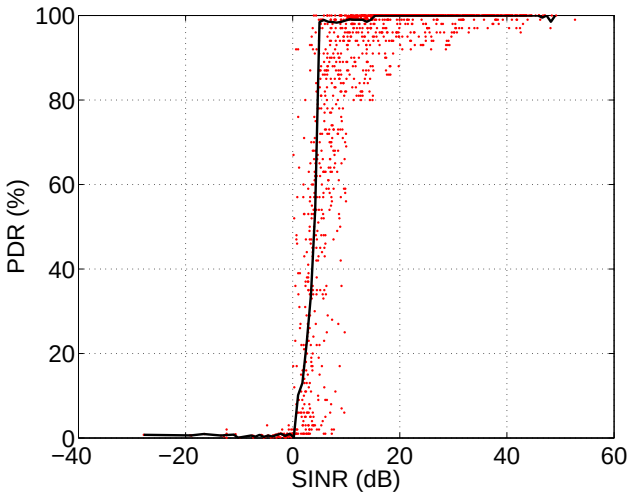

Figure 3.14: PDR vs. SINR for the CC2420 radio in MoteLab

transmission power is $0dBm$ and $-3dBm$, and Figure 3.16 shows the histogram of background noise power in MoteLab. We see that there is a high degree of spatial variability in link PDRs and background noise power. Thus the testbed enables us to do experiments in non-uniform

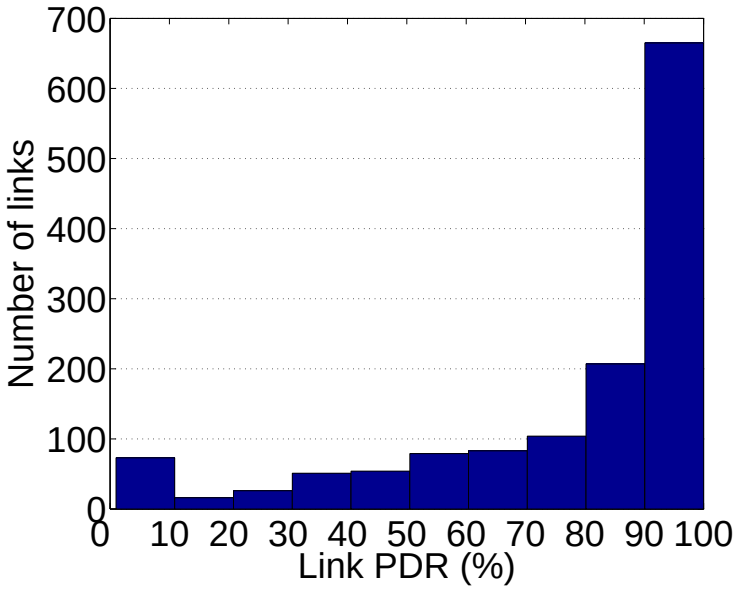

(a) Transmission power: $0dBm$

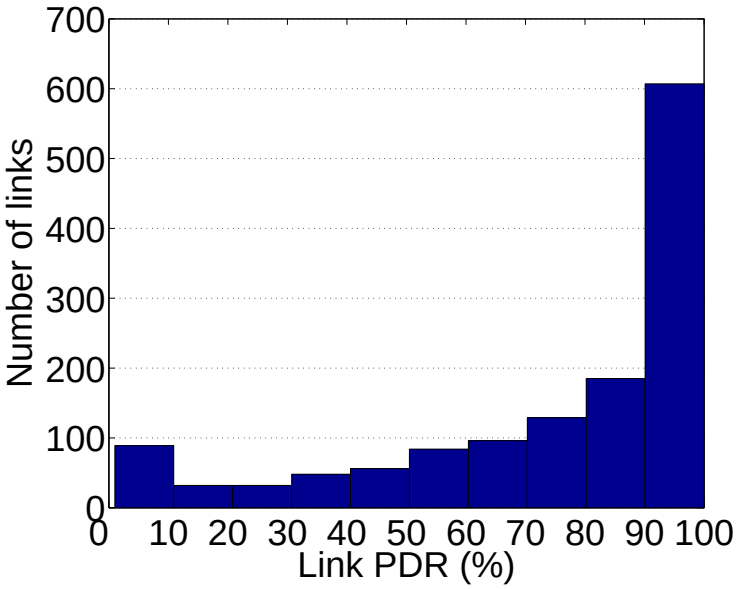

(b) Transmission power: $-3dBm$

Figure 3.15: Histogram of link PDRs in MoteLab

settings.

To generate the traffic load for scheduling, we consider convergecast where data packets generated by all the nodes need to be delivered to a base station node. More specifically, we let mote #115 at the center of the second floor be the base station to which the remaining 100 motes deliver their packets (mostly via multi-hop paths). Then we build the routing tree by identifying, for each non-base-station mote, a reliable minimum-hop path to the base station where each link of the path has a receiver-side SNR of no less than $\gamma_t + \gamma_b$ in the absence of interference. Similar to simulation, we set γ_t and γ_b as $5dB$ and $1dB$ respectively. Figure 3.17 shows the histogram of the routing hop length when different transmission power is used. We see that the maximum hop count is 5 and 9 when the transmission power is $0dBm$ and $-3dBm$ respectively.

Given a routing tree, we generate the traffic load as follows: each mote generates 30 packets, and then the number of packets that need to be delivered across a link is the number of packets generated in the subtree rooted at the transmitter of the link. Then the traffic load is used as the input to iOrder and LQF to generate the transmission schedule. Experiment with each schedule is repeated 10 times to gain statistical insight. To experiment with a schedule

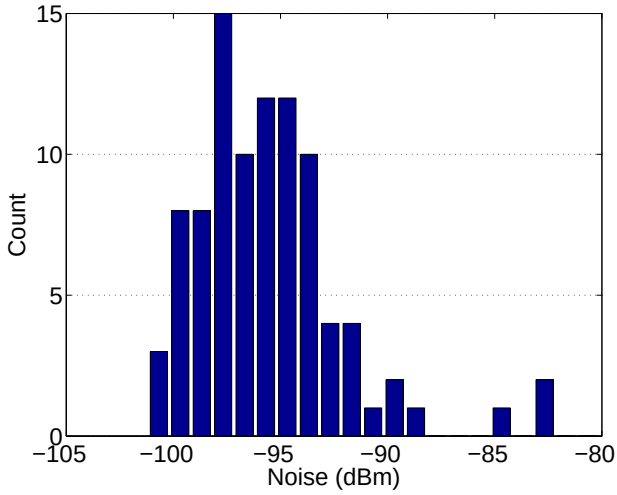

Figure 3.16: Histogram of background noise power in MoteLab

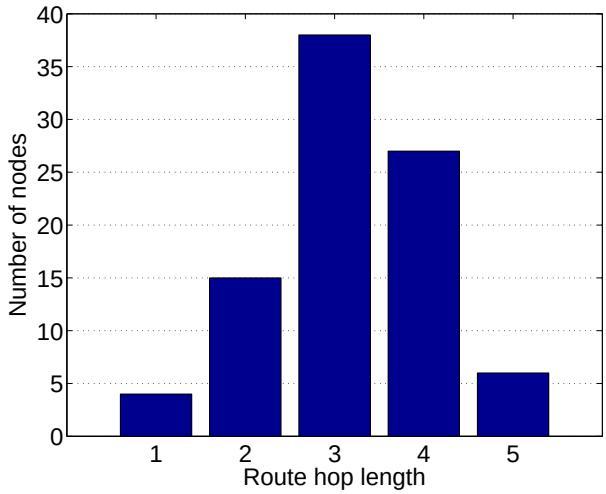

(a) Transmission power: $0dBm$

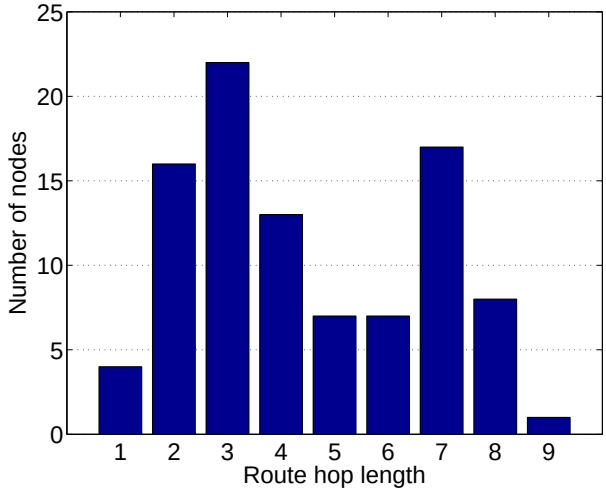

(b) Transmission power: $-3dBm$

Figure 3.17: Histogram of routing hop length

in MoteLab, we use the TinyOS Flooding Time Synchronization Protocol (FTSP) [42] to synchronize transmissions such that the links in the same time lot of the schedule transmit at the same time; each slot is repeated 30 times before moving onto the next slot so that we can get 30 samples on the transmission status (i.e., success or failure) along each link of the slot to understand the behavior of each slot.

3.5.2 Measurement results

Figure 3.18(a) shows the network-wide throughput (measured in the total number of packets delivered per time slot) in LQF and iOrder when different transmission powers and thus different routing trees are used. We see that iOrder consistently outperforms LQF, by 22.6% and 28.9% when the transmission power is $0dBm$ and $-3dBm$ respectively. Given that MoteLab is housed in an indoor environment where the path loss exponent $\alpha \approx 3.5$ and that the size (i.e., 101 motes) of our measurement network is between those of the 5×5 and 7×7

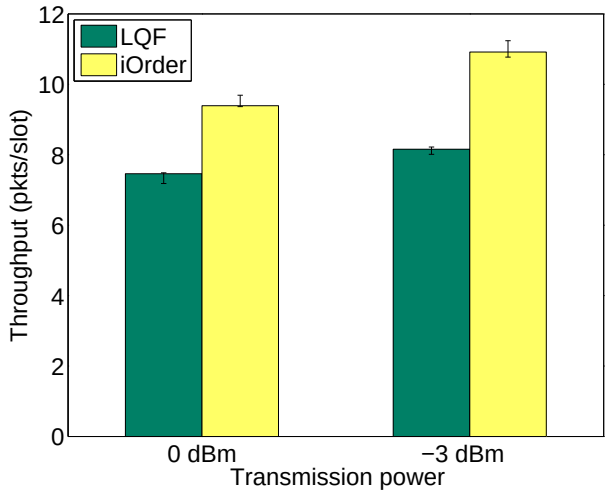

(a) Median throughput

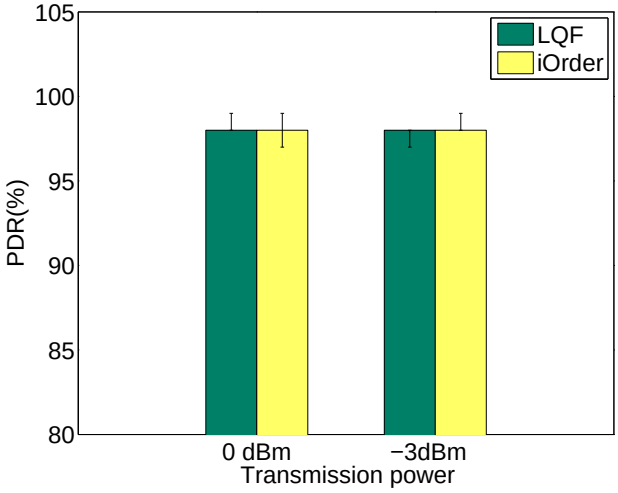

(b) Mean link PDR

Figure 3.18: MoteLab-based measurement

simulation networks (which have 70 and 140 nodes respectively), the MoteLab-based measurement data very much agrees with the simulation data shown in Figure 3.3, thus validating the simulation results. When the transmission power decreases from $0dBm$ to $-3dBm$, the diameter of the network connectivity graph and the depth of the routing tree increases (as shown in Figure 3.17), and thus the opportunity of optimizing spatial reuse increases. Therefore, the throughput enhancement increases from 22.6% to 28.9% when the transmission power decreases.

The intention of setting γ_t as $5dB$ is to ensure a $\sim$100% link reliability in scheduling. To verify the correctness of our schedule, Figure 3.18(b) presents the actual link PDRs during experiments. We see that the links are very reliable and have a mean PDR of $\sim$98%, which implies that the TDMA scheduling is able to ensure the required link reliability. From Figures 3.18(a) and 3.18(b), we also see that iOrder improves network throughput without sacrificing link reliability.

3.6 Discussion: distributed implementation

As a first step towards addressing the limiting impact of interference on wireless scheduling, our objective in this paper is to characterize the impact of link ordering on the throughput of TDMA scheduling, thus we have focused on centralized TDMA scheduling. In terms of implementation, even though distributed scheduling algorithms are preferred in general, centralized scheduling has also found its use in settings of slowly-varying network and traffic conditions. In wireless networked sensing for oil field instrumentation, for instance, the wireless link properties tend to be slowly-varying only, and the monitoring nodes generate packets at fixed, pre-specified frequencies; in these cases, centralized TDMA scheduling (possibly together with frequency scheduling) has been employed in both engineering practice [62] and industry standards such as WirelessHART [70]. That said, for cases where distributed scheduling is more desirable, the scheduling algorithm iOrder can be implemented in a distributed manner, and we discuss the potential approaches as follows.

To implement iOrder in a distributed manner, we need to design mechanisms that generate transmission schedules similar to those in iOrder; more specifically, we need to generate the effect of interference-budget- and queue-length-based scheduling of iOrder. The effect of *interference-budget-based scheduling* is that the SINRs at the receivers of a slot-schedule are close to the required threshold γ_t. This fact lends iOrder to distributed implementation via the physical-ratio-K (PRK) interference model [16], because PRK-based scheduling makes the SINRs at the receivers close to the desired threshold γ_t. The PRK model also integrates the high-fidelity of the physical interference model with the locality of the protocol interference model, thus PRK-based scheduling enables reliable, high-throughput communication while only requiring coordination among nodes close-by (i.e., no global information is needed in PRK-based scheduling) [16].

For the effect of *centralized, queue-length-based scheduling*, Le et al. [35] and Ni et al. [47] have recently developed distributed, queue-length-based priority scheduling mechanisms that, only with localized, asynchronous coordination among neighboring nodes, achieve a performance close to the centralized, queue-length-based scheduling. In iOrder, the link with the highest queue length is selected as the first link of a slot-schedule, but, as we have discussed in Section 3.4.2, the number of links that can be scheduled for a time slot is *insensitive* to the location of the first link picked for the slot.

From the above observations, we believe that iOrder can be implemented in a distributed manner by leveraging the PRK model [16] and the distributed queue-length-based priority scheduling [35, 47], and we will investigate this in detail in our future work.

3.7 Related work

As a basis of wireless scheduling, different interference models have been studied extensively [40, 44, 14, 56]. It was found that the physical interference model (a.k.a. the SINR model) is more accurate than the basic protocol interference model and can enable higher scheduling performance in general [40, 44]. For distributed protocol design, we also discov-

ered that it is possible to effectively instantiate the protocol interference model via local feedback control [16]. Focusing on gaining insight into the impact of link ordering on wireless scheduling instead of distributed protocol design, we employ the physical model in this paper for the sake of its high accuracy.

Different interference-oriented TDMA scheduling algorithms have been proposed in the literature. They include LQF and its variants [35, 30, 36, 54, 8, 9], GreedyPhysical and its variants [10, 66], as well as LengthDiversity [23]. The throughput and delay performance [36, 32, 46] as well as the distributed implementation [36, 24, 31] of these algorithms have also been studied, and scheduling based on dominant interferers has been considered by Badia et al. [8]. Nonetheless, these work have not focused on the impact of link ordering on interference-limited scheduling; the analysis of these algorithms has also mostly focused on the asymptotic behavior without characterizing the impact of potentially large constants in the analysis. Our study fills this gap by proposing the algorithm iOrder for optimizing link ordering in wireless scheduling and by examining the detailed behavior of different protocols through analysis, simulation, and testbed-based measurement.

Interference-oriented distributed scheduling has also been well studied [12, 73, 11, 80, 53, 13, 65], but the existing work has mostly focused on contention resolution and collision avoidance without explicitly optimizing network-wide spatial reuse. Yang et al. [71] have studied how to induce spatial clustering for the purpose of improving spatial reuse in densely deployed spread-spectrum networks. Spatial clustering may not be generically applicable since it is most useful only when network deployment is dense and the spreading factor of the spread spectrum radios is large (e.g., a spreading factor of 512 was considered in [71]). The performance of spatial clustering has only been compared with the traditional CSMA/CA random access schemes too.

Scheduling has also been considered together with transmission power control in wireless networks [23, 45] where nodes adapt their transmission power to further increase network

capacity and to reduce delay. Focusing on characterizing the limiting impact of interference on wireless scheduling, we have assumed fixed transmission power in this paper. How to leverage controllable transmission power in addressing the limiting impact of interference on scheduling will be an interesting topic to pursue, but detailed study of this is beyond the scope of this paper.

Several studies [22, 27] recently proposed mechanisms for interference cancellation where a single receiver could simultaneously receive packets from multiple senders. These results challenge the traditional paradigm where a receiver can only receive one packet at a time, and they suggest new ways of interference management. Nonetheless, interference still needs to be controlled due to the constraints of these interference cancellation mechanisms [37]. For instance, ZigZag decoding [22] works the best when the number of interferers is small (e.g., less than 6). How to schedule transmissions to take advantage of interference cancellation is an interesting problem to study, and there has been some recent effort on this [37]. But the detailed study of this issue is beyond the scope of this paper.

3.8 Concluding remarks

Co-channel interference control is important for the reliability and predictability of wireless networks. Towards understanding the importance of explicitly addressing the limiting impact of interference on wireless scheduling, we have formulated the notion of interference budget to characterize a schedule's tolerance of additional interference, and we have designed the algorithm iOrder that schedules links in a decreasing order of the enabled interference budget. Through analysis, simulation, and testbed-based measurement, we have demonstrated the benefits of explicitly addressing the limiting impact of interference by showing the significantly better performance of iOrder as compared with the well-known algorithms such as LQF, GreedyPhysical, and LengthDiversity. By discovering and understanding the surprisingly low performance of LengthDiversity, our study has also demonstrated the importance of examining the constant factors involved in asymptotic analysis. As a side result, our study has characterized the relative goodness of the existing algorithms, which is of independent inter-

est. The findings of this paper shed new insight into the behavior of wireless scheduling and, via algorithm iOrder, constructively shows the benefit of optimizing link ordering to address the limiting impact of interference. Therefore, the findings of this paper open up new avenues for future research and for optimizing wireless network performance; one of the future directions is to investigate mechanisms for realizing iOrder (or interference budget optimization in general) in a distributed manner.

CHAPTER 4

PRK MODEL IN MULTI-CHANNEL

4.1 Preliminaries

With successful commercialization of IEEE802.11 WiFi standard, more devices are expected to function in these 2.4GHz and 5GHz ISM(Industrial, scientific and medical) radio bands. In order to avoid and decrease co-channel interference, one method is to use different orthogonal channels in scheduling. It can also greatly increase the network throughput in multi-hop wireless mess network. In this section, we want to use our PRK model in milt-channel scheduling and see its potential for multi-channel distributed MAC protocols. More specifically, we want to understand the impact of available channel number on the performance of PRK model, since the number of channels available in practice is usually limited due to both economical and policy reasons We will study the performance gain of PRK model with different number of channels that can be used for wireless scheduling. We hope that our study in this section will shed light into the work of designing multi-channel PRK scheduling.

4.2 Problem definition

In order to get a more representative result, we consider a 2D Poisson networks, where nodes are distributed with an average density λ node per unit area. The traffic pattern is such that the average link length is ℓ; each transmitter T sends packets to a receiver R such that the distance between T and R is the closest to ℓ, and if multiple such receivers exist, T randomly picks one as its receiver. We assume that each transmitter has data packets buffered for transmission with probability β at any moment in time.

Given a single link and its exclusive region, there are two ways to use the multi-channel option. First, we can use the multi-channel option to enable the nodes' transmission within the exclusive region; Second, we can use the multi-channel option for the nodes outside or on the

boundary of the exclusive region. We notice that the first method will have little change of the total interference level at the receiver, as this method will not affect the link distribution in a Poisson distribution. It will only create channel overlaps in a 2D space. However, the second method will affect the co-channel interference level at the receiver side, thus affect in choice of K in our PRK model. So our study will focus on the second method.

Based on the analysis above, we can compute the total interference I at an arbitrary receiver R as follows:

Proposition 9. *With ratio-K-based scheduling, the expected total interference I at a receiver R in an infinite Poisson random network is as follows:*

$$I = \frac{2\pi\lambda_t P_t \beta}{C(\alpha-2)}(K\ell)^{2-\alpha} \tag{4.1}$$

where λ_t is given by Equation 2.20, P_t is the transmission power, β is the node transmission probability, α is the wireless path loss exponent, C is the number of available channels and ℓ is the link length. □

Proof. From the analysis in single channel Poisson network, we know that the total interference at an arbitrary receiver R is

$$I = \frac{2\pi\lambda_t P_t \beta}{(\alpha-2)}(K\ell)^{2-\alpha}$$

as we assume that each link can pick their channel individually and with an equal probability, the interference then can be computed as

$$I = \frac{2\pi\lambda_t P_t \beta}{C(\alpha-2)}(K\ell)^{2-\alpha}$$

Q.E.D. □

4.3 Numerical analysis

Using the radio model describe in 2.1 and Formula 4.1, we numerically analyze the impact of multiple channels on model. Given a certain channel number, we want to understand how much the link quality (PDR) will change. We also want to see how the value of minimum K will change because of multi-channel scheduling. Because the PRK model uses the minimum K that ensures a certain link quality requirement. This will help us understand the performance of PRK model in the multi-channel scheduling and shed light into its potential in helping the multi-channel protocol design.

4.3.1 methodology

We exam a wide range of system configuration for our ratio-K model. To examine the impact of wireless attenuation in different environments, we consider the set $\{2.1, 2.6, 3, 3.3, 3.6, 3.8, 4, 4.5, 5\}$ of wireless path loss exponents αs, which represent a wide range of real-world environments [57]; we also set the shadowing variance σ^2 based on measurement data from [57]. We vary their parameters such as traffic load, link length, and node distribution density to examine the impact of network properties. Link length is chosen so that the link reliability varies from 1% to 100% in the absence of interference. More specifically, for each specific path loss exponent α, we choose a link length ℓ_0 corresponding to an interference-free packet delivery rate (PDR) of 1%, and another link length ℓ_1 corresponding to a signal-to-noise-ratio (SNR) of 5dB more than the minimum SNR for ensuring 100% interference-free PDR; then we take 60 sample link lengths that are uniformly distributed between ℓ_0 and ℓ_1. (Note that the transmission power level is set at -25dBm in our study.) For each average link length ℓ in random networks, we select a set of node distribution densities λs so that the average number of nodes in a circular area of radius ℓ is 5, 10, 15, 20, 30, and 40 respectively. The number of channels considered are $\{1, 2, 3, \ldots, 32\}$. We find that in our set up $C = 32$ or larger will not have significant increase in link quality.

we regard each setting of network and environment parameters as a *system configuration*

hereafter. Thus our study examines 68,040 different system configurations, and the boxplots, medians, and distributions to be presented in the rest of the section are mostly based on the distribution of the corresponding metrics across different system configurations. For each system configuration, we analyze the network performance when the ratio-K model is instantiated with different Ks. The set of Ks we consider are $\{1, 1.5, 2, 2.5, \ldots, 10\}$ for Poisson random networks. $K = 10$ is is large enough to serve as the largest K in our study.

Using the numerical results on network throughput and link reliability in these 68,040 system configurations, we analyze 1) how the PDR will change as a result of using multiple channels. and 2) the relation between the minimum K that ensure a certain link reliability will change and the number of channels used in the transmission.

4.4 Simulation result

To understand the impact of the channel number on the link quality, we define $\Delta PDR(c)$ as

$$\Delta PDR(c) = PDR(c) - PDR(1)$$

where $\Delta PDR(c)$ is the link PDR when the available channel number used in scheduling is c. So $\Delta PDR(c)$ describes the benefit of multi-channel scheduling comparing to the single channel case.

PDR gain In order to show potential PDR gain, we choose the link with the PDR $< 10\%$ when only one channel is available in the network, and compare it to the PDRs when different channel numbers are used.The results are presented in Figure 4.1. We can see that the channel number has a positive impact on the link quality. As more channels are used in the network, the link quality keep increasing until it reaches almost 100% PDR.

Second, for both indoor and outdoor environment, the link quality improvement will be very small when there are only 2 or 3 channels to choose from. For example, when the channel

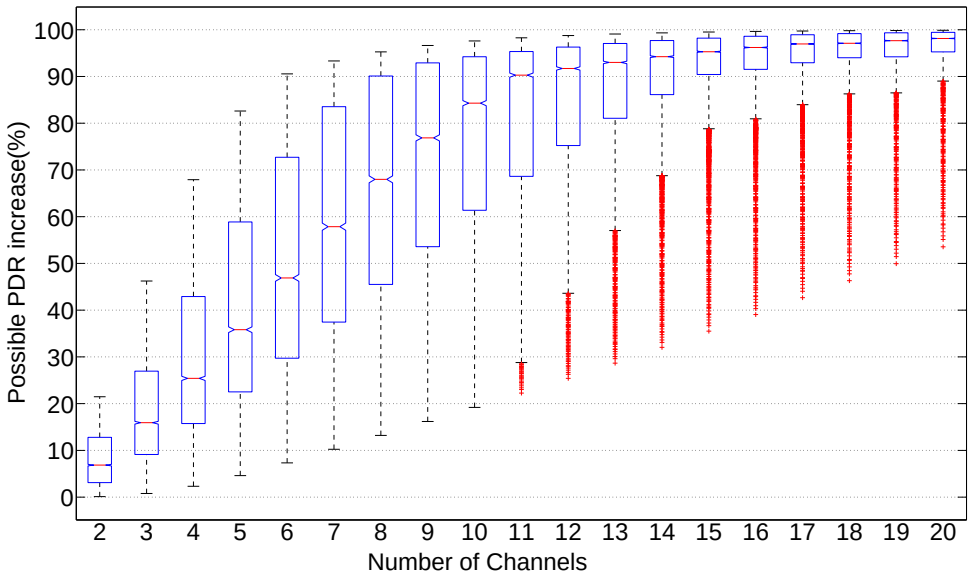

(a) indoor environment $\alpha = 3.6$

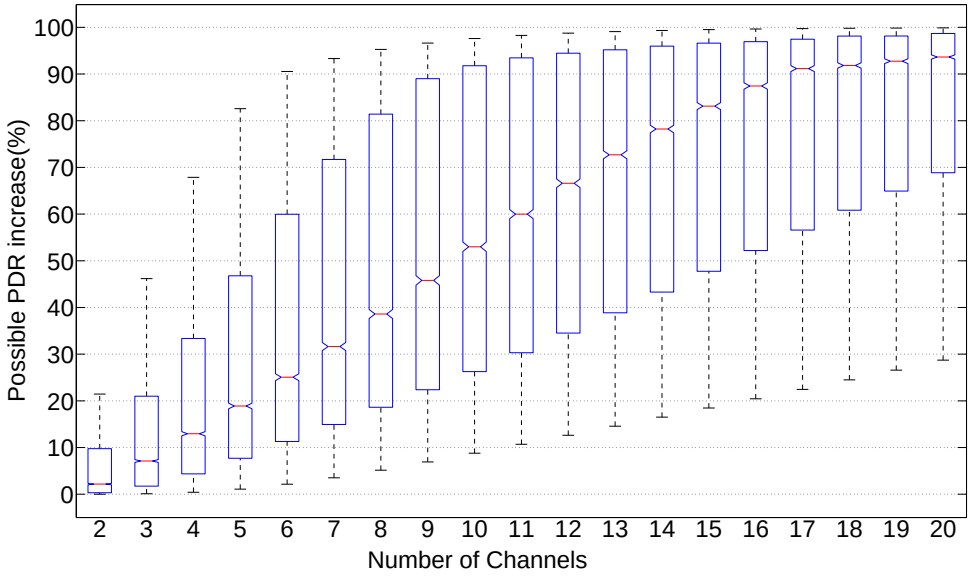

(b) outdoor environment $\alpha = 4.5$

Figure 4.1: PDR gain when different number of channels are used

number is 2, the median link quality improvement is only 6.8% for indoor environment and 2% for outdoor environment.This implicates that we cannot expect that a MAC protocol with 2 or 3 channels can improve the link quality significantly.

Third, the number of channels needed to maintain a relative good link quality (e.g. 80% PDR) does not have to be very large. if we regard 80% PDR as a relative good link quality, it is about 70% PDR increase in Figure 4.1. For indoor environment, the channel needed to have a median 80% PDR is 10. For outdoor environment, the channel number is 15. The channel number difference may contradict to our expectation. In a single channel setup, the number of channels needed to maintain a certain PDR is less in an outdoor environment. This is because that the signal attenuates faster in the outdoor environment and the interference accumulates much slower in a outdoor environment. However, in a multi-channel setup, as the aggregate interference has less impact on the link quality in the outdoor environment, the advantage of spatial reuse from the use of multiple channel will be also less in the outdoor environment. So the number of the channel required in outdoor environment is bigger.

Fourth, we find that if the channel number in scheduling is more than a certain number, its benefit on the PDR will be very small. For example, when channel number is bigger than a certain number (e.g. 15 for indoor environment and 17 for outdoor environment, respectively), the PDR improvement is very lmited. This is because the link quality for most of cases is already or very close to 100%. From this result, we know that more channels to be used in scheduling does not always guarantee a better link quality in practice. 15 - 20 channels will be fair enough to handle most of indoor and outdoor environment. This could be a helpful guideline for us in the network planning.

We also look at PDR gain when the link quality is different with respect to the number of available channels. From Figure 4.2 and 4.3, we can see that when PDR gain is higher when the single channel link quality is lower. The channel number does not improve the link quality when it is greater than 4. More importantly, we know that, from the figure, the multi-channel

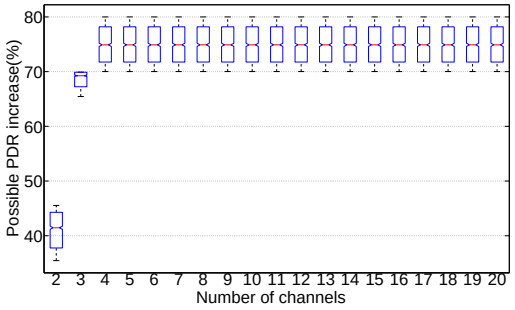

(a) $PDR = 20\%$

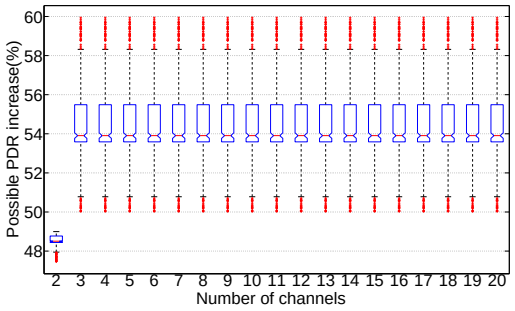

(b) $PDR = 40\%$

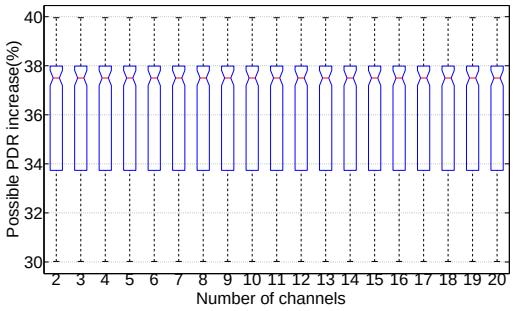

(c) $PDR = 60\%$

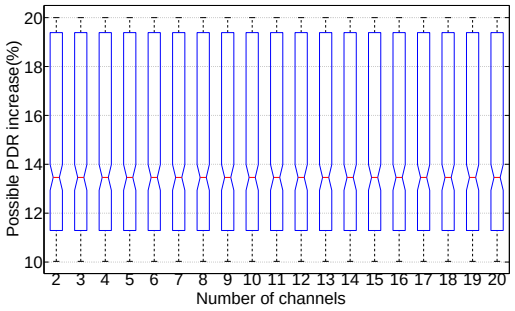

(d) $PDR = 80\%$

Figure 4.2: the PDR gain of different link PDR in indoor environment

scheduling will help a lot when the original link quality is very low.

Minimum K in multi-channel In the single channel PRK study, we find that the minimum K to ensure a certain PDR does not always fall into the number 2 or 3. Sometimes it is as large as to 9 or 10. The drawbacks of a large K value are two folds at least. First, when a larger number K is used in the network, there will be fewer concurrent transmissions and the network throughput will be low. Second, a big K value means that a bigger exclusive region is required. In order to suppress the transmission of the far-away nodes in the exclusive region, it requires either to use larger transmission power to improve the delivery of the singaling message, or more complex schemes to synchronize the nodes in the exclusive region. Neither is good for a distributed protocol. Based on the reasons above, we want to understand how the choice of multiple channels will help to decrease the value of minimum K that ensures a certain PDR.

We choose certain system configurations in which a larger ratio-K is needed in a single channel setup and see how does the minimum K is changed as the number of channels used in the network increases. We choose the PDR requirements to be 0.6, 0.7, 0.8 and 0.9, which should cover the most common requirement. We present the result in the indoor(alpha = 3.5) and outdoor(alpha=.45) environment.

From the Figure 4.6, we can see that the help of multiple channels on the mimim K is significant. Moreover, the value of minimum K drops very fast when the channel number changes from 1 to 2. For example, in both the indoor and outdoor environment, the minimum K for 80% PDR requirement drops from 10 to 4. That 60% decrease implicates a great reduction in the exclusive region and more possible concurrent transmissions.

Second, the minimum K drops to 2 when the channel number increases to 7, for both indoor and outdoor environment, for all the PDR requirement in the figures. It suggest that we do not need a large number of channels to decrease the number K to 2. It also implicates that with a choice of a multiple channels, the schemes for exchanging controlling message within the exclusive region will be much easier and more reliable than a single channel case.

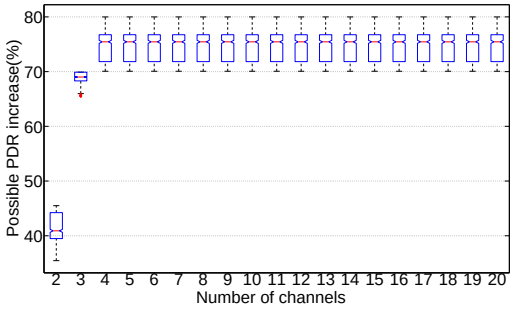

(a) $PDR = 20\%$

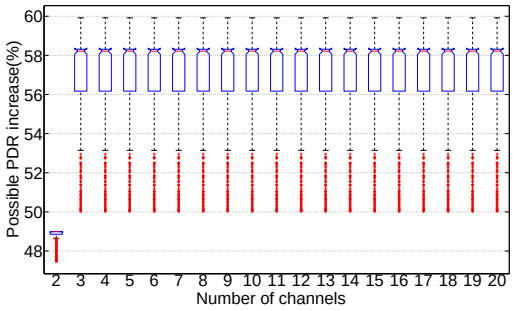

(b) $PDR = 40\%$

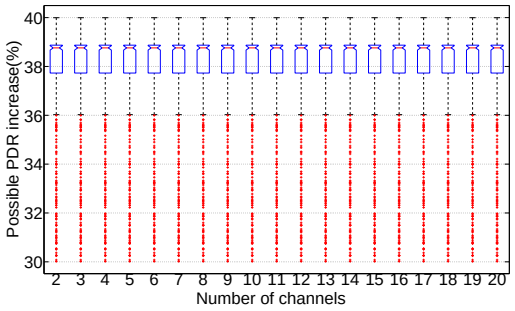

(c) $PDR = 60\%$

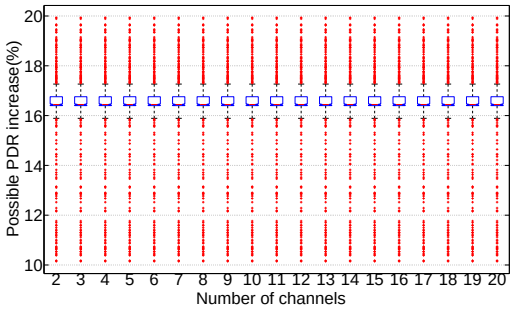

(d) $PDR = 80\%$

Figure 4.3: the PDR gain of different link PDR in outdoor environment

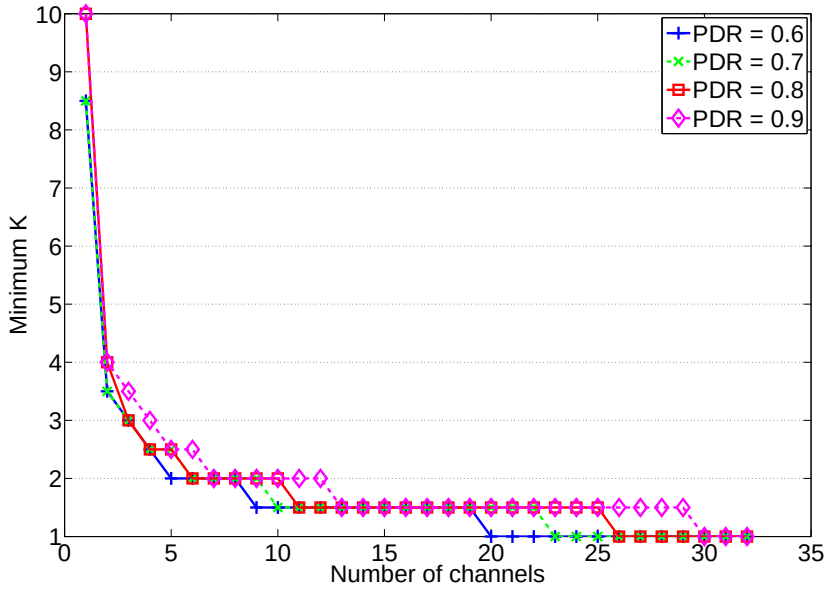

(a) indoor environment $\alpha = 3.5$

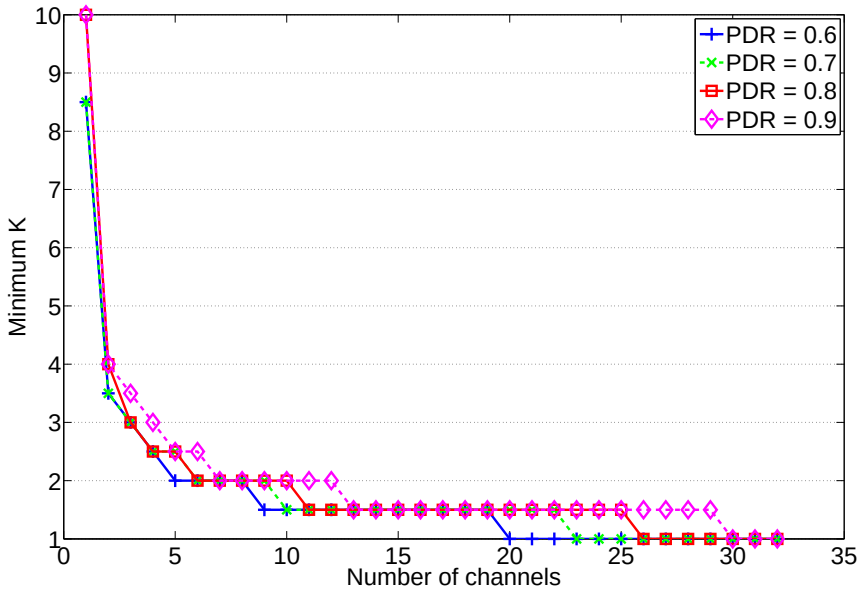

(b) outdoor environment $\alpha = 4.5$

Figure 4.4: Minimun K when different channels are used in the network

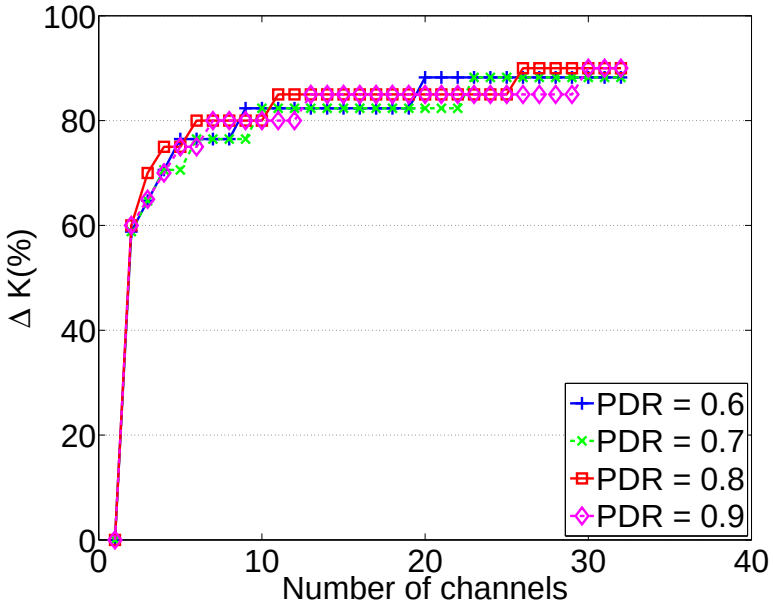

(a) indoor environment $\alpha = 3.5$

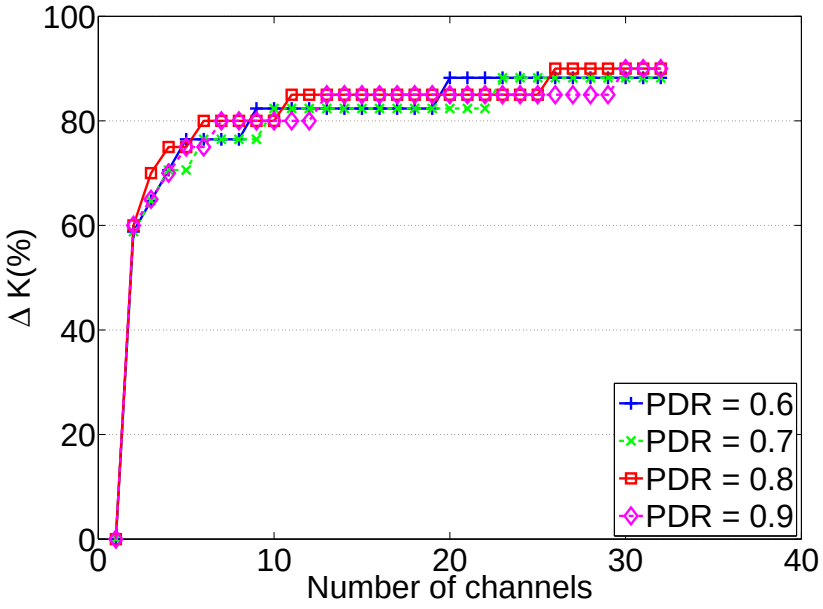

(b) outdoor environment $\alpha = 4.5$

Figure 4.5: Minimun K reduction when different channels are used in the network

Third, this result also tells us that the minimum K does not decrease further after the number of channel reaches a certain number. For example, for 80% PDR requirement in a indoor environment, the minimum K does not further decrease when the number of channel is between 11 and 25. The same scenario is found in the outdoor environment in figure 4.4(b). This implies that the larger number of channel to use in scheduling does not always lead to a reduction of minimum K and the exclusive region. We should carefully choose the number of channels used in the network, considering the value of the channel resource.

We also look at the minimum K for all the indoor and outdoor cases and show the result in figure 4.6. We can tell that the minimum K will decreases as the channel number increases for both type of environments. The minimum K will be not greater than 2 when the channel number is 2. More over, the minimum K decrease to 1 when the channel number is greater than 12, even for 90% PDR requirement.

4.5 Concluding remarks

In this section, we study the potential of using PRK model in multi-channel scheduling. We first formulate the interference in Poisson network using PRK model under the condition that multiple transmission channels can be used. Through the simulation under a wide range of system configurations, the potential of using PRK model with multi-channel scheduling is carefully studied. Our results show that the channel number in scheduling has a great impact on the link quality. A scheduling with 2 or 3 channels cannot improve the link quality significantly. On the other side, the number of channels needed by ratio-K model to have a relative good link quality(e.g. 80% PDR) does not have to been very large. In our setup, the number is 10 for indoor environment and 15 for outdoor environment. If the channel number is greater than that, it will not have significant PDR improvement for most of the system configurations. 10 - 15 is our recommendation to use ratio-K model in multi-channel MAC protocols.

We also study how the minimum K will change if multiple channels are used in the scheduling. Our results shows that the benefits of multiple channels on the minimum K is significant,

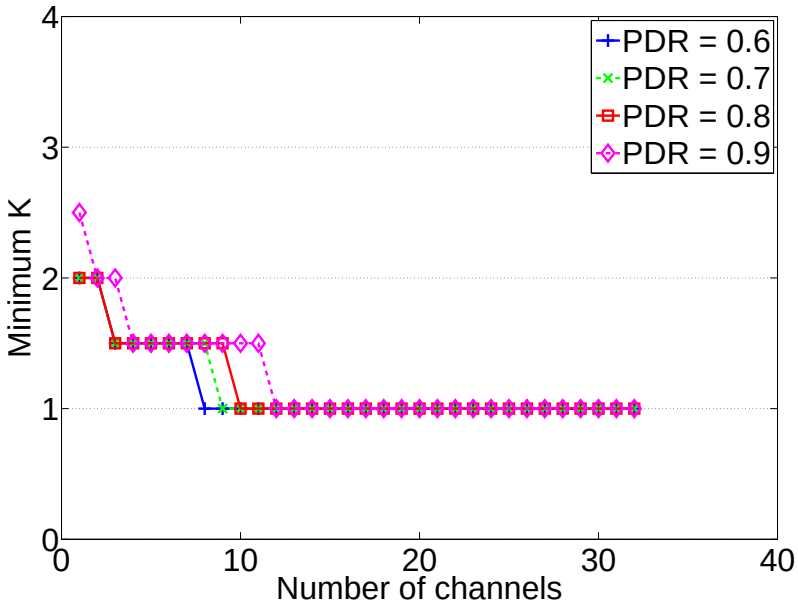

(a) indoor environment $\alpha = 3.5$

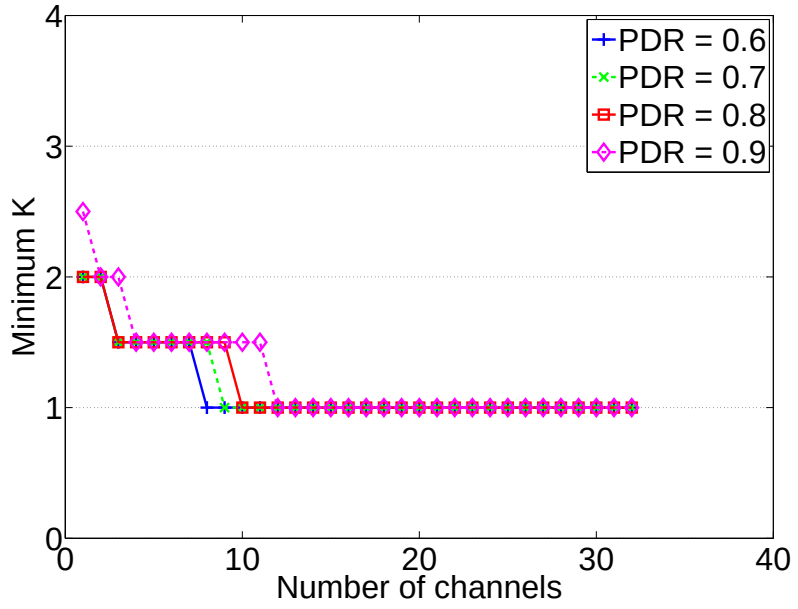

(b) outdoor environment $\alpha = 4.5$

Figure 4.6: Minimun K reduction when different channels are used in the network

especially for the cases that a large value minimum K is required. Moreover, we find that the minimum K drops to 2 when channel number increases to 7, for both indoor and outdoor environment. This good message suggests that ratio-K models can perform very well in a multi-channel scheduling and be a good model for distributed protocol design. We also find that the minimum K does not further decrease when the channel number increases from 11 to 25. This result implies that the larger number of channel to use in scheduling does not always lead to a reduction of minimum K and the exclusive region

CHAPTER 5

CONCLUSION AND FUTURE WORK

5.1 Conclusion

Interference model is the basis of MAC protocol design in wireless networks, and it directly affects the efficiency and predictability of wireless messaging. To enable the design of distributed MAC protocols for agile, predictable interference control, this thesis tries to answer the *open question*: whether it is possible to develop an interference model that has both the locality of the ratio-K model and the high fidelity of the SINR model.

Given that the ratio-K model is local and can enable agile, distributed protocols, we explore the possibility of extending the ratio-K model to preserve its locality while addressing the low performance issue of ratio-K-based scheduling. To this end, we first study the behavior of ratio-K-based scheduling, and analyze how network traffic load, link length, and wireless signal attenuation affect the effective instantiation of the ratio-K model. We find that fixing K to a constant number, as in most existing studies [14, 40, 44], can lead to significant performance loss when network and environmental settings change. For instance, deviation from the optimal K by up to 1 can cause up to 68% throughput loss, and fixing K to 2 may lead to a link reliability less than 80%.

These findings suggest that, when designing and evaluating ratio-K-based scheduling algorithms, it is important to choose the right parameter K according to network and environmental conditions. We also find that there is inherent tradeoff between reliability and throughput when instantiating the ratio-K model. Maximum network throughput is usually achieved not at the minimum K for ensuring certain link reliability, but at a smaller K. For instance, $\sqrt{2}$ is the optimal K for maximizing throughput in many scenarios, but, with non-negligible probability, $\sqrt{2}$ is unable to guarantee an 80% link reliability.

Our findings (in particular, those on the reliability-throughput tradeoff in ratio-K-based scheduling) suggest that, in wireless networked sensing and control where high link reliability is critical not only for reliable data delivery but also for small latency and latency jitter, we can use link reliability requirement as the basis of instantiating the ratio-K model. Based on that, we propose the *physical-ratio-K (PRK) interference model* as a reliability-oriented instantiation of the ratio-K model, where the link-specific choice of K adapts to network and environmental conditions as well as application QoS requirements to ensure certain minimum reliability of every link. Through simulations and testbed experiments, we find that, for a given requirement on link reliability, PRK-based scheduling achieves a network spatial throughput very close to what is enabled by SINR-based scheduling, for instance, at least 95% in many scenarios we study. Moreover, as link reliability requirement increases, the throughput loss in PRK-based scheduling further decreases.

During the research in ratio-K based scheduling, we notice one interesting thing: the interference among the transmissions, when scheduling them for a same time slot, limits the number of concurrent transmissions in the slot. Optimal interference-oriented scheduling in wireless networks has been shown to be NP-complete in general [23, 54], and the research community has proposed different polynomial-time approximation algorithms accordingly. Most approximation algorithms are greedy in nature, and two representatives are Longest-Queue-First (LQF) [35, 30, 9] and GreedyPhysical [10, 66]. In approximation algorithms where links are added to a time slot in a sequential manner until reaching the interference limit,[1] the order in which links are added determines the accumulation of interference at the receivers and thus affects the number of concurrent links schedulable in the slot. Nonetheless, existing scheduling algorithms either do not take this ordering effect into account (e.g., in LQF) or do not explicitly optimize for the ordering effect (e.g., in GreedyPhysical and LengthDiversity). Thus we try to answer those *open questions* are: 1) how to explicitly optimize the ordering of link addition

[1] For example, the SINR at some receiver falls below a minimum threshold.

in wireless scheduling? and 2) how does link ordering affect the throughput and delay of data delivery?

To address these open questions for insight into wireless scheduling, we formulate the concept of *interference budget* that, given a set of scheduled transmissions in a time slot, characterizes the additional interference power that can be tolerated by all the receivers without violating the application requirement on link reliability. Then, by modeling the scheduling problem as a knapsack problem, we propose the scheduling algorithm *iOrder* that optimizes link ordering by considering both interference budget and queue length in scheduling. When constructing the schedule for a time slot, iOrder first picks a link with the maximum number of queued packets; then iOrder adds links to the slot one at a time in a way that maximizes the interference budget at each step; this process repeats until no additional link can be added to the slot without violating the application requirement on link reliability.

To understand the impact of link ordering on scheduling, we first analytically prove the approximation ratio of iOrder in Poisson random networks, then we comparatively study the performance of iOrder and existing algorithms via simulation and testbed-based measurement. We observe that optimizing link ordering can improve the performance of existing algorithms by a significant margin in the case of both backlogged and online traffic, for instance, doubling the throughput and reducing the latency of LQF by a factor up to 24, and improving the throughput of LengthDiversity by a factor up to 19.6. Thus our study demonstrates the importance of explicitly optimizing link ordering in wireless scheduling, which opens up new avenues for future research and for optimizing wireless network performance. Our detailed simulation study also discover the surprisingly low performance of LengthDiversity despite its good asymptotic approximation ratio. We find that this is due to the large constant factor hidden in the analysis of LengthDiversity [23]. Therefore, it is important to examine the constant factors when analyzing wireless scheduling algorithms.

5.2 future work

PRK model is proposed to bridge the gap between the protocol model and the physical interference model. Our work showed that the performance of ratio-K-based scheduling is highly sensitive to the choice of K. If correctly instantiated via the PRK model, ratio-K-based scheduling can achieve a close-to-optimal performance. It is important to take this into account in both protocol design and performance evaluation. These findings showed the feasibility of integrating the high fidelity of the SINR model with the locality of the ratio-K model, and suggested new approaches to MAC protocol design in dynamic, unpredictable network and environmental settings. For example, if we can let the receiving of each link locally choose K, the MAC protocol will be able to satisfy application-specific link reliability requirement. So one extension to PRK work is to implement protocols that can enable link-specific, local search of K via feedback on packet delivery reliability, since link reliability is locally measurable metric. This also addresses the challenge of how to efficiently adapt K according to dynamic, potentially unpredictable network and environmental settings, which has been recognized as an open problem by Shi $et\ al.$ [56] who studied the ratio-K model in parallel with our work here.

By utilizing the orthogonal channels, the interference among the multiple concurrent transmissions could be greatly reduced. One of the key challenge to design distributed PRK protocols is to ensure the signaling message correctly received by all the nodes in the exclusive region, especially when the value of K is large. In our multi-channel PRK study, our result show that the minimum K to ensure a certain link quality will be greatly reduced. This is a very promising message for designing multi-channel PRK-based protocols. So one of the future work is to use the PRK model in multi-channel scheduling and design multi-channel distributed protocols that uses PRK model in the wireless networks.

BIBLIOGRAPHY

[1] NetEye testbed. http://neteye.cs.wayne.edu/neteye/home.php.

[2] IEEE Std 802.15.4-2006. Wireless Medium Access Control (MAC) and Physical Layer (PHY) Specifications for Low-Rate Wireless Personal Area Networks (WPANs), September 2006.

[3] 802.15.4A WORKING GROUP, I. IEEE 802.15.4a channel model - final report. Tech. rep.

[4] AKYILDIZ, I., MELODIA, T., AND CHOWDURY, K. Wireless multimedia sensor networks: A survey. *Wireless Communications, IEEE 14* (December 2007).

[5] AKYILDIZ, I., SU, W., SANKARASUBRAMANIAM, Y., AND CAYIRCI, E. Wireless sensor networks: A survey. In *Computer Networks (Elsevier) Journal* (2002).

[6] AKYILDIZ, I., WANG, X., AND WANG, W. Wireless mesh networks: A survey. In *Computer Networks (Elsevier) Journal* (2005).

[7] ARORA, A., RAMNATH, R., ERTIN, E., SINHA, P., BAPAT, S., NAIK, V., KULATHUMANI, V., ZHANG, H., CAO, H., SRIDHARA, M., KUMAR, S., SEDDON, N., ANDERSON, C., HERMAN, T., TRIVEDI, N., ZHANG, C., GOUDA, M., CHOI, Y. R., NESTERENKO, M., SHAH, R., KULKARNI, S., ARAMUGAM, M., WANG, L., CULLER, D., DUTTA, P., SHARP, C., TOLLE, G., GRIMMER, M., FERRIERA, B., AND PARKER, K. Exscal: Elements of an extrem scale wireless sensor network. In *IEEE RTCSA* (2005).

[8] BADIA, L., ERTA, A., LENZINI, L., ROSSETTO, F., AND ZORZI, M. A physical model scheduler for multi-hop wireless networks based on local information. In *IEEE MASS* (2008).

[9] BLOUGH, D. M., DAS, S., RESTA, G., AND SANTI, P. A framework for joint scheduling and diversity exploitation under physical interference in wireless mesh networks. In *IEEE MASS* (2008).

[10] BRAR, G., BLOUGH, D. M., AND SANTI, P. Computationally efficient scheduling with the physical interference model for throughput improvement in wireless mesh networks. In *ACM MobiCom* (2006).

[11] BRAR, G., BLOUGH, D. M., AND SANTI, P. The SCREAM approach for efficient distributed scheduling with physical interference in wireless mesh networks. In *ICDCS* (2008).

[12] CAI, L. X., CAI, L., SHEN, X., MARK, J. W., AND ZHANG, Q. MAC protocol design and optimization for multi-hop ultra-wideband networks. *IEEE Transactions on Wireless Communications 8*, 8 (2009).

[13] CESANA, M., MANIEZZO, D., BERGAMO, P., AND GERLA, M. Interference aware (IA) MAC: an enhancement to ieee 802.11b DCF. In *IEEE VTC* (2003).

[14] CHAFEKAR, D., KUMAR, V. A., MARATHE, M. V., PARTHASARATHY, S., AND SRINIVASAN, A. Approximation algorithms for computing capacity of wireless networks with sinr constraints. In *IEEE INFOCOM* (2008).

[15] CHE, X., JU, X., AND ZHANG, H. The case for addressing the limiting impact of interference on wireless scheduling. In *IEEE ICNP* (2011).

[16] CHE, X., LIU, X., JU, X., AND ZHANG, H. Adaptive instantiation of the protocol interference model in mission-critical wireless networks. In *IEEE SECON* (2010).

[17] CHE, X., LIU, X., JU, X., AND ZHANG, H. Adaptive instantiation of the protocol interference model in mission-critical wireless networks. Tech. Rep. WSU-CS-DNC-

TR-08-04, Wayne State University (http://www.cs.wayne.edu/~hzhang/group/TR/DNC-TR-08-04.pdf), December 2008.

[18] CHINTALAPUDI, K., AND VENKATRAMAN, L. On the design of mac protocols for low-latency hard real time latency applications over 802.15.4 hardware. In *ACM/IEEE IPSN* (2008).

[19] CHOI, J. I., JAIN, M., KAZANDJIEVA, M., AND LEVIS, P. Granting silence to avoid wireless collisions. In *ICNP* (oct. 2010), pp. 82 –91.

[20] DAS, S. M., KOUTSONIKOLAS, D., HU, Y. C., AND PEROULIS, D. Characterizing multi-way interference in wireless mesh networks. In *ACM WiNTECH* (2006).

[21] GOBRIEL, S., MELHEM, R., AND MOSSE, D. A unified interference/collision analysis for power-aware adhoc networks. In *IEEE INFOCOM* (2004).

[22] GOLLAKOTA, S., AND KATABI, D. Zigzag decoding: Combating hidden terminals in wireless networks. In *ACM SIGCOMM* (2008).

[23] GOUSSEVSKAIA, O., OSWALD, Y. A., AND WATTENHOFER, R. Complexity in geometric sinr. In *ACM MobiHoc* (2007).

[24] GUPTA, A., LIN, X., AND SRIKANT, R. Low-complexity distributed scheduling algorithms for wireless networks. *IEEE/ACM Transactions on Networking 17*, 6 (2009).

[25] GUPTA, P., AND KUMAR, P. R. The capacity of wireless networks. *IEEE Transactions on Information Theory 46*, 2 (2000).

[26] HAENGGI, M., AND GANTI, R. K. Interference in large wireless networks. *Foundations and Trends in Networking 3*, 2 (2009), 127–248.

[27] HALPERIN, D., ANDERSON, T., AND WETHERALL, D. Taking the sting out of carrier sense: Interference cancellation for wireless LANs. In *ACM MobiCom* (2008).

[28] HELLERSTEIN, J., DIAO, Y., PAREKH, S., AND TILBURY, D. M. *Feedback Control of Computing Systems*. Wiley-IEEE Press, 2004.

[29] HOCHBAUM, D. S. *Approximation Algorithms for* NP*-hard Problems*. PWS Publishing Company, 1997.

[30] JOO, C., LIN, X., AND SHROFF, N. B. Understanding the capacity region of the greedy maximal scheduling algorithm in multi-hop wireless networks. In *IEEE INFOCOM* (2008).

[31] JOO, C., AND SHROFF, N. B. Performance of random access scheduling schemes in multi-hop wireless networks. In *IEEE INFOCOM* (2007).

[32] KAR, K., LUO, X., AND SARKAR, S. Delay guarantees for throughput-optimal wireless link scheduling. In *IEEE INFOCOM* (2009).

[33] KATZ, B., VOLKER, M., AND WAGNER, D. Link scheduling in local interference models. In *AlgoSensors* (2008).

[34] KIM, T.-S., LIM, H., AND HOU, J. C. Improving spatial reuse through tuning transmit power, carrier senses threshold, and data rate in multihop wireless networks. In *ACM MobiCom* (2006).

[35] LE, L. B., MODIANO, E., JOO, C., AND SHROFF, N. B. Longest-queue-first scheduling under SINR interference model. In *ACM MobiHoc* (2010).

[36] LECONTE, M., NI, J., AND SRIKANT, R. Improved bounds on the throughput efficiency of greedy maximal scheduling in wireless networks. In *ACM MobiHoc* (2009).

[37] LI, L. E., ALIMI, R., SHEN, D., VISWANATHAN, H., AND YANG, Y. R. A general algorithm for interference alignment and cancellation in wireless networks. In *IEEE INFOCOM* (2010).

[38] MA, H., ALAZEMI, H. M., AND ROY, S. A stochastic model for optimizing physical carrier sensing and spatial reuse in wireless ad hoc networks. In *IEEE MASS* (2005).

[39] MAHESHWARI, R., CAO, J., AND DAS, S. Physical interference modeling for transmission scheduling on commodity wifi hardware. In *IEEE INFOCOM miniconference* (2009).

[40] MAHESHWARI, R., JAIN, S., AND DAS, S. A measurement study of interference modeling and scheduling in low-power wireless networks. In *ACM SenSys* (2008).

[41] MAHESHWARI, R., JAIN, S., AND DAS, S. R. On estimating joint interference for concurrent packet transmissions in low power wireless networks. In *ACM WiNTECH* (2008).

[42] MAROTI, M., KUSY, B., SIMON, G., AND LEDECZI, A. The flooding time synchronization protocol. In *ACM SenSys* (2004).

[43] MENON, R., BUEHRER, R. M., AND REED, J. H. Impact of exclusion region and spreading in spectrum-sharing ad hoc networks. In *ACM Workshop on Technology and Policy for Accessing Spectrum* (2006).

[44] MOSCIBRODA, T., WATTENHOFER, R., AND WEBER, Y. Protocol design beyond graph based models. In *ACM HotNets* (2006).

[45] MOSCIBRODA, T., WATTENHOFER, R., AND ZOLLINGER, A. Topology control meets SINR: The scheduling complexity of arbitrary topologies. In *ACM MobiHoc* (2006).

[46] NEELY, M. J. Delay analysis for maximal scheduling with flow control in wireless networks with bursty traffic. *IEEE/ACM Transactions on Networking 17*, 4 (2009), 1146–1159.

[47] NI, J., TAN, B., AND SRIKANT, R. Q-CSMA: Queue-length based CSMA/CA algorithms for achieving maximum throughput and low delay in wireless networks. In *IEEE INFOCOM* (2010).

[48] NIKOOKAR, H., AND HASHEMI, H. Statistical modeling of signal amplitude fading of indoor radiopropagation channels. In *Personal Communications: Gateway to the 21st Century* (1993).

[49] QIAO, D., CHOI, S., AND SHIN, K. G. Interference analysis and transmit power control in IEEE 802.11a/h wireless LANs. *IEEE/ACM Transactions on Networking 15*, 5 (2007).

[50] RAPPAPORT, T. *Wireless Communications*. Prentice-Hall, Upper Saddle River, NJ, 2002.

[51] RHEE, I., WARRIER, A., MIN, J., AND XU, L. DRAND: Distributed randomized TDMA scheduling for wireless ad hoc networks. In *ACM MobiHoc* (2006).

[52] SEIDEL, S. Y., AND RAPPAPORT, T. S. 914 mhz path loss prediction model for indoor wireless communication in multi floored buildings. 207–217.

[53] SHA, M., XING, G., ZHOU, G., LIU, S., AND WANG, X. C-MAC: Model-driven concurrent medium access control for wireless sensor networks. In *IEEE INFOCOM* (2009).

[54] SHARMA, G., MAZUMDAR, R. R., AND SHROFF, N. B. On the complexity of scheduling in wireless networks. In *ACM MobiCom* (2006).

[55] SHARMA, G., SHROFF, N., AND MAZUMDAR, R. Maximum weighted matching with interference constraints. In *Pervasive Computing and Communications Workshops, 2006. PerCom Workshops 2006. Fourth Annual IEEE International Conference on* (2006).

[56] SHI, Y., HOU, Y. T., LIU, J., AND KOMPELLA, S. How to correctly use the protocol interference model for multi-hop wireless networks. In *ACM MobiHoc* (2009).

[57] SOHRABI, K., MANRIQUEZ, B., AND POTTIE, G. J. Near ground wideband channel measurement.

[58] SON, D., KRISHNAMACHARI, B., AND HEIDEMANN, J. Experimental analysis of concurrent packet transmissions in low-power wireless networks. In *ACM SenSys* (2006).

[59] STOYAN, D., KENDALL, W. S., AND MECKE, J. *Stochastic Geometry and its applications*. Wiley, 1995.

[60] TABET, T., AND KNOPP, R. Spatial throughput of multi-hop wireless networks under different retransmission protocols. In *Allerton* (2004).

[61] CC 2420 RADIO. http://focus.ti.com/docs/prod/folders/print/cc2420.html.

[62] DUST NETWORKS. Time synchronized mesh protocol (TSMP). http://www.dustnetworks.com/cms/ sites/default/files/TSMP_Whitepaper.pdf.

[63] ISA SP100.11A. http://www.isa.org//MSTemplate.cfm?MicrositeID= 1134&CommitteeID=6891.

[64] TOBAGI, F., AND KLEINROCK, L. Packet switching in radio channels: Part ii–the hidden terminal problem in carrier sense multiple-access and the busy-tone solution. *IEEE Transactions on Communications COM-23*, 12 (1975), 1417–1433.

[65] WANG, P., AND ZHUANG, W. A collision-free MAC scheme for multimedia wireless mesh backbone. *IEEE Transactions on Wireless Communications 8*, 7 (2009).

[66] WANG, W., WANG, Y., LI, X.-Y., SONG, W.-Z., AND FRIEDER, O. Efficient interference-aware TDMA link scheduling for static wireless networks. In *AMC MobiCom* (2006).

[67] WANG, X., AND BERGER, T. Spatial channel reuse in wireless sensor networks. *Wireless Networks*, 14 (2008), 133–146.

[68] WEBER, S., YANG, X., ANDREWS, J. G., AND DE VECIANA, G. Transmission capacity of wireless ad hoc networks with outage constraints. *IEEE Transactions on Information Theory 51*, 12 (December 2005).

[69] WERNER-ALLEN, G., SWIESKOWSKI, P., AND WELSH, M. Motelab: A wireless sensor network testbed. In *IEEE/ACM IPSN/SPOTS* (2005).

[70] WIRELESSHART. http://www.hartcomm2.org/hart_protocol/wireless_hart/ wireless_hart_main.html.

[71] YANG, X., AND DE VECIANA, G. Inducing spatial clustering in MAC contention for spread spectrum ad hoc networks. In *ACM MobiHoc* (2005).

[72] YEDAVALLI, K., AND KRISHNAMACHAR, B. 'enhancement of the IEEE 802.15.4 MAC protocol for scalable data collection in dense sensor networks. In *International Symposium on Modeling and Optimizationin Mobile, Ad Hoc, and Wireless Networks* (2008).

[73] YI, Y., VECIANA, G. D., AND SHAKKOTTAI, S. On optimal MAC scheduling with physical interference model. In *IEEE INFOCOM* (2007).

[74] YING, L., AND SHAKKOTTAI, S. Scheduling in mobile ad hoc networks with topology and channel-state uncertainty. In *IEEE INFOCOM* (2009).

[75] ZAMALLOA, M. Z. N., AND KRISHNAMACHARI, B. An analysis of unreliability and asymmetry in low-power wireless links. *ACM Trans. Sen. Netw.* (2007).

[76] ZHANG, H., ARORA, A., RI CHOI, Y., AND GOUDA, M. Reliable bursty convergecast in wireless sensor networks. *Computer Communications (Elsevier), Special Issue on Sensor-Actuator Networks 30*, 13 (2007).

[77] ZHANG, H., ARORA, A., AND SINHA, P. Link estimation and routing in sensor network backbones: Beacon-based or data-driven? *IEEE Transactions on Mobile Computing* (May 2009).

[78] ZHANG, Y., AND BROWN, A. K. Data rate for ds-uwb communication systems in wireless personal area networks. In *ICUWB* (2008).

[79] ZHOU, G., HE, T., KRISHNAMURTHY, S., AND STANKOVIC, J. Models and solutions for radio irregularity in wireless sensor networks. *ACM Transactions on Sensor Networks 2*, 2 (2006).

[80] ZHOU, G., HE, T., STANKOVIC, J. A., AND ABDELZAHER, T. RID: Radio interference detection in wireless sensor networks. In *IEEE INFOCOM* (2005).

[81] ZUNIGA, M., AND KRISHNAMACHARI, B. An analysis of unreliability and asymmetry in low-power wireless links. *ACM Transactions on Sensor Networks 3*, 2 (2007).

ABSTRACT

INTERFERENCE MODELING AND CONTROL IN WIRELESS NETWORKS

by

XIN CHE

August 2014

Advisor: Dr. Hongwei Zhang

Major: Computer Science

Degree: Doctor of Philosophy

With the successful commercialization of IEEE802.11 standard, wireless networks have become a tight-knit of our daily life. As wireless networks are increasingly applied to real-time and mission-critical tasks, how to ensuring real-time, reliable data delivery emerges as an important problem. However, wireless communication is subject to various dynamics and uncertainties due to the broadcast nature of wireless signal. In particular, co-channel interference not only reduces the reliability and throughput of wireless networks, it also increases the variability and uncertainty in data communication [64, 80, 77].

A basis of interference control is the interference model which *predicts* whether a set of concurrent transmissions may interfere with one another. Two commonly used models, the *SINR model* and the *radio-K model*, are thoroughly studied in our work. To address the limitations of those models, we propose the *physical-ratio-K(PRK)* interference model as a reliability-oriented instantiation of the ratio-K model, where the link-specific choice of K adapts to network and environmental conditions as well as application QoS requirements to ensure certain minimum reliability of every link.

On the other hand, the interference among the transmissions, limits the number of concurrent transmissions. We formulate the concept of *interference budget* that, given a set of scheduled transmissions in a time slot, characterizes the additional interference power that can

be tolerated by all the receivers without violating the application requirement on link reliability. We propose the scheduling algorithm *iOrder* that optimizes link ordering by considering both interference budget and queue length in scheduling. Through both simulation and real-world experiments, we observe that optimizing link ordering can improve the performance of existing algorithms by a significant.

Based on the strong preliminary research result on interference modeling and control, we will extend our method into distributed protocol designs. One future work will focus on implementing the *PRK model* in distributed protocols. We will also explore the benefits of using multiple channels in the interference control.

AUTOBIOGRAPHICAL STATEMENT

XIN CHE

Xin Che is a Ph.D. candidate in Computer Science at Wayne State University. He received his Bachelor degrees (2004) in Computer Science and Communication Systems respectively, from Huazhong University of Science and Technology(HUST), Wuhan, China. He also received his Master degree(2007) in Signal Processing from HUST. His research interests include computer networks, distributed systems, operating systems, communication systems and signal processing. Several of his research papers have been published at top journals and international conferences.